Revisiting Fluorescent Calixarenes: From Molecular Sensors to Smart Materials

Rajesh Kumar,[‡,†,§] Amit Sharma,[‡,§] Hardev Singh,[‡,ǁ,§] Paolo Suating,[⊥,§] Hyeong Seok Kim,[‡] Kyoung Sunwoo,[‡] Inseob Shim,[‡] Bruce C. Gibb,[⊥,*] Jong Seung Kim[‡,*]

[‡] Department of Chemistry, Korea University, Seoul 02841, Korea.

[†] Present address: CanAm Bioresearch Inc. Winnipeg, Manitoba, Canada.

[ǁ]Present address: Department of Biosystems Engineering, University of Manitoba, Winnipeg, Canada.

[⊥] Department of Chemistry, Tulane University, New Orleans, LA 70118, USA.

* Corresponding authors: jongskim@korea.ac.kr (J. S. Kim); bgibb@tulane.edu (B. C. Gibb)

[§] Equally contributed.

Abstract

Calix[*n*]arenes (n = 4, 5, 6, 8), "chalice-like" phenol-based macrocycles, are one of the most fascinating and highly-studied scaffolds in supramolecular chemistry. This stems from the functional and tunable diversity at both their upper and lower rims, their pre-organized non-polar cavities and pre-organized ion-binding sites, and their well-defined conformations. Conjugation of calixarene scaffolds with various fluorogenic groups leads to the development of smart fluorescent probes that have been utilized toward molecular sensors, bio-imaging, drug- and gene-delivery, self-assembly/aggregation, and smart materials. The fine-tuning and incorporation of different ligating sites in the calix[4]arene scaffolds has given numerous molecular sensors for cations, anions, and biomolecules. Moreover, the aqueous solubility of *p*-sulfonatocalix[4]arenes has engendered their potential use in drug/gene-delivery, and enzymatic assays. In addition, owing to their strong optical properties, fluorescent calix[4]arenes have been used to develop smart

materials including gels, nonlinear, OLED and multi-photon materials. Finally, significant developments in the utility of fluorescent higher-calixarenes have been made for bio-applications. This review critically summarizes the recent advances made in all of these different areas.

Contents

1. Introduction

Supramolecular chemistry – the chemistry beyond the molecule – has occupied the minds of a significant proportion of the chemical community over the last few decades.[1] Utilizing the gamut of non-covalent interactions such as hydrogen bonding, electrostatics, and π-π stacking, Nature itself forms a vast array of supramolecular complexes from smaller chemical entities. Utilizing such non-covalent interactions, numerous synthetic molecular systems have been developed and investigated for different applications including switches, smart materials, molecular machines, catalysis, sensing, and nanomedicine.[2-5] The development of next-generation materials and devices must incorporate more carefully crafted molecular design and supramolecular interactions to expand or enhance their function. In healthcare, for example, defined photophysical responses tied to precise supramolecular interactions are central to sensor materials and diagnostics, as well as treatment strategies. Moreover, the emerging field of theranostics doubly relies on this precise control.[2] In this regard materials possessing distinct photophysical and supramolecular properties represent key platforms for a wide range of disciplines.

Advances in organic synthesis, supramolecular chemistry, and fluorimetry over the last 50 years now mean that chemists are poised to address the design of new materials for these goals. Towards this, supramolecular chemists have a unique set of tools at their disposal: a wide range of macrocycles possessing the required rigid architectures and synthetic tailorability. These macrocycles include calixarenes,[6] crown ethers,[7] cyclodextrins,[8,9] cryptands,[10] and cucurbiturils;[11,12] and among these it is arguably fluorescent calixarenes (Figure 1A) that offer the greatest opportunity for the development of future applications; their facile synthesis, distinct conformational preferences, π-electron rich cavities, ease of derivatization, and their signaling capabilities, all combine to give unparalleled opportunities.

Calixarenes are a class of “chalice-like” phenol-based macrocycles (Figure 1A) and are one of the most investigated molecular scaffolds in supramolecular chemistry.[13] This is in large part because they are so readily accessible. Additionally, calixarenes offer several advantages compared to other macromolecules, specifically: a) a pre-organized non-polar cavity; b) a pre-organized ion binding site; c) well-defined conformations that

are both substituent- and guest-dependent, and; d) tuneable functionalization of their lower and upper rims.

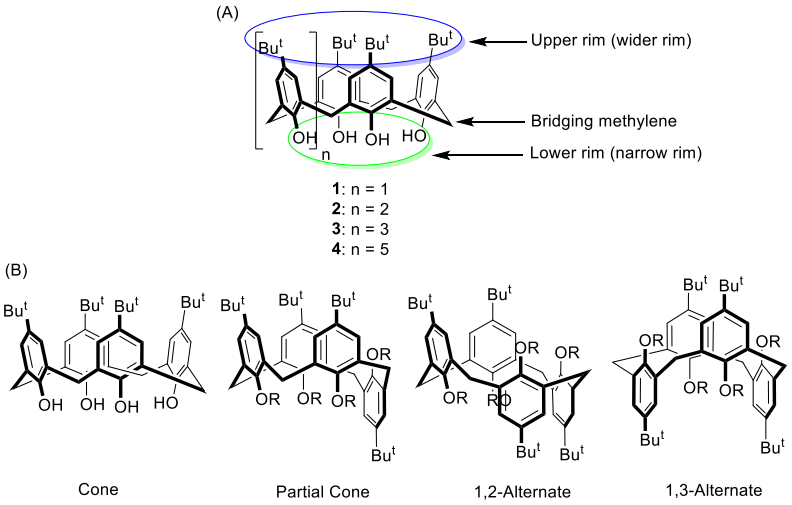

Figure 1. (A) Structure of calix[n]arenes **1**-**4** and (B) different conformations of calix[4]arene **1**.

The pre-organization of the non-polar cavity of calixarenes leads to excellent size- and shape-specific binding of guests. Complexation can be driven by the hydrophobic effect, cation-π interactions, or by adorning various hydrogen bond-donor/acceptor groups on the upper rim. On the other hand, selective ion binding is readily accomplished by incorporating suitable functional groups on the lower rim of the host.

As this review highlights, amongst the various calix[n]arenes it is the calix[4]arene scaffold that is the most investigated, primarily because of its facile synthesis and ease of derivatization. Calix[4]arenes can themselves adopt four different diastereomeric conformations: cone, partial cone, 1,2-alternate, and 1,3-alternate (Figure 1B). Perhaps more importantly, by chemical modification, a calixarene can be "frozen" in any one of these conformations (four hosts in one!), or if desired, the host can be designed in such a way as to allow it to switch between different conformations. Such switching can be precisely controlled so that, for example, the calixarene changes form (and therefore photophysical properties) in response to guest binding. Among the four different conformations, it is the cone[14] and 1,3-alternate[15] conformations that have been the most widely investigated. The cone conformation can be selectively derivatized into mono-, di-, tri-, and tetra-derivatives with flexible binding properties. On the other hand, 1,3-alternate conformation exhibits two binding sites, each consisting of two phenolic oxygens and

benzene rings, resulting in a π-basic tunnel.[16] Collectively, these unique properties are the foundation of the success of calixarenes as so-called “third generation” hosts.[17]

Much of the success of calixarenes, in general, can be attributed to fluorescent derivatives.[18] Fluorescence spectroscopy is among the best non-invasive spectral modality for observing and monitoring events at the molecular level, whether it be molecular recognition *in vitro*, or molecular recognition *in vivo*. Numerous reports have been published in which calixarene-based, smart fluorogenic materials have been utilized by either covalently or non-covalently conjugating various fluorophores. These include coumarinyl, dansyl, naphthalimide, pyrenyl, perylenyl, quinolyl, and anthranyl moieties. These fluorophores translate binding events into an optical signal *via* exciplex formation, photoinduced electron transfer (PET), intramolecular charge transfer (ICT), intermolecular excited state proton transfer (ESPT), and metal-to-ligand charge transfer (MLCT), resulting in fluorescence enhancement, quenching, or ratiometry responses.

Several strategies have been formulated to generate fluorescent calixarenes, including: a) covalently appending fluorophores to calixarenes; b) decorating fluorogenic polymeric backbones with calixarenes; c) developing amphiphilic self-assembled nanoparticles, and; d) engineering silica or metal nanoparticles coated with calixarenes. The eventual goal of these formulations is to develop efficient and sensitive systems for monitoring cellular events, diagnostics, drug delivery, and high-performance optical materials, to name a few examples (Scheme 1).

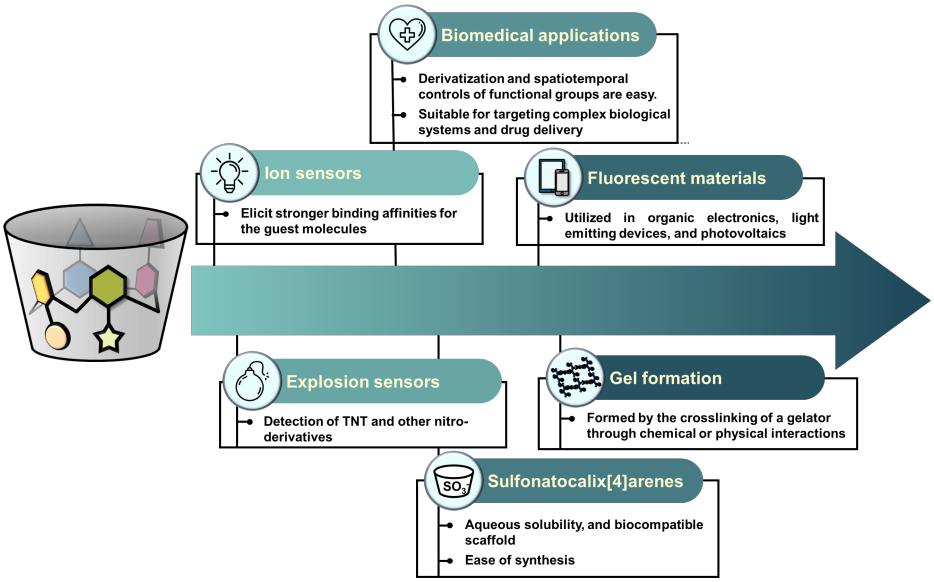

Scheme 1. A representation of applications of fluorescent calix[4]arenes.

In the last few years, a number of elegant fluorogenic probes based on calixarenes have been developed. However, despite numerous developments of fluorescent calixarenes and their utilities, no comprehensive review has been recently published. Therefore, this review summarizes the advances made in the development and applications of fluorescent calixarene hosts in the last ten years. The review has been broken down into two main sections: one on calix[4]arenes, and one on larger calix[5/6/8]arene-based receptors. As the calix[4]arene scaffold is the most investigated, its applications have been sub-categorized according to the type of guest binding (cation, anions, biomolecules and bifunctional), bio-application (bio-sensors, enzymatic assays, and drug carriers), and materials application.

2. Calix[4]arene based receptors

2.1 Fluorescent receptors for metal ions

Metal ions play essential roles in countless biological processes and are consequently key to many aspects of medicine. However, if a metal ion is out of context, present in abnormally high concentrations, or is intrinsically toxic, then detrimental impacts on the environment and human health become key. Consequently, the selective and sensitive detection of hard and/or soft metal ions is essential in a multitude of scenarios. To meet this challenge, finely-tuned calixarene fluorescent probes with both suitable ligating sites (O, N, and S) and attendant fluorophores have been developed. This section will focus on the recent developments of calix[4]arene probes for selective detection of different metal ions in environmental and biological systems. The summarized binding properties including stoichiometries, binding constants, and detection limits of various probes for the respective metal cations and have been listed in Table 1.

2.1.1 Detection of alkali metal cations

The direct conjugation of four phenanthridine moieties to the lower rim of calix[4]arene **5** (Figure 2) has been investigated as a strategy for the detection for alkali metal cations.[19] In a mixed MeOH-CH_2Cl_2 solvent, probe **5** revealed enhancement in fluorescence emission at 375 nm with Na^+, whilst with K^+ and Rb^+ ions induced quenching

of fluorescence. To gain insight into the different binding pattern of probe **5** with Na^+, and K^+ and Rb^+ ions, molecular dynamics (MD) simulations were performed. In the **5**·Na^+ complex (in MeOH–CH_2Cl_2), Na^+ ion bound with the oxygen atoms of the ether groups and methanol of crystallization which resulted in fluorescence enhancement and the suppression of PET. On the other hand, due to their larger size, K^+ and Rb^+ bound to both the oxygen atoms of the ether groups and the phenanthridine nitrogens, resulting in quenching of the fluorescence emission and enabled PET.

Cesium cation (Cs^+) is of interest owing to its intrinsic toxicity. For example, it can displace potassium ions in red blood cells and muscles causing cardiac diseases and cancer.[20] Leray *et al*. developed 1,3-alternate BODIPY-modified fluorescent probe **6A** (Figure 2) for selective Cs^+ detection.[21] The method of BODIPY conjugation to the crown-6 ether of **6A** was found to be essential; whilst the *meso*-position conjugation of BODIPY in **6B** resulted in no detection, conjugation of BODIPY with the styryl linker in probe **6A** furnished sensitive detection of Cs^+. Theoretical calculations using a B3LYP hybrid functional of density functional theory (DFT) indicated that BODIPY and the styryl unit of **6A** share the delocalization of electron density for the highest occupied molecular orbitals (HOMO). On the other hand, the *meso*-phenyl ring of **6B**, was perpendicular to the BODIPY groups and interrupted π-conjugation. Upon titration with Cs^+, a hypsochromic shift in the absorption and fluorescence spectra of **6A** was observed, along with an increase in fluorescence quantum yield. Probe **6A** exhibited 1:1 and 2:1 binding stoichiometries toward Cs^+, with stronger binding compared to other studied metal ions. This observation was attributed to the better fit of Cs^+ in the crown-ether cavity.

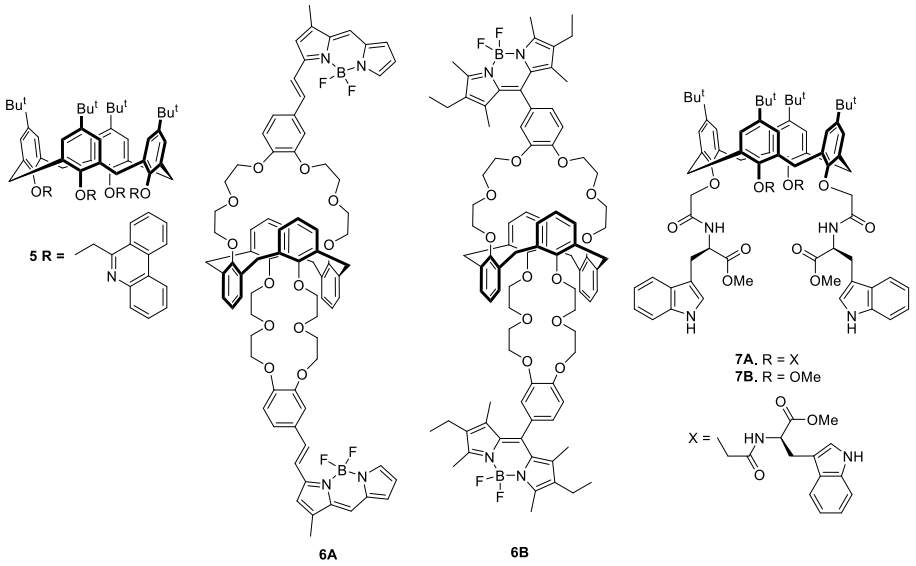

Figure 2. Structures of calixarene based probes **5**-**7** for detection of alkali metal cations.

Fluorescent peptidocalix[4]arenes **7A** and **7B** (Figure 2) bearing four and two tryptophan units, respectively, have been investigated for their binding of alkali metal and Eu^{3+} ions using UV-Vis, fluorescence, potentiometric, and conductometric titrations.[22] Probes **7A** and **7B** showed strong and moderate emission, respectively, but insignificant fluorescence changes were observed with alkali metal ions. However, using UV-Vis, potentiometric and conductometric titrations probes **7A** and **7B** displayed stronger binding for small alkali metal ions Li^+ (log $K_{Li\text{-}7A} > 6$, log $K_{Li\text{-}7B} > 6$) and Na^+ (log $K_{Na\text{-}7A} = 8.25$, log $K_{Na\text{-}7B} = 6.94$). In contrast, due to poorer accommodation in the calixarene cavities binding of K^+ was weaker (log $K_{K\text{-}7A} = 5.09$, log $K_{K\text{-}7B} = 4.09$), whilst Cs^+ and Rb^+ ions showed no evidence of complexation. The larger number of coordination sites of probe **7A** enabled binding with europium ion (Eu^{3+}, log $K = 6.16$), with notable quenching in the fluorescence emission. In contrast, with fewer coordination sites probe **7B** did not show Eu^{3+} complexation.

Table 1. Various fluorescent receptors **5**-**45** and their binding stoichiometries and constants, and detection limits toward various metal cations.

Probe number (L)	Guest species (G)	Stoichiometry ratio (L:G)	Binding constant	Detection limit	Reference
5	Na^+ K^+ Rb^+	1:1	log K = 5.19 [a] log K = 4.49 [a] log K = 2.94 [a]	- [g]	19
6A **6B**	Cs^+ Cs^+	1:1 2:1 1:1 2:1	log K = 6.09 [b] log K = 3.70 [b] log K = 5.87 [b] log K = 3.50 [b]	- [g]	21
7A **7B**	Li^+ Na^+ Eu^{3+} Li^+ Na^+ Eu^{3+}	1:1 1:1 1:1 1:1 1:1 1:1	log K >6 [c] log K = 8.25 [d] log K = 6.16 [e] log K > 6 [c] log K = 6.94 [d] - [g]	- [g]	22
8	Ca^{2+}	1:1	$K = 5.2 \times 10^7\ M^{-1}$ [e]	- [g]	26
9	Ca^{2+}	1:1	$K = 1.23 \times 10^4\ M^{-1}$ [e]	5.0×10^{-5} M	27
10	Ag^+	1:1 1:2	$K = 4.46 \times 10^3\ M^{-1}$ [e] $K = 9.20 \times 10^4\ M^{-1}$ [e]	- [g]	31
11A **11B**	Ag^+ Ag^+	1:1 1:1	$K = 7.11 \times 10^3\ M^{-1}$ [e] $K = 1.83 \times 10^4\ M^{-1}$ [e]	- [g]	32
12	Al^{3+}	- [z]	- [g]	1.8 μM	35
13	Al^{3+}	1:1	$K = 8.7 \times 10^3\ M^{-1}$ [e]	- [g]	36
14	Co^{2+}	1:1	$K = 4.8 \times 10^5\ M^{-1}$ [e]	0.92 μM	39
15	Cu^{2+}	1:1	$K = 4.9 \times 10^5\ M^{-1}$ [e]	3.05 ng ml^{-1}	46
16	Cu^{2+}	1:1	$K = 3.67 \times 10^7\ M^{-1}$ [e]	$2.71 \times 10^{-8}\ M^{-1}$	47
17	Cu^{2+}	2:1	$K = 7.24 \times 10^9\ M^{-2}$ [e]	- [g]	48
18	Cu^{2+}	1:1	log K = 4.83 [e]	- [g]	49
19A **19B** **19C** **19D** **19E**	Cu^{2+} Cu^{2+} Cu^{2+} Cu^{2+} Cu^{2+}	1:2 1:2 1:2 1:2 1:2	log K = 4.25 [e] log K = 4.37 [e] log K = 3.92 [e] log K = 4.15 [e] log K = 4.19 [e]	- [g] - [g] - [g] - [g] - [g]	50
20	Cu^{2+}	1:2	$K = 2.02 \times 10^9\ M^{-2}$ [e]	- [g]	51
21	Cu^{2+}	1:1	$K = 1.58 \times 10^4\ M^{-1}$ [e]	- [g]	53
22	Cu^{2+}	1:1	$K = 1.74 \times 10^3\ M^{-1}$ [e]	10 nM	56
23	Fe^{3+}	1:1	$K = 2.2 \times 10^5\ M^{-1}$ [e]	0.334 μM	59
24	Fe^{3+}	1:1	$K = 6.0 \times 10^4\ M^{-1}$	3×10^{-7} M	60
25	Fe^{3+}	- [z]	- [g]	- [g]	61
26	Hg^{2+}	1:1	K = 39,070 M^{-1} [e]	- [g]	67
27	Hg^{2+}	1:2	- [g]	5.0 μM	68
28	Hg^{2+}	1:1	log K = 5.94 [b]	1×10^{-7} M	69
29	Hg^{2+}	1:1	$K = 2.6 \times 10^4\ M^{-1}$ [e]	8.0×10^{-7} M	71
30	Hg^{2+}	1:1	$K = 2.93 \times 10^5\ M^{-1}$ [e]	3.41×10^{-6} M	72
31	Hg^{2+}	- [z]	- [g]	1.56 μM	74
32	Hg^{2+}	1:1	log K = 5.34 [e]	70 nM	75
33	Hg^{2+}	1:1	- [g]	1.95×10^{-5} M	76
34	Hg^{2+}	1:1	K = 20966 M^{-1} [e]	1.4 ppm	77
35	Hg^{2+}	1:1	$K = 8.527 \times 10^3\ M^{-1}$ [e]	- [g]	78
36	Pb^{2+}	1:1	$K = 5.0 \times 10^5\ M^{-1}$ [e]	- [g]	83
37	Pb^{2+}	1:1	- [g]	2.5 ppb	84

38	Pb^{2+}	1:1	log K = 4.08	- [g]	85
39	Pb^{2+}	1:1	log = 4.74	42ppb	86
40	Zn^{2+}	1:1	K = 1.49 x 10^5 M^{-1} [e]	36 ppb	89
41	Zn^{2+}	1:2	K = 6.2×10^4 M^{-1} [e]	- [g]	91
42	Zn^{2+}	1:1	K = 37150 M^{-1} [e]	183 ppb	92
43	Zn^{2+}	1:2	- [g]	- [g]	93
44	Zn^{2+}	1:2	- [g]	- [g]	93
45	Zn^{2+}	1:1	- [g]	- [g]	94

[a] Calculated using spectrophotometric titrations, [b] SPECFIT software, [c] spectrophotometric and conductometric titrations, [d] potentiometric titrations, [e] fluorescence titrations, [g] not reported by the original article.

2.1.2 Detection of calcium (Ca^{2+}) ion

Calcium is an important metal ion in human health and also been widely used in the electronic and metallurgic industries.[23-25] The direct conjugation of BODIPY moieties to the upper rim of calix[4]arene **8** (Figure 3) resulted in a host that showed strong fluorescence quenching upon binding Ca^{2+} ions.[26] In this sensor, photoinduced electron transfer (PET) from the donor BODIPY groups to the carbonyl group acceptors was modulated by the strong binding of Ca^{2+} to the oxygen lone pairs of the latter. Further, Ca^{2+} binding was enhanced by additional ligation of the two proximal hydroxyl groups. Probe **8** exhibited selective binding of Ca^{2+} over the other investigated alkali, alkali earth, and transition metal cations.

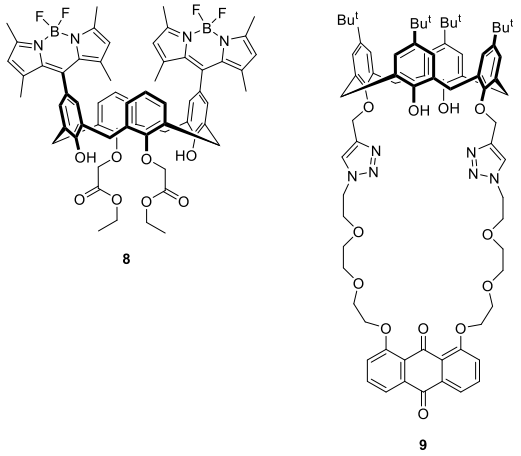

Figure 3. Structures of calixarene-based probes **8** and **9** for detection of alkali metal cations.

Li *et al*. synthesized an anthraquinone appended fluorescent calix[4]arene **9** bearing polyether chains and triazole binding units.[27] In its fluorescence spectrum, probe **9**

displayed weak emission at 510 nm in acetonitrile with small bands at 442 nm and 585 nm attributed to the Raman scattering and π-π stacking interactions. The fluorescence emission at 510 nm was greatly enhanced by the addition of Ca^{2+} ions – a phenomenon ascribed to the suppression of intramolecular PET. Thus, Ca^{2+} binding to the N atoms of each triazole withdraws electron density and increases the charge transfer from the oxygen atoms of the anthraquinone. The binding of Ca^{2+} was further supported by MALDI-TOF and the downfield shifting of the proton signal from the triazole ring in ^1H NMR spectroscopy.

2.1.3 Fluorescent sensors for transition metal ions

2.1.3.1 Detection of silver ion (Ag^+)

Silver is a useful metal that has been used in many applications in the biomedical and pharmaceutical sciences,[28] and the photographic industry. For example, in the biomedical field it has been shown to inhibit (benign) bacteria and inactivate enzymes by binding to sulfhydryl groups.[29] Consequently, accumulation of Ag^+ in the environment can cause toxicity concerns. The complexation of Ag^+ and other precious metal ions has been recently reviewed.[30]

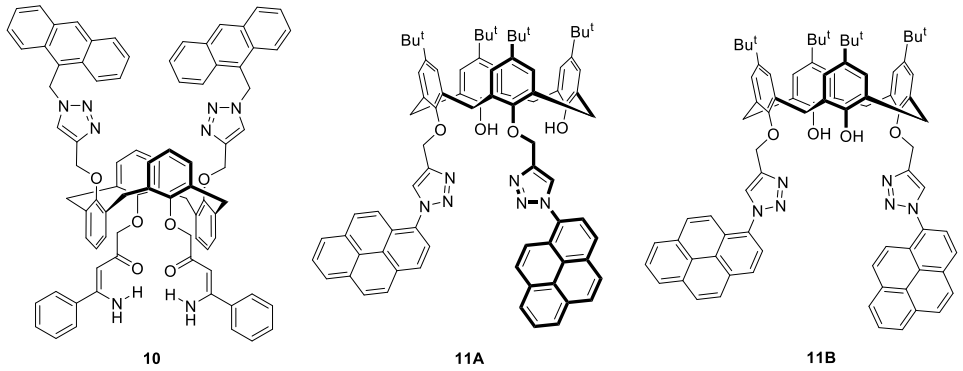

Figure 4. Structures of calixarene-based probes **10** and **11** for the detection of Ag^+ ions.

Chung *et al*. developed homo-binuclear ditopic calixarene **10** (Figure 4) bearing two binding sites of *bis*-enaminones and *bis*-triazoles for selective Ag^+ ion binding.[31] UV-Vis, fluorescence and ^1H NMR spectral analysis demonstrated that the first equivalent of Ag^+ bound at the triazole units of host **10**, exerting a positive allosteric effect for the binding of a second equivalent to the *bis*-enaminone site. No tunneling effect of Ag^+ was

observed through the 1,3-alternate calix[4]arene tube, illustrating that the strong binding of Ag^+ by the bis-triazoles and bis-enaminones sites was facilitated by cation-π interactions.

Chung *et al*. also synthesized calix[4]arene-based fluorogenic probes bearing proximal (**11A**) and distal (**11B**) triazolylpyrenes on their lower rims (Figure 4).[32] Both these probes exhibited selective binding toward Ag^+ ion over other metal ions. The positioning of the triazolylpyrenes moieties on probes **11A** and **11B** plays an important role in Ag^+ binding. Probe **11A** bearing proximal triazolylpyrene groups showed a ratiometric response toward Ag^+, whereas the distal positioning of the triazolylpyrene groups in probe **11B** led to turn-on emission changes in a MeOH–$CHCl_3$ mixed solvent. The different binding pattern of probes **11A** and **11B** toward Ag^+ was revealed by ^1H NMR titrations. Significant chemical shift of the signals from the OCH_2 and pyrene protons, along with small shift in those from the triazolyl protons, were observed for probe **11A** upon titrating with one equivalent of Ag^+. These results suggest that Ag^+ binding involves the phenoxy oxygens and triazole nitrogens of probe **11A**, and that as a result the pyrene groups moved apart, enhancing monomer emission and diminishing excimer emission. On the other hand, triazolyl protons of probe **11B** showed significant chemical shift upon binding with Ag^+ while other protons were barely shifted, suggesting only the triazole groups are involved in Ag^+ binding. This resulted in the overall enhancement of monomer and excimer emissions of probe **11B**. The binding stoichiometry of probes **11A** and **11B** with Ag^+ were found to be 1:1, with binding constants of $7.11 \times 10^3\ M^{-1}$ and $1.83 \times 10^4\ M^{-1}$ respectively. The higher binding constant of **11B** compared to **11A** toward Ag^+ was attributed to the distal positioning of the triazolylpyrenes moieties.

2.1.3.2 Detection of aluminum ion (Al^{3+})

Aluminum, the most abundant metal on the Earth's crust, has properties which have proved useful in myriad industrial applications. However, numerous health concerns have been associated with high concentration of Al^{3+} in the environment including neurotoxicity,[33] and Alzheimer's disease.[34] Thus, sensitive and selective detection of Al^{3+} using non-invasive fluorescent probes is highly desirable.

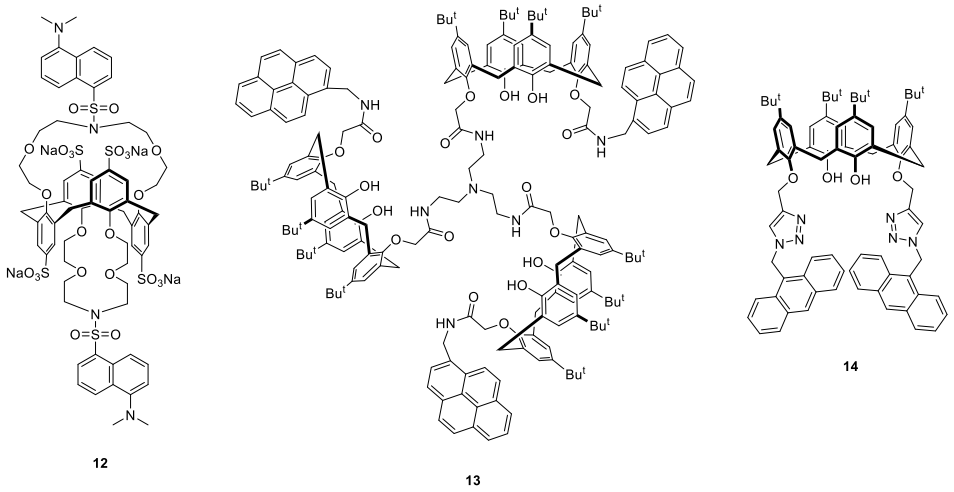

Figure 5. Structures of calixarene based probes **12** and **13** for the detection of Al^{3+} and probe **14** for Co^{2+} ions.

Leray *et al*.[35] utilized dansyl appended sulfonated calixarene **12** (Figure 5) in the 1, 3-alternate conformation for the selective detection of Al^{3+} ions. The dansyl fluorophore, which generally shows intramolecular charge transfer, exhibited aggregation-induced emission when conjugated with the sulfonated calixarene. In an aqueous system, negatively charged probe **12** showed strong complexation of Al^{3+} ions and formed large aggregates with increased anisotropy values from 0.05 to 0.23. This resulted in the inhibition of rotational diffusion rate and micro-environmental polarity. Hence ratiometric fluorescence emission was observed. Probe **12** exhibited high selectivity for Al^{3+} over the other investigated alkali, alkaline and transition metal ions.

Vicens *et al.* developed a fluorescent probe **13** (Figure 5) in which a TREN (*tris*(2-aminoethyl)amine) unit was conjugated to three calix[4]arene units bearing peripheral pyrene groups.[36] Probe **13** exhibited monomer and excimer emission in acetonitrile and showed strong binding towards Al^{3+} with significant emission changes. Thus, with the addition of 60 equivalents of Al^{3+}, excimer emission at 480 nm decreased, whilst monomer emission increased. This was attributed to the complexation of Al^{3+} with the TREN unit leading to decreased π-π interactions and decreased excimer emission. Upon further addition of Al^{3+} (500 equivalents), monomer and excimer emissions of probe **13** increased due to Chelation-Enhanced Fluorescence (CHEF).[37] Proton NMR spectroscopy indicated substantial downfield shift of TREN CH_2 protons, indicating that Al^{3+} binding involved the

nitrogen atoms of the TREN unit. The association constant (K_a) calculated using fluorescence titrations between probe **13** and Al^{3+} was found to be 8,700 M^{-1}.

2.1.3.3 Detection of cobalt (Co^{2+}) ion

Cobalt, an essential micronutrient, plays vital roles in hemoglobin synthesis and iron metabolism, and is an integral part of vitamin B_{12} (cobalamin coenzyme).[38] However, perturbed concentrations of Co^{2+} in the biochemical milieu leads to severe toxicity, retarded growth, and anemia. For sensitive detection of Co^{2+} ion, Rao *et al.* developed calix[4]arene probe **14** (Figure 5) bearing two anthracenyl units conjugated through triazole groups.[39] Among the investigated metal ions **14** revealed selective binding of Co^{2+} ions, with quenching in fluorescence emission and a detection limit of 55 ppb (0.92 μM). The binding stoichiometry was found to be 1:1, with an K_a of 4.8 ± 0.2 × 10^5 M^{-1}. The binding of Co^{2+} to probe **14** was further supported by ^1H NMR titrations, transmission electron microscopy (TEM), and atomic force microscopy (AFM) analysis. For example, an upfield shift in the anthracenyl -CH_2 group indicated the involvement of anthracene units in the binding process. Significant changes in the shape and size of probe **14** particles upon addition of Co^{2+} in TEM and AFM images supported its binding pattern. A single-armed reference compound demonstrated that the calixarene backbone was essential for the preorganized binding of Co^{2+}.

2.1.3.4 Detection of copper ion (Cu^{2+})

Copper is the third essential transition metal cation found in humans.[40] Ranging from mammals[41] to bacteria, copper has been occupied in many physiological processes controlled by metallo-enzymes.[42] However, excessive amounts of copper produce increased concentrations of reactive oxygen species (ROS) detrimental to many biological processes.[43] On the other hand, its deficiency leads to neurological[44] and hematological disorders.[45] Not surprisingly, sensitive copper detection is highly desirable.

Yang *el al*.[46] developed a salicylhydrazide-conjugated calix[4]arene probe **15** (Figure 6), for the fluorogenic detection of Cu^{2+}. Quenching in the fluorescence emission was observed upon complexation of Cu^{2+}, and this response was further increased in the presence of non-ionic surfactant Triton X-100. The double reciprocal plot between [Cu^{2+}]

and fluorescence of probe **15** gave a linear quenching relationship validating a 1:1 complexation, a binding constant of 4.9×10^5 M^{-1}, and a detection limit of 3.05 ng ml^{-1}. Probe **15** was highly selective towards Cu^{2+} in the presence of other metal ions.

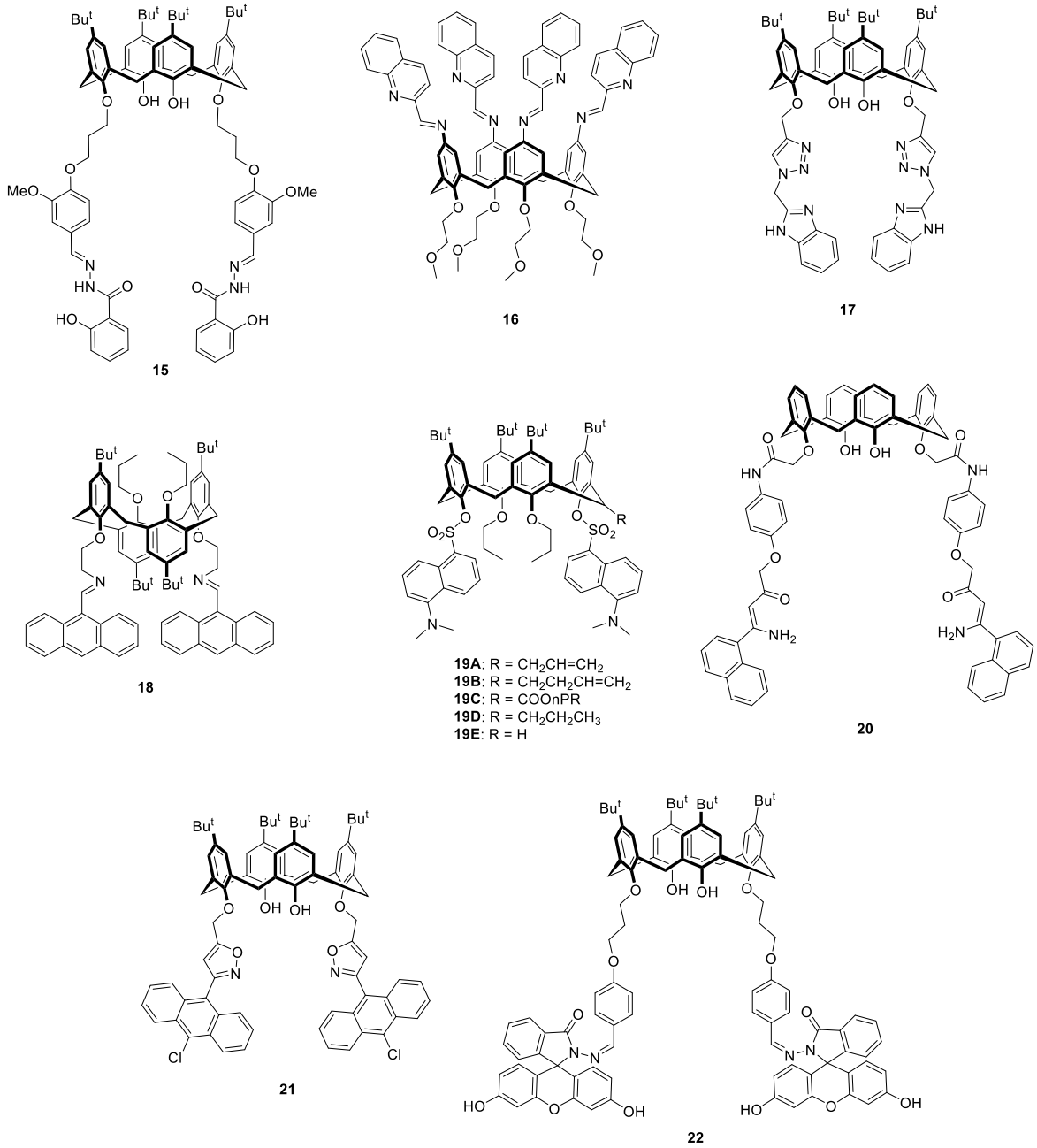

Figure 6. Structures of calixarene based probes **15-22** for the detection of Cu^{2+} ions.

Huang *et al*.[47] developed highly selective turn-on fluorescent probe **16** (Figure 6) bearing four iminoquinoline groups on the upper rim of a cone calix[4]arene. In this sensor, the iminoquinoline units play dual roles of ionophore and fluorophore. Probe **16** displayed very weak fluorescence emission at 412 nm due to PET from the lone pair of electrons of the imine nitrogens to the quinolines. Upon binding of Cu^{2+} to the lone pairs of the quinolines and the imines, a 1,200-fold enhancement in the fluorescence emission was observed. This blocking of PET was attributed to an increase in the energy of the n→π* transition of quinoline and a decrease in the energy of the π→π* transition. The binding stoichiometry of Cu^{2+} and probe **16** was 1:1, with a K_a of 3.67×10^7 M^{-1} and a detection limit of 2.71×10^{-8} M^{-1}. Probe **16** was found to be highly selective for Cu^{2+} among the investigated alkali, alkali earth, and transition metal cations.

Rao *et al.* reported a ratiometric off-on-off fluorogenic probe for Cu^{2+} in an aqueous buffer medium (MeOH–buffer, 2:1 v/v). Host **17** (Figure 6) possesses two triazoles appended benzimidazoles.[48] Two to three equivalents of Cu^{2+} lead to a decrease in the fluorescence emission of compound **17** around 311 nm and the formation of a new band around 380 nm attributed to excimer formation between the benzimidazole groups. With further addition of equivalents of Cu^{2+} excimer emission at 380 was efficiently quenched due to the paramagnetic nature of the ion. Job plot and mass analysis illustrate the formation of a di-nuclear Cu^{2+} complex with a K_a of 7.24×10^9 M^{-2}. That the complexation processes being observed were not due to adventitious Cu^{+} was confirmed by electron paramagnetic resonance. Similarly, anthracene-appended calix[4]arene probe **18** (Figure 6) showed weak fluorescence in 1:1 CH_2Cl_2–CH_3CN due to PET from its nitrogen lone pairs, and a 10-fold enhancement in fluorescence emission at 437 nm upon binding Cu^{2+} ions.[49]

Calix[4]arene derivatives **19A-E** (Figure 6) bearing two dansyl units on the lower rim and different substituents on one methylene bridge were reported to form strong complexes with Cu^{2+} ions.[50] Each dansyl unit bound one Cu^{2+} and resulted in strong fluorescence quenching of the emission at 546 nm. It was observed that the presence of substituents on the methylene bridge have little effect on the emission properties and Stokes shift of probes **19A-E** and induced only minor variation in the quantum yield.

Chung *et al.*[51] developed fluorogenic probe **20** (Figure 6) bearing bis-chelating β-amino α,β-unsaturated ketone, amide, and phenolic sites. As a result, **20** could selectively bind two Cu^{2+} ions at its lower rim. Enhanced fluorescence emissions at 431 nm (4-fold) and 452 nm (40-fold) from the naphthalene fluorophores of **20** were observed with the addition of excess Cu^{2+} ions. The overall binding constant for both events was 2.02×10^9 M^{-2}. The binding of one Cu^{2+} to the β-amino α,β-unsaturated ketone groups resulted in conformational restriction and CHEF. In contrast, the binding of a second equivalent of Cu^{2+} ion to the phenolic OH groups resulted in the formation of a new absorption band at 438 nm.[52] It was also observed by electron paramagnetic resonance (EPR) that the complexation of Cu^{2+} led to its reduction to Cu^{+}. Both the amine units and phenolic OH groups of **20** were involved in this reduction illustrated by ^1H NMR experiments. However, reduction was not complete with 12% of the original EPR signal intensity persisting.

The same group also reported fluorescent calix[4]arene **21** (Figure 6) bearing two anthracene-isoxazolyl-methyl groups for the selective binding of Cu^{2+} ions.[53] Probe **21** exhibited both structured monomer emission at 430 nm and structureless excimer emission at 511 nm – bands characteristic of the anthracene groups. Two isoxazole moieties along with the phenolic units provided appropriate and selective binding site for Cu^{2+} that resulted in the quenching of the fluorescence emission. This was attributed to either reverse PET[54] or the heavy metal effect.[55] The binding of Cu^{2+} to the oxygen atoms of the isoxazole and phenol moieties of the calix scaffold was confirmed by ^1H NMR analysis. Here, too, it was observed that the phenolic hydroxyl units of the calixarene scaffold induced the reduction of Cu^{2+} to Cu^{+}.

Chawla *et al*. reported a calix[4]arene probe **22** (Figure 6) bearing two fluorescein groups with a turn-on recognition response towards Cu^{2+} in acetonitrile.[56] Significant enhancement in the emission bands of probe **22** was observed at 460 nm and 550 nm upon 1:1 binding of Cu^{2+} ions. On the other hand, in a partial aqueous medium (CH_3CN–H_2O, 1:1, v/v) a slight quenching was tentatively attributed to the paramagnetism of Cu^{2+} or the heavy metal effect.

Comparing the structural features of probes **15** – **22**, different fluorescence outputs were observed upon complexation with Cu^{2+} ions. Fine tuning in the ligating sites, such

as imine and carbonyl groups in probe **15** or imine units in probes **16** and **18**, change the optical behavior from “quenched fluorescence due to reverse PET” to “enhanced fluorescence due to blocked PET”, respectively. On the other hand, ring opening of imine-appended fluorescein of probe **22** was observed upon Cu^{2+} binding, resulting in the fluorescence enhancement. Incorporation of triazole and imidazole groups in probe **17** resulted in the ratiometric fluorescence changes, with Cu^{2+} binding illustrating the participation of both groups in binding. Further, the participation of the hydroxyl groups of calix[4]arene scaffold was also observed along with other ligating sites in probes **20** and **21** toward Cu^{2+} binding that resulted in its reduction to Cu^{+}. Thus, these results suggest that ostensibly trivial variations in the position and type of binding sites in the fluorescent probe lead to a wide range of fluorescence output upon ion binding.

2.1.3.5 Detection of iron (Fe^{3+})

Iron is key to biological systems,[57] where it is associated with various proteins as a redox-active cofactor. Like copper, it too is associated with the formation of ROS that, in turn, are involved in lipid metabolism and cellular dysfunction.[58] Thus, the optical detection of iron at the cellular level could provide precise analysis of its concentration and its associated roles in diseases.

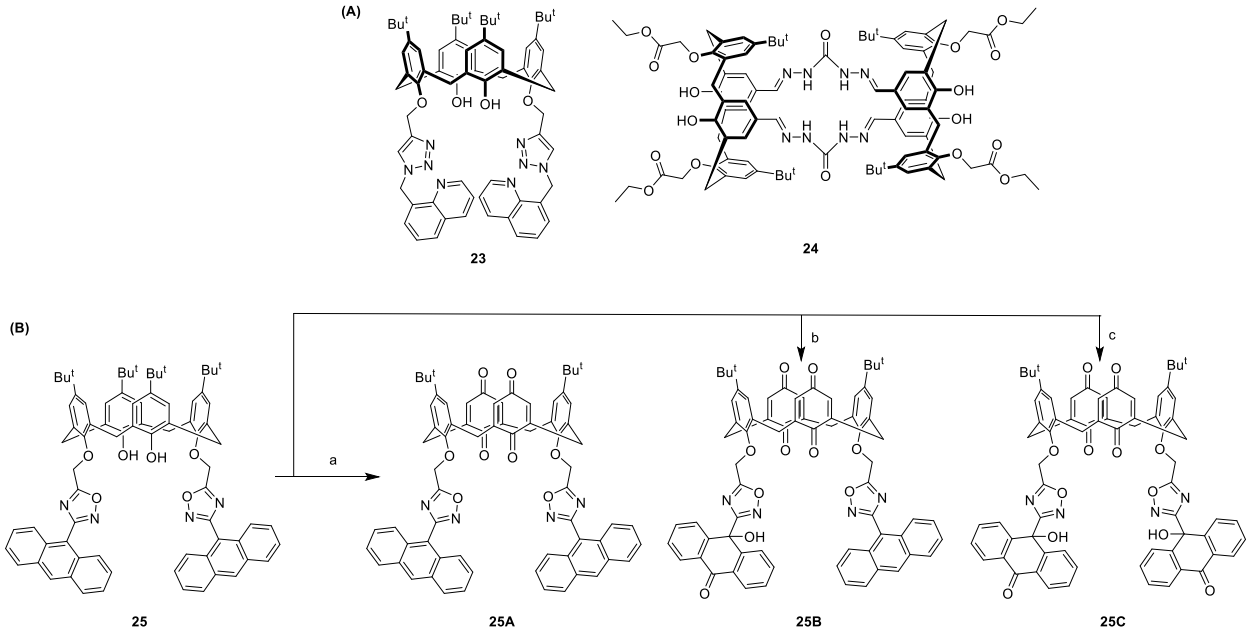

Figure 7. (A) Structures of calixarene-based probes **23** and **24** for the detection of iron. (B) Oxidative products **25A-C** of probe **25** with different equivalents of Fe^{3+} for 1 h: a) 10, b) 15, and c) 50 equivalents, respectively.

Rao *et al.* have developed optical probe **23** (Figure 7A) bearing two triazole-linked quinolines on the calix[4]arene core for the selective detection of Fe^{3+} over Fe^{2+} and other biologically important cations.[59] The binding of Fe^{3+} to probe **23** in acetonitrile resulted in an ~900-fold enhancement in emission at 418 nm. The selectivity was so high that no other tested metal ions induced any change in the emission band of the probe. As visualized by the formation of a charge transfer band at 685 nm (colorless to blue), the first equivalent of Fe^{3+} bound to the phenol groups of the probe. However, at higher equivalents, Fe^{3+} was found to form a complex with the inward-turned quinoline and triazole groups resulting in a strong enhancement in the fluorescence emission. Furthermore, this **23**·Fe^{3+} complex was used as an intracellular fluorescent agent for labelling MDA-MB-231 cells. Thus, upon incubation with **23**·Fe^{3+} overnight, MDA-MB-231 cells clearly showed blue fluorescence in the cytoplasm indicating its facile uptake.

Chawla *et al*. reported upper-rim conjugated bis-calixarene **24** (Figure 7A) using a carbohydrazine moiety as a sensitive turn-on fluorescent probe for Fe^{3+} ions.[60] Generally, probes possessing urea moieties (*vide infra*; section 2.2.2) are sensitive toward different anions. However, probe **24** with carbohydrazine units showed high selectivity for Fe^{3+}. The interactions of Fe^{3+} with probe **24** resulted in ratiometric absorption with the formation of a new band at 370 nm and decrease of absorption at 308 and 321 nm. On the other hand, an enhancement in the fluorescence emission was observed at 445 nm with Fe^{3+} ions because of its binding with the carbonyl oxygen of each carbohydrazine unit. The detection of Fe^{3+} was however limited by the cross-sensitivity for other metal ions such as Cu^{2+} and Hg^{2+}.

Chung *et al*. used a chemodosimetric approach to develop a Fe^{3+}-sensitive probe **25** (Figure 7B) bearing two 3-(anthracen-9-yl)-1,2,4-oxadiazol-5-yl moieties on the 1,3 positions at the lower rim.[61] Significant quenching in the fluorescence emission of probe **25** at 440 nm was observed upon the addition of Fe^{3+}. However, the phenol groups of **25** also allowed Cu^{2+} complexation and sensing. The authors also observed and separated the reaction products of **25** with different concentrations of Fe^{3+}. With the addition of ten equivalents of Fe^{3+}, the phenols of calix[4]arene were oxidized into di-quinone **25A**. With fifteen equivalent addition of Fe^{3+}, one anthrany unit of probe **25** was also oxidized to the

10-hydroxy-9-anthranone **25B**. Higher concentrations (50 equivalents) of Fe^{3+} fully oxidized probe **25** into **25C**. These observations were fully supported by ^{1}H NMR spectroscopy, and mass and X-ray crystallographic analyses. Hence, this approach not only allowed the selective detection of Fe^{3+}, but also provided a facile method to obtain oxidized calixarenes.

2.1.3.6 Detection of mercury ion (Hg^{2+})

Because of neurological and nephrological ill-effects, mercury is one of the most toxic metals known.[62] Consequently, its bioaccumulation is of considerable concern. There are various sources of mercury contamination including volcanic emission,[63] and multiple human activity,[64] including gold mining.[65] Widespread mercury contamination is thought to be due to its conversion from inorganic mercury to methylmercury by bacterial or chemical processes.[66] For the sensitive detection of Hg^{2+}, several optical sensors have been developed using various approaches.

Kim *et al.* reported a Förster resonance energy transfer (FRET) based fluorescent probe **26** (Figure 8) bearing two pyrene-appended calixarene units and a rhodamine B unit on a central TREN core.[67] Due to their proximity, the pyrene moieties in **26** displayed strong monomer (< 400 nm) and excimer emission (475 nm). Furthermore, the excimer emission of pyrene (as a donor) overlapping with the absorbance of the "open" form of rhodamine (as an acceptor) induced the observed FRET. Upon binding Hg^{2+}, an increase in the monomer and an excimer emission of pyrene and the rhodamine were observed. Instead of observing a decrease in the excimer emission of pyrene due to FRET to rhodamine, an increased excimer emission was observed. It was postulated that the increase of the pyrene excimer and monomer emission upon binding with Hg^{2+} was due to suppression of PET from the tertiary N atom (possessing a lone pair of electrons) to the pyrene units thereby increasing the CHEF. In the absorption spectra of **26**, a new absorption band at 555 nm was observed upon binding with Hg^{2+}, attributed to the CHEF effect, and the color of the solution changed from colorless to pink.

To build a more FRET-efficient probe, Kim *et al*. used a 1,3-alternate calixarene to develop probe **27** (Figure 8).[68] The close proximity of the two pyrene units in **27** led to strong excimer (~460 nm) and weak monomer emission (< 400 nm) upon excitation at

343 nm. Furthermore, the excimer emission band of the pyrene units significantly overlap with the absorption band of rhodamine, leading to strong FRET. Upon the titration of Hg^{2+} ion and excitation at 343 nm, the excimer emission of pyrene decreased and a new emission band at 576 nm corresponding to a ring-open rhodamine. Such ratiometric fluorescence changes in the presence of Hg^{2+} illustrate the efficient energy transfer from the pyrene excimer to the rhodamine unit of probe **27**.

Kumar *et al*. used mono-dansyl appended partial-cone calixarene **28** (Figure 8) for the selective detection of Hg^{2+}.[69] The binding of Hg^{2+} resulted in the formation of a blue-shifted absorption band at 286 nm (55 nm hypsochromic shift) and a decrease in the dansyl absorption at 340 nm attributed to the protonation of dimethylamino group. Binding also induced strong fluorescent quenching at 502 nm (λ_{ex} = 338 nm) and the formation of blue-shifted emission bands around 435 nm and 412 nm. New absorption and emission bands at 286 nm, 435 nm, and 412 nm of **28** were also observed upon protonation with trifluoroacetic acid. These results supported the idea that Hg^{2+} binding induces the intramolecular proton transfer from the phenol to the amine. Similar deprotonation of the phenolic groups of a calixarene scaffold was previously reported with lead and indium ions.[70] Probe **28** showed high selectivity for Hg^{2+} over other metal ions tested, except for Cu^{2+} which upon binding also resulted in quenching of the fluorescence emission. The different optical signals of probe **28** with Hg^{2+} and Cu^{2+} resulted in mimicking of YES and NOR molecular logic gates.

Talanova *et al.* used the di-sodium salt **29** (Figure 8) for the detection of Hg^{2+} in the presence of high concentration of Na^{+} and other relevant metal cations.[71] Thus, in the presence of Hg^{2+} ions strong fluorescence quenching at 468 nm was observed. The detection limit of **29** towards Hg^{2+} concentration was 8.0×10^{-7} M^{-1}. In contrast, the neutral (protonated) analogue showed little selectivity for Hg^{2+}.

Huang *et al*. developed an upper-rim substituted tetra-dansyl appended calix[4]arene probe **30** (Figure 8) for the selective detection of Hg^{2+} ions.[72] Strong quenching in the fluorescence emission and a hypsochromic shift of 32 nm was observed with the addition of four equivalents of Hg^{2+} to a partial aqueous solution (CH_3CN–H_2O, 1:1, v/v) of the probe. Quenching was attributed to PET, whereas the hypsochromic shift was attributed to the deprotonation of the sulfonamide NH with Hg^{2+}.[73] The four

preorganized dansyl arms formed a strong coordinating site for one equivalent of Hg^{2+} ion. The detection limit for Hg^{2+} was found to be 3.41×10^{-6} M^{-1}.

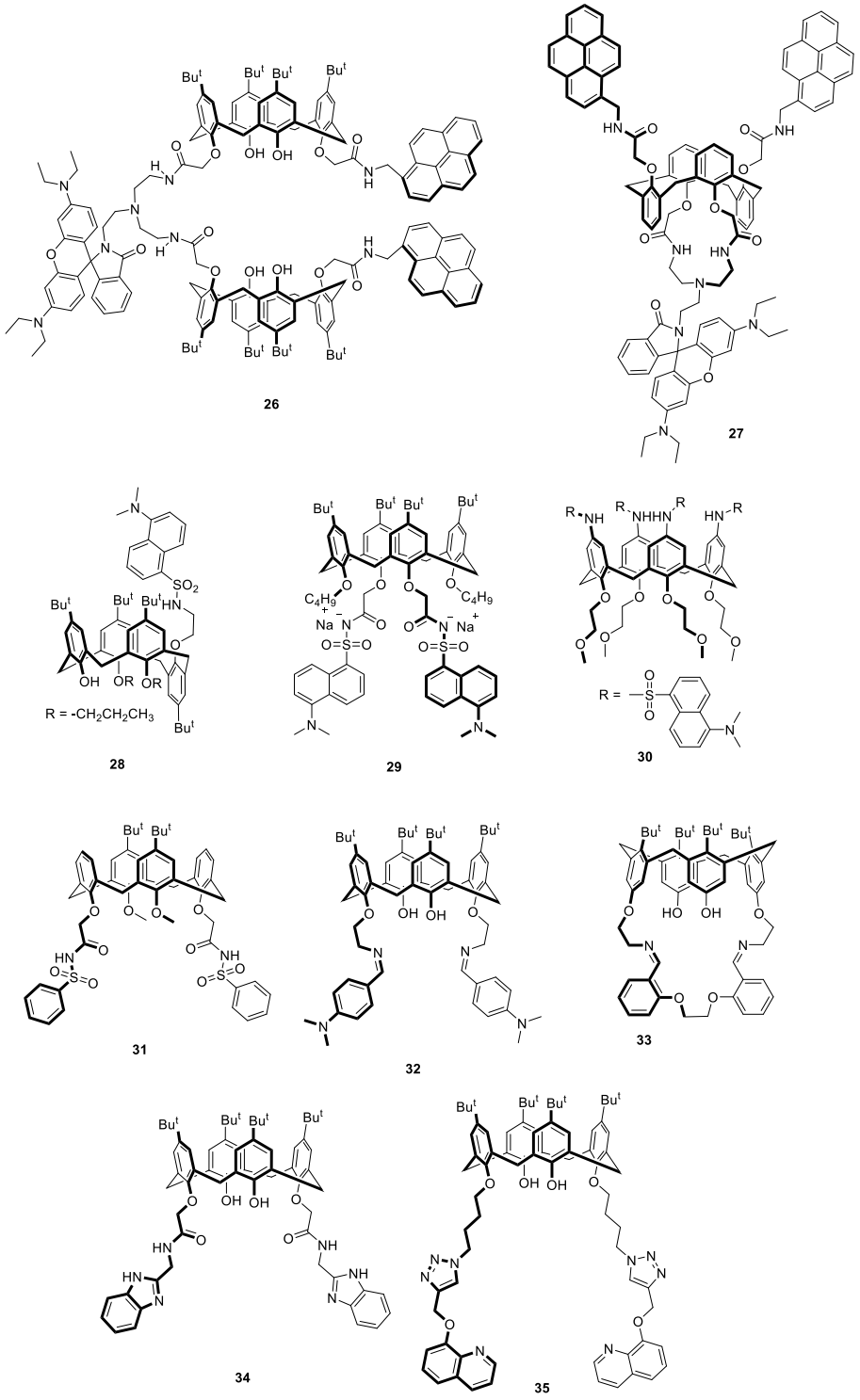

Figure 8. Structure of calixarene based probes **26-35** for detection of Hg^{2+}.

Sgarlata *et al*. reported fluorescent probe **31** (Figure 8) that selectively detects Hg^{2+} *via* the relatively acidic NH groups of the N-(phenyl)sulfonyl carboxamide side arms.[74] In CH_3CN a remarkable quenching in the fluorescence emission of probe **31** in the presence of Hg^{2+}, $Pb^{2+,}$ and Cd^{2+} occurred, resulting from the formation of multiple complex species, however, no selectivity was observed. On the other hand, upon using mixed solvents of water and CH_3CN (1:1, v/v), the Hg^{2+} selectivity of probe **31** significantly improved. With the addition of one equivalent of Hg^{2+} the fluorescence of **31** was quenched by about 70%, whereas no change was observed in the presence of Pb^{2+} or Cd^{2+}. The quenching in fluorescence of probe **31** was due to the proton displacement of the acidic sulfonyl carboxamide NH-groups upon Hg^{2+} complexation.

The fluorescent probe **32** (Figure 8), bearing dimethylaminophenyl units linked with imine units on the lower rim, showed high turn-on selectivity for Hg^{2+}.[75] It was shown that Hg^{2+} ions complex with the nitrogen atoms of the imine units, increasing their electron-withdrawing ability and leading to enhanced ICT and consequently an enhanced emission band at 444 nm. The lowest limit of Hg^{2+} detection was found to be 70 nM; low enough for utilization in many biological and environmental applications.

Rao *et al*. reported that salicylidene-di-capped calix[4]arene conjugate **33** (Figure 8) underwent turn-on fluorescence in the presence of Hg^{2+}.[76] The binding of Hg^{2+} resulted in the enhancement of emission at ~310 nm, attributed to coordination to the four phenolic oxygens and the imine units. DFT studies show that the binding of Hg^{2+} led to a complex with a distorted square pyramidal geometry.

The same group have also used pendent 1,3-dibenzimidazoles at the lower rim of a calixarene scaffold (**34**, Figure 8) for the selective detection of Hg^{2+} in aqueous mixtures.[77] Thus, in an equimolar mixture of H_2O and CH_3CN **34** exhibited strong and selective complexation of Hg^{2+}. The selectivity of probe **34** changed from Hg^{2+} to Cu^{2+} upon changing the water-acetonitrile ratio, under the optimal 1:1 solvent ratio strong quenching in the fluorescence emission of **34** was observed upon binding with Hg^{2+} in the presence of other competitive metal ions.

Another calixarene, probe **35** (Figure 8) bearing two 8-oxyquinoline subunits conjugated by triazole linkers, showed strong PET quenching upon binding with Hg^{2+} ions

$CH_3CN–H_2O$ (3:1, v/v).[78] The quenching in emission was attributed to binding through the two 8-oxyquinoline and two triazole units.

These results show a complex relationship between the fluorescence outcome of Hg^{2+} binding and the type of ligating sites and fluorophore present in the probe. Probes **26** and **27** bearing rhodamine B on a TREN core and pyrenes showed enhanced fluorescence emission upon binding with Hg^{2+} due to the ring-opening of the spirolactam and causing FRET between the excimer emission of pyrene and the rhodamine B. The fluorescence enhancement was also observed for **32** and **33**, but in this case it was due to enhanced ICT upon binding Hg^{2+} to the imine groups. On the other hand, replacing the binding sites from spirolactam/imine units to sulfonamide/hydroxy group, and fluorophore from rhodamine/ pyrene to dansyl on the calix[4]arene altered the fluorescence outcome of probes **28** and **30**. Probes **28** and **30** bearing dansyl moieties exhibited deprotonation of phenolic hydroxyl group and sulfonamide group respectively in the presence of Hg^{2+}, resulting in ratiometric fluorescence emission. Probe **31** also showed deprotonation of sulfonamide group with Hg^{2+} but resulted in quenched fluorescence emission due to PET. In contrast to probes **28** and **30**, probe **29** complexes Hg^{2+} through its two carbonyl- and four phenolic oxygen atoms. While, probes **34** and **35** containing 1,3-dibenzimidazoles and 8-oxyquinoline units, respectively showed involvement of their N atoms for the complexation of Hg^{2+} ions resulting in PET quenching. In totality, these results demonstrate that the relationship between the fluorescence outputs and the ligating sites, type of fluorophore, and conformation of calix[4]arene is complex and still not fully understood.

2.1.3.7 Detection of lead ion (Pb^{2+})

The toxicity of lead has been appreciated for at least the past two thousand years.[79] Lead ion can accumulation in soft tissues and affect digestion, development, and cardiovascular diseases.[80] However, its persistent use in the automotive industry (gasoline) and in batteries and pigments, as well as its emission from coal-fired power stations, has led to a very significant environment presence.[81] According to current regulations, the concentration of Pb^{2+} should not exceed 10 mg L^{-1} (equivalent to ~10

ppb).[82] Thus, the highly sensitive and selective detection of Pb^{2+} is of the utmost importance.

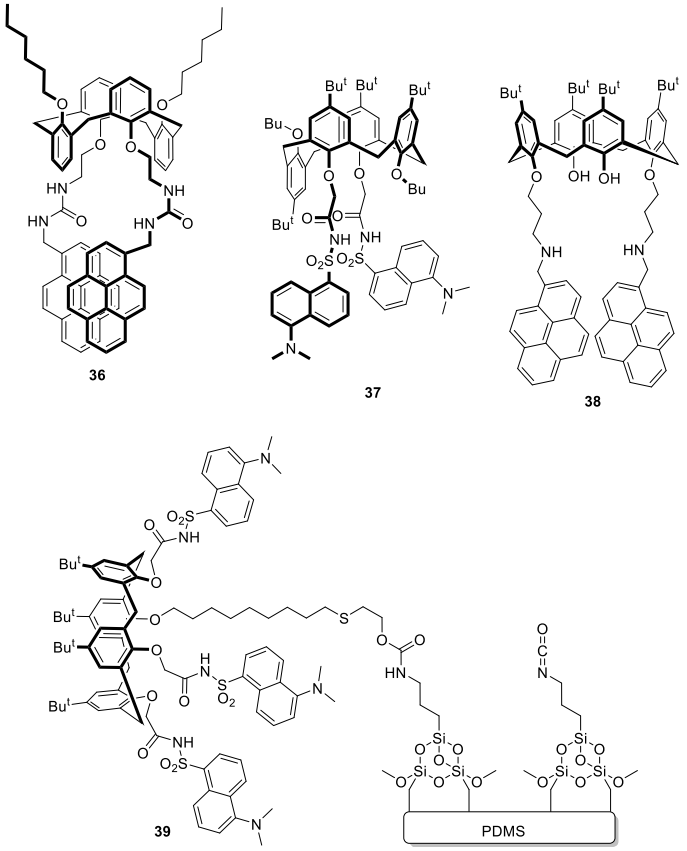

Figure 9. Structure of calixarene based probes **36-39** for detection of Pb^{2+}.

Nam *et al*. reported a pyrene appended fluorescent calixarene probe **36** (Figure 9) for the selective detection of Pb^{2+}.[83] Probe **36** showed strong excimer emission at 475 nm and weak monomer emission at 375 nm, signifying that the two pyrene units are in close proximity to one another. Upon addition of Pb^{2+}, a significant quenching in excimer and monomer emissions was observed. Monomer quenching was attributed to reverse PET from the pyrene units to the oxygen atoms of the urea moiety binding Pb^{2+}, whilst the decrease in excimer emission was attributed to the conformational changes of the pyrene arm upon Pb^{2+} binding. It was observed that addition of F^- led to the formation of PbF_2 and the reestablishment of monomer and excimer emission.

To further enhance the selectivity for Pb^{2+} over other metal ions, Talanova *et al*. utilized the partial cone conformation of calix[4]arene and incorporated two dansyl amide units in probe **37** (Figure 9).[84] The preorganized nature of probe **37** provided the

appropriate cavity for the selective binding of Pb^{2+}. At pH 4.0 the host formed a 1:1 complex with Pb^{2+} in MeCN-H_2O (1:1 v/v), and an enhanced fluorescence emission at 496 nm was observed due to the deprotonation of the dansylcarboxamide N–H. The fluorescence titrations of probe **37** allowed very low-level detection of Pb^{2+} (2.5 ppb), without any significant interference from other tested metal cations.

Yilmazz *et al.* reported another pyrene-appended calixarene probe **38** (Figure 9) bearing amine groups for the detection of Pb^{2+} and Cu^{2+} in CH_3CN–CH_2Cl_2 (1:1 v/v).[85] Significant quenching in monomer and excimer emissions were found with the addition of Pb^{2+} and Cu^{2+} ions, attributed to reverse PET and/or the heavy metal ion effect.

To evaluate the applicability of the above for lead detection, Leray *et al*. developed a fluorescent calixarene probe **39** (Figure 9) bearing three dansyl units grafted onto a polydimethylsiloxane (PDMS) microfluidics chip.[86] In CH_3CN–H_2O (3:2, v/v), free probe **39** showed strong fluorescent emission band at 572 nm upon excitation at 347 nm. Upon interacting with Pb^{2+} ions, a hypsochromic shift from 572 nm to 520 nm was observed in the emission spectrum of probe **39** attributed to the deprotonation of the sulfonamide N–H proton. The association constant for 1:1 complexation was found to be log (K_{11}) = 4.74. Upon grafting to the PDMS matrix the fluorescence intensity of the probe with Pb^{2+} was lower. However, the probe still showed excellent selectivity for Pb^{2+} against competitive metal ions, and a detection limit of 42 ppb.

2.1.3.8 Detection of zinc ion (Zn^{2+})

Zn^{2+} is an important micronutrient in humans whose deficiency may cause severe metabolic and developmental detriments.[87] The concentration of Zn^{2+} in the blood serum is approximately 19 μM, and deviation from this concentration is associated with various disorders including Alzheimer's disease, hyperalgesia, and diabetes.[88]

Rao *et al.* developed a triazole appended calixarene probe **40** (Figure 10) for the selective detection of Zn^{2+} in solution and in blood serum.[89] Probe **40** displayed very weak fluorescence at 450 nm (λ_{ex} = 380 nm) in H_2O–MeOH (1:4 v/v) at pH 7.4. Upon titration with Zn^{2+}, an enhanced fluorescence emission at 450 nm with a tenfold increase in quantum yield from 0.028 to 0.32 was observed. The binding constant for this 1:1 event was $1.49 \times 10^5\ M^{-1}$. The *in-situ* prepared complex **40**–Zn^{2+} was tested against blood

proteins such as human serum albumin (HSA), bovine serum albumin (BSA), and α-lactalbumin (LA) and serum, and no significant fluorescence change was observed. The detection limit of probe **40** for the Zn^{2+} in blood serum was found to be 332 ppb.

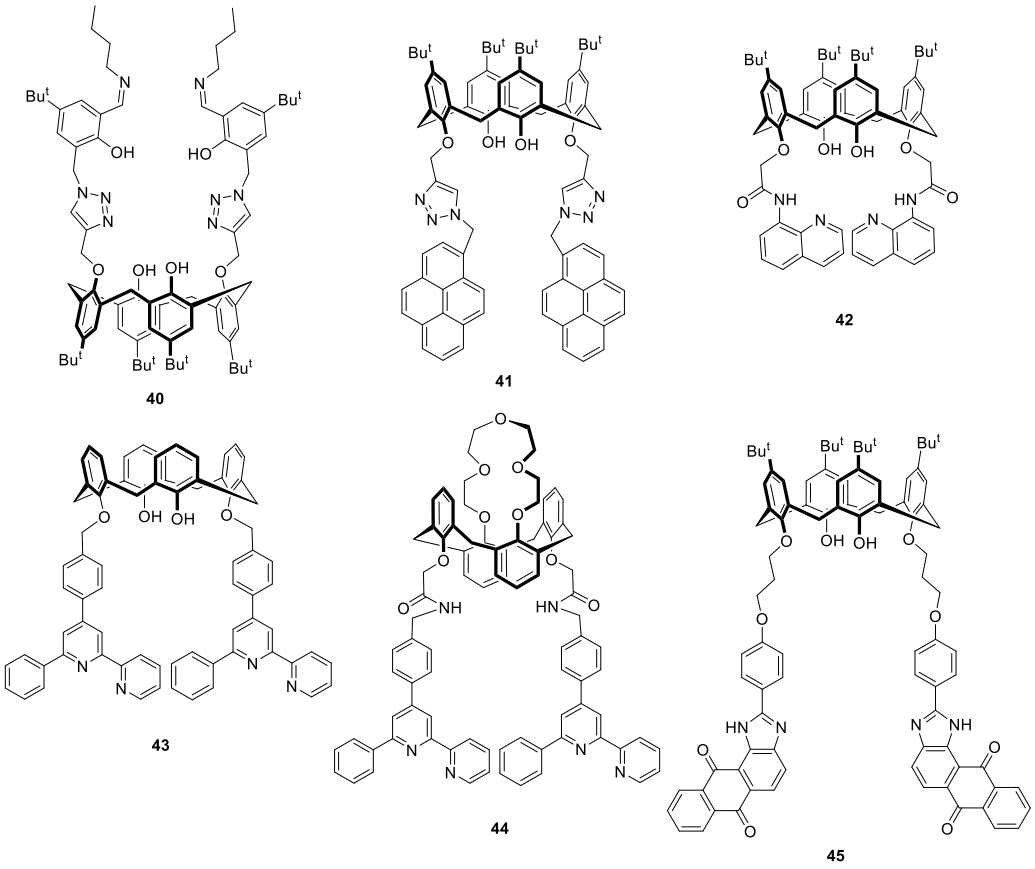

Figure 10. Structure of calixarene based probes **40-45** for detection of Zn^{2+}.

Zhu *et al*. reported another probe containing triazole-linked pyrene moieties, **41** (Figure 10), for the ratiometric detection of Zn^{2+}. Probe **41** showed weak monomer emission and strong excimer emission indicating a face-to-face overlap of the two pyrene units. Monomer emission was enhanced and excimer emission quenched upon binding Zn^{2+}, whilst with other metal cations, specially Cu^{2+} and Hg^{2+} ions, strong quenching in both monomer and excimer was observed.[90] ^1H NMR studies indicated that this ratiometric emission behavior arose *via* binding with the triazole nitrogen atoms of the host. On the other hand, quenching with Cu^{2+} and Hg^{2+} was due to their binding with both the triazole nitrogens and the phenol oxygen atoms of the calixarene. This resulted in reverse PET from the pyrene to the nitrogen atoms. The different optical outputs of probe

41 with Zn^{2+} (ratiometric) and Cu^{2+} (quenching) was utilized to mimic "inhibition" (INH) and "joint denial" (NOR) logic gates.

Kim *et al*. also reported on the same calixarene probe **41** (Figure 10) for the ratiometric detection of Zn^{2+} and Cd^{2+} ions.[91] With the addition of Zn^{2+} and Cd^{2+} ions to a solution of **41**, a ratiometric response with an increase in monomer emission and a decrease in excimer emission was observed. In contrast, other metal ions tested led to strong quenching in both monomer and excimer emission.

Rao *et al.* synthesized carboxamidoquinoline probe **42** (Figure 10) for the ratiometric detection of Zn^{2+}.[92] Upon excitation at 320 nm, probe **42** displayed a fluorescence emission at 410 nm in MeOH. Binding of Zn^{2+} led to a decrease in emission at 410 nm and a formation of new band at 490 nm. The 9-fold ratiometric enhancement of probe **42** was only observed with Zn^{2+}, with a detection limit of 183 ppb and a fluorescent color change to green. Studies with other metal ions demonstrated the selectivity of **42** towards Zn^{2+}. DFT calculations suggested the distorted tetrahedral geometry of Zn^{2+} in the core of four N atoms of **42**. Zinc ion binding was also investigated by AFM and TEM. AFM revealed that the observed spherical particles of **42** changed to elongated topologies upon binding with Zn^{2+}. TEM studies also supported the transformation of spherically shaped particles into Koosh nano-flowers upon binding Zn^{2+} ion.

Kim *et al*. developed two fluorescent probes **43** and **44** (Figure 10) bearing bipyridine moieties on the lower rim of a cone, and 1,3-alternate calix respectively.[93] In acetonitrile both probes showed enhanced binding of Zn^{2+} against a range of potential metal cations competitors. Absorption and fluorescence titrations of **43** and **44** with Zn^{2+} showed ratiometric changes in their spectra. With Zn^{2+}, a decrease in absorption at 260 nm and the formation of a band at 282 nm were observed for both probes **43** and **44**. In the fluorescence spectra of probe **43**, the emission band at 363 nm decreased and a new emission band at 408 nm formed upon addition of Zn^{2+}. Similarly, ratiometric changes with a decrease in emission at 356 nm and a new band at 414 nm was found for probe **44** with Zn^{2+}. These changes in the fluorescence and absorption spectra were attributed to ICT. Insignificant changes were also observed in the presence of other metal ions. The stoichiometry of probes **43** and **44** with Zn^{2+} were evaluated to be 1:2, with K_a values of 218 M^{-2} and 492 M^{-2}, respectively.

Chawla *et al*. reported anthraquinone-appended calixarene probe **45** (Figure 10) for Zn^{2+} detection.[94] Probe **45** exhibited strong emission at 565 nm upon excitation at 420 nm in 1:4 $CHCl_3$–CH_3CN (v/v). In the presence of Zn^{2+} a 1:1 complex was formed, and strong quenching occurred. In contrast, no change in fluorescence emission was found with other metal ions, including Cd^{2+}, indicating that the probe was highly selective for Zn^{2+}.

2.2 Fluorescent receptors for anions

Anions are ubiquitous and play significant roles in many biological processes required for sustaining life, for example in energy production, cell signaling, and homeostasis.[95,96] Unsurprisingly, imbalances in intracellular anion concentration are implicated in many disorders including cystic fibrosis and amyloid-related diseases.[97,98] Anions also potentially pose a grave threat to human life in many other ways. Naturally occurring anions such as toxic arsenate are a problem in many parts of the world, and long-term exposure to these have been associated with increased risks of diabetes, skin diseases, hypertension, and various types of cancer.[99,100] Similarly, naturally occurring phosphate and sulfate anions have been found to cause renal failure in humans, whilst anthropogenic anions such as pertechnetate (a by-product of nuclear fuel reprocessing) and perchlorate (arising from explosives manufacturing) are also of considerable environmental concern.[101,102] Increasing awareness of these issues has resulted in greater efforts to develop synthetic receptors for determining and monitoring anion levels. Designing artificial fluorescent probes for anions is, however, more demanding than designing hosts for cations and neutral species since monovalent anions tend to have higher free-energies of solvation than monovalent cations, lower charge densities, and strong pH dependence.[103] This section outlines recent progress made in anion recognition and sensing using fluorescent calixarenes. Table 2 lists the binding stoichiometries, binding constants, and detection limits for various anions binding to calixarene-based probes.

2.2.1 Detection of fluoride ion (F^-)

Fluoride (F^-) has received considerable attention because of its benefits to dental health[104] and for its administration in the treatment of osteoporosis.[105,106] Conversely, however, excessive accumulation of this anion in the body can lead to dental or even skeletal fluorosis[107,108] and nephrological problems.[109] For the selective recognition of this anion, various calixarene derivatives bearing upper or lower rims decorated with suitable recognition moieties such as amine and amide groups have been reported.

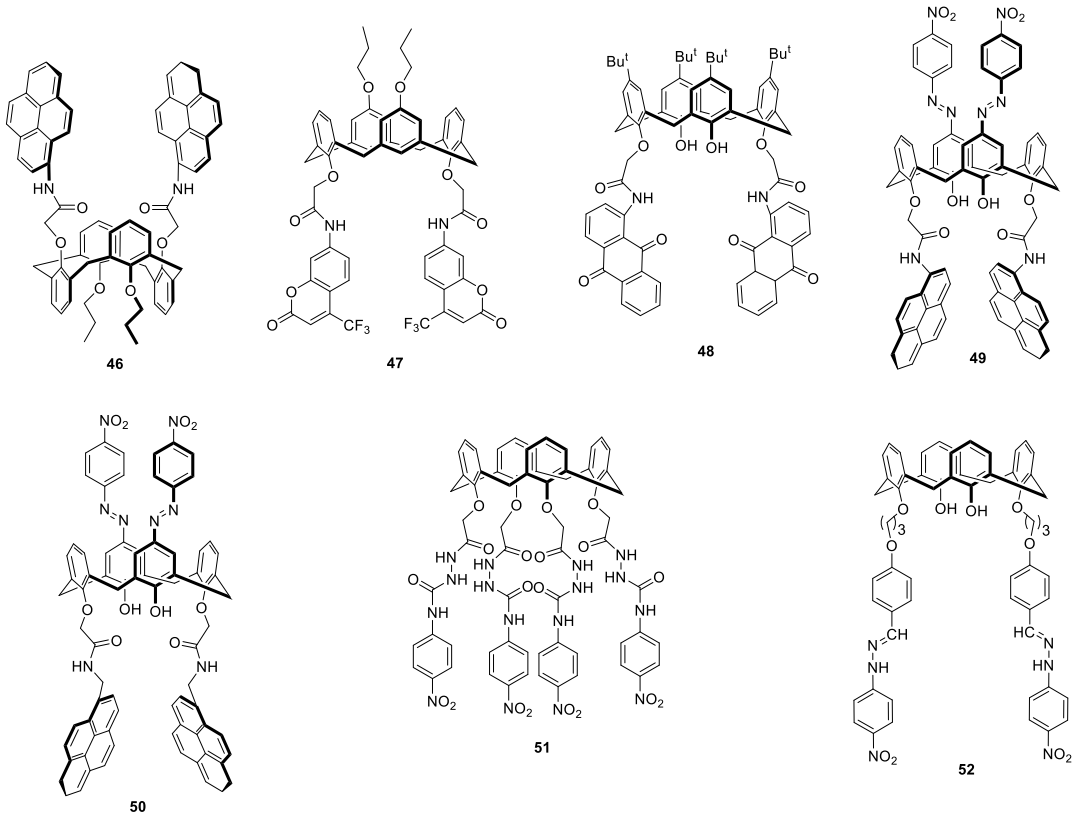

Figure 11. Molecular structures of fluoride (F^-)-selective chemosensors **46-52**.

Kim *et al*.[110] reported photo-induced charge transfer (PCT) chemosensor **46** (Figure 11) possesing pyrene signaling subunits appended to a calixarene framework through anion-recognizing amide groups. ^{1}H NMR spectroscopy revealed that the addition of F^- to **46** led to hydrogen bonding with the amide -NH- groups, and at higher equivalents, deprotonation and delocalization of electrons from the anionic nitrogen atoms to the pyrene moiety. NMR spectroscopy studies implicate PCT in the recognition process.[111-

[113] The selectivity of **46** towards F^- ion was demonstrated using UV-Vis and fluorescence spectroscopy. The absorption band was significantly red-shifted from 346 to 400 nm in the presence of F^-, with a concomitant color transition from colorless to yellow. Upon excitation at 346 nm, **46** exhibited monomer and excimer emissions at 385 and 482 nm respectively. However, complexation of F^- ions caused quenching of the monomer emission whilst excimer emission showed enhancement with a slight hypsochromic shift of 12 nm. This hypsochromically-shifted band was attributed to static excimer formation based on excitation spectra and DFT calculations.[114] No significant response was observed with any other anions tested.

Another PCT-based chemosensor **47** (Figure 11) by the same author[115] was designed by replacing the pyrene moieties of **46** with coumarin units. The selective interaction of **47** with F^- over other anions was confirmed by following the changes in the spectral behavior of the coumarin moiety. Upon titration with F^-, the band at 335 nm corresponding to the absorption of the coumarin decreased and moved to a shorter wavelength. A new band at 408 nm, attributable to deprotonation of the NH group by F^- ions, also appeared. The fluorescence quenching of **47** (λ_{ex} = 335 nm, λ_{em} = 420 nm) upon titrating with F^- was ascribed to a PET process[116-118] involving electron transfer from the deprotonated amide groups to the coumarins.

With the aim of extending their studies, Kim *et al*.[119] further reported *p-tert*-butylcalix[4]arene **48** (Figure 11) substituted with two amido-anthraquinone groups (AAQ) at the lower rim as a chemosensor for F^-. Upon gradual addition of F^-, the spectrum of **48** showed a decrease of the absorption band at 405 nm and the concomitant formation of a bathochromically-shifted band at 510 nm, mainly ascribed to an ICT process caused by F^--induced deprotonation of the amide groups.[120] Excitation of probe **48** at 455 nm gave two bands at 527 nm and 560 nm corresponding to normal and tautomer emissions, respectively, arising from excited state intramolecular proton transfer (ESIPT). In the presence of F^-, a significant enhancement in the normal emission was observed accompanied by a slight change in tautomer emission, indicating that ESIPT was inhibited by the presence of F^-.

In another investigation, Kim *et al*.[121] reported bifunctional (fluorogenic and chromogenic) calix[4]arene probes **49** and **50** (Figure 11). The 4-nitrophenylazo groups

of these sensors were introduced as chromogenic moieties[122] to affect the naked-eye detection of F^- ions. Probe **49** showed a characteristic fluorescence band at 480 nm originating from the excimer formed by the pyrene moieties. However, probe **50** did not exhibit an analogous excimer emission band. The reason for this difference was attributed to the methylene spacer between the pyrene moiety and amide group in **50** reducing the extent of excimer formation. This was supported by DFT calculations wherein the optimized structures showed that the pyrene moieties were orthogonal to one other. Probe **50** displayed a very drastic change in the absorption spectra upon F^- binding, namely a strong bathochromically-shifted band and a color change from yellow to blue. While **49** showed small red shift of 54 nm with F^-. In the fluorescence spectra, probe **49** showed quenching in excimer emission at 480 nm with 300 equivalents of F^- due to PET from F^- to pyrene units. With further addition of F^-, a new emission band at 460 nm, as static excimer, was observed attributed to the H-bonding between amide NH proton and F^-.

A related example is **51** (Figure 11) wherein four semicarbazide groups as anion recognition moieties were attached to the calix[4]arene scaffold.[123] Probe **51** exhibited a strong band at 335 nm which was ascribed to an ICT process induced by the electron withdrawing 4-nitrophenyl moieties. In the presence of F^- however, this band decreased in intensity and underwent a concomitant bathochromic shift attributed to hydrogen bonding interactions between an anion and the NH groups of the semicarbazides. The addition of higher equivalents of F^- led to the deprotonation of NH groups.[124,125] This resulted in a significant perturbation of the ICT process which was also reflected in a color change from colorless to dark red. Another example of the colorimetric detection of F^- ions is probe **52** (Figure 11), in which the lower rim of a calix[4]arene scaffold was decorated with hydrazone functionalities on the distal (1,3-) positions.[126]

These results reveal that a common motif for the recognition of F^- are weakly acidic amide or amide-like N–H amide groups. The spectroscopic response to anion recognition can occur via conformational changes induced by hydrogen bonding, or by deprotonation of the amide NH proton. The fluorescence outcome of F^- binding depends upon: a) the spacer length between an amide NH and fluorophore; b) type of fluorophore; and c) type

of calix[4]arene conformation. Furthermore, naked-eye detection of F^- can be performed by incorporating 4-nitrophenylazo groups into the calix[4]arene scaffold.

Table 2. Various fluorescent receptors **46**-**64** and their binding stoichiometries and constants, and detection limits toward various anions.

Probe number (L)	Guest species (G)	Stoichiometry ratio (L:G)	Binding constant	Detection limit	Reference
46	F^-	1:1	$K = 2.5 \times 10^2\ M^{-1}$ [b]	- [c]	110
47	F^-	1:1	$K = 1.08 \times 10^4\ M^{-1}$ [b]	- [c]	115
48	F^-	1:1	$K = 279\ M^{-1}$ [b]	- [c]	119
49	F^-	- [c]	- [c]	- [c]	121
50	F^-	- [c]	- [c]	- [c]	121
51	F^-	1:1	log K = 5.68 [b]	- [c]	123
		1:2	log K = 4.79 [b]		
52	F^-	1:1	$K = 9.9 \times 10^6$ [a]	- [c]	126
53	Cl^-	1:1	$K = 2.4 \times 10^4\ M^{-1}$ [b]	8 μM	127
54A	I^-	1:1	$K = 1.49 \times 10^4\ M^{-1}$ [b]	1.81 ppm	128
54B	I^-	1:1	$K = 1.79 \times 10^4\ M^{-1}$ [b]	0.23 ppm	128
54C	I^-	1:1	$K = 2.01 \times 10^4\ M^{-1}$ [b]	0.22 ppm	128
55	HSO_4^-	- [c]	$K = 2.0 \times 10^4\ M^{-1}$ [b]	- [c]	131
56	F^-	1:1	log K = 3.87 [b]	- [c]	132
		1:4	log K = 21.2 [b]		
	CH_3COO^-	1:1	$K = 4.6 \times 10^5\ M^{-1}$ [b]		
	$H_2PO_4^-$	1:1	log K = 3.16 [b]		
		1:4	log K = 18.3 [b]		
	$PhCOO^-$	1:1	$K = 3.9 \times 10^4\ M^{-1}$ [b]		
57	D-*N*-Boc-Ala	1:1	$K = 53.56\ M^{-1}$ [b]	- [c]	133
58	D-mandelate	1:1	$K = 1.04 \times 10^3\ M^{-1}$ [b]	- [c]	
59	L-phenylalaninol	1:1	$K = 25\ M^{-1}$ [b]	- [c]	
	D-phenylalaninol	1:1	$K = 124\ M^{-1}$ [b]		
60A	R-phenylglycinol	1:1	$K = 88.5\ M^{-1}$ [b]	- [c]	134
60B	R-phenylglycinol	1:1	$K = 110.8\ M^{-1}$ [b]	- [c]	
60C	R-phenylglycinol	1:1	$K = 145.7\ M^{-1}$ [b]	- [c]	
60D	R-phenylglycinol	1:1	$K = 564.5\ M^{-1}$ [b]	- [c]	
61	Citrate	1:1	$K = 4200\ M^{-1}$ [b]	- [c]	137

62	Aspartic acid	1:1	K = 6.44 × 10^4 M^{-1} [b]	- [c]	142
	Glutamic acid	1:1	K = 3.88 × 10^4 M^{-1} [b]	- [c]	
63A	Tryptophan	1:1	- [c]	1 μM	143
64	ATP	1:1	K = 40000 M^{-1} [b]	2.34 μM	147
	UTP	1:1	K = 21665 M^{-1} [b]	4.26 μM	
	CTP	1:1	K = 19000 M^{-1} [b]	4.35 μM	
	TTP	1:1	K = 17000 M^{-1} [b]	6.34 μM	
	GTP	1:1	K = 9316 M^{-1} [b]	13.4 μM	

[a] Calculated using spectrophotometric titrations, [b] fluorescence titrations, [c] not reported by the original article.

2.2.2 Detection of chloride (Cl^-), iodide (I^-) and hydrogen sulfate (HSO_4^-) ions

Diamond *et al*.[127] reported compound **53** (Figure 12), decorated with urea linked pyrene units whose orientation relative to each other changes with Cl^- inclusion. Compound **53** showed a strong excimer emission and a weak monomer emission in MeCN–$CHCl_3$ (95:5, v/v). The addition of Cl^- exclusively lead to a ratiometric fluorescence change with a sharp decline in excimer emission and a corresponding increase in monomer emission. These results suggested that Cl^- ions selectively coordinated with the urea protons, thereby reducing the extent of the pyrene units π-π stacking (excimer emission) and promoting monomer emission. The binding of **53** with Cl^- was further supported by the downfield shift of the signals from the urea protons in NMR titration studies. From the ratio of excimer to monomer, the K_a for Cl^- was found to be 2.4 × 10^4 M^{-1}.

Saitz *et al*.[128] reported a series of calix[4]arenes **54A-C** (Figure 12**)** bearing benzothiazole, benzoxazole, and benzoimidazole groups for detection of iodide ions (I^-). All the three derivatives displayed selective fluorescence responses to I^- in MeOH. No significant response was observed even with titration with F^- ions, which can readily deprotonate thiourea and amide groups.[129,130] The rationale for this observation was that F^- is too small to effect cooperative binding with the sidearms of the calixarene. Derivatives **54A**-**C** were found to have detection limits of 1.81 ppm, 0.23 ppm, and 0.22 ppm respectively. Considering their binding constants, however, **54C** (K_a = 2.01 × 10^{-4} M^{-1}) was found to be most suitable candidate among the three. NMR spectroscopy titration studies of compound **54C** with I^- showed a significant upfield shift of amide NH proton, clearly depicting the involvement of the amide groups in complex formation.

In 2009, Nam *et al*.[131] reported pyrene-appended calix[4]arene derivative **55** (Figure 12) for the selective fluorescence detection of tetrahedral HSO_4^- ion. Probe **55** exhibited weak monomer emission at 375 nm and strong excimer emission at 475 nm, pointing to strong π-π stacking of the pyrene moieties. However, in the presence of HSO_4^- ions these bands changed ratiometrically with an enhancement of monomer emission and a quenching of excimer emission. These results suggested that HSO_4^- ions selectively coordinate with urea NH groups in the cavity of probe **55** and inhibited efficient π-π stacking between pyrene units. Thus, depending upon the conformation of calix[4]arene, the nature of the appended ligating urea moieties, and the degree of cooperative binding, either Cl^-(1,3-alternate probe **53**) or HSO_4^- (cone conformation **55**) can be targeted.

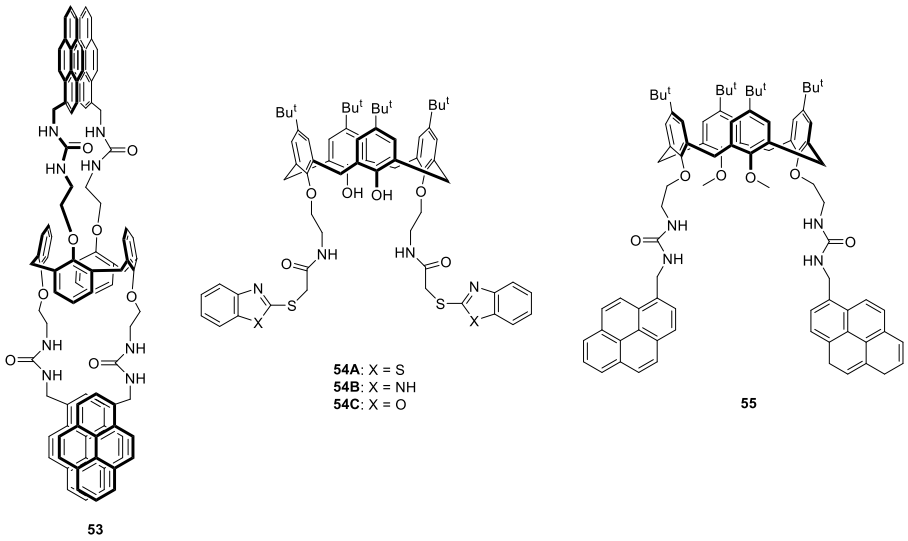

Figure 12. Calixarene-based chemosensors **53** for Cl^-, **54A-C** for I^- ions, and **55** for HSO_4^-.

2.2.3 Detection of carboxylate anions ($RCOO^-$)

Shuang *et al*.[132] reported *tetrakis*-(4-carbamoylphenyl)-substituted calix[4]arene **56** (Figure 13) with chelating carbamate groups as a fluorescent sensor for carboxylates ($RCOO^-$). Probe **56** displayed differential fluorescence quenching in the presence of $RCOO^-$ depending on the nature of the R group. For example, the addition of $RCOO^-$ to a MeCN solution of probe **56** led to a sequential decrease in the fluorescence band centered at 350 nm with a slight hypsochromic shift. In contrast, the addition of a small excess of F^- or $H_2PO_4^-$ led to greater fluorescence quenching, suggesting that the binding mode of these anions to **56** is different. Job plot analyses indicated that at low anion

concentrations, probe **56** initially formed 1:1 complexes with F^- or $H_2PO_4^-$, whereas at high concentrations a 1:4 complex predominated. However, only 1:1 binding was observed at all concentrations of acetate (AcO^-) and benzoate (BzO^-). The K_a values for the binding of AcO^- and BzO^- were found to be 4.6×10^5 M^{-1} and 3.9×10^4 M^{-1} respectively. The greatly enhanced binding affinity and selectivity of probe **56** towards $RCOO^-$ was attributed to hydrogen bonding interactions between $RCOO^-$ and two opposite -NH- groups of carbamates.

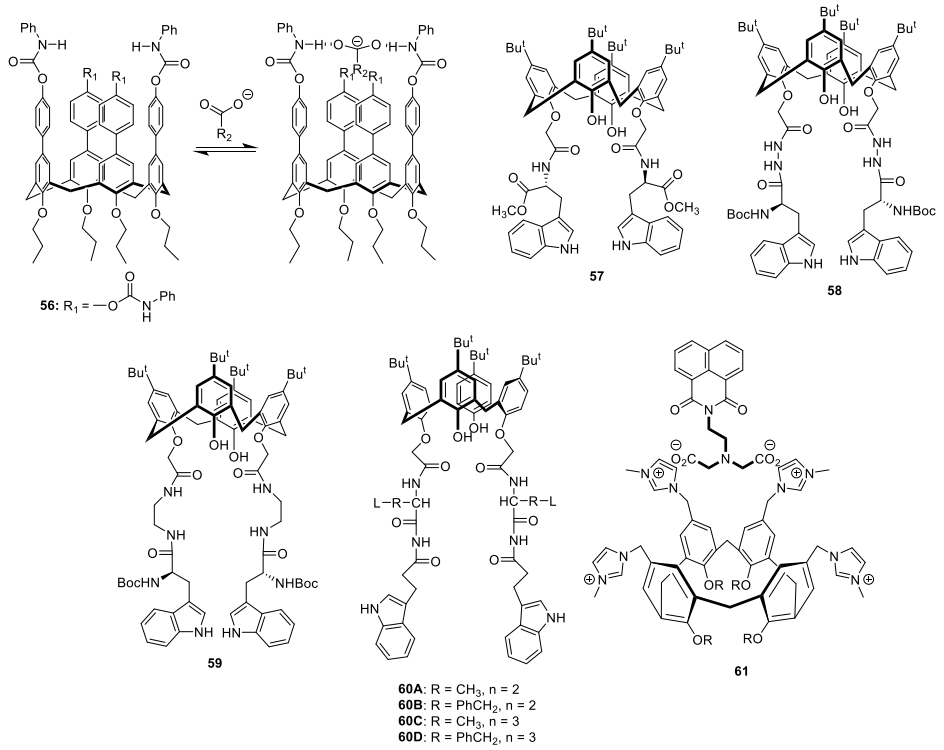

Figure 13. Molecular structures of calix[4]arene derivatives **53**-**58** for recognition of carboxylate anions.

In another investigation, He *et al*.[133] reported a series of calix[4]arene derivatives **57-59** (Figure 13) bearing L-tryptophan units at the lower rim for the chiral recognition of carboxylate ions. In DMSO, probe **57** displayed dramatically different fluorescence responses to the binding of L- and D-alanine, with the D- isomer causing about 48% fluorescence quenching at 346 nm, whilst the L-isomer showed only 10% quenching at the same concentration. The formation of a 1:1 complex between **57** and D-alanine was confirmed and a K_a of 54 M^{-1} determined (K_a was calculated for D-N-Boc-Ala). The binding of L-alanine was too weak for a K_a to be calculated. Similar behavior was

observed with probe **58** and the recognition of D-mandelate from L-mandelate. Probe **58** exhibited a dramatic decrease in fluorescence intensity at 345 nm upon the addition of D-mandelate (K_a value of 1.04 ×103 M^{-1}) compared to L-mandelate (K_a value was not calculated). Probe **59** showed good chiral recognition towards phenylalaninol with binding constants of 25 and 124 M^{-1} for the L- and D- isomers, respectively. However, probe **59** exhibited a strong fluorescence band at 445 nm, hypsochromically shifted compared to probes **57** and **58**. Considering their structures, it was presumed that the ethylene linkers in probe **59** bestowed it with enough flexibility such that two indole moieties can approach each other to induce excimer emission. Moreover, in stark contrast to the fluorescence quenching in the case of probe **57** and **58**, the intensity of the excimer emission was gradually enhanced upon the addition of L-Ala anion. The fluorescence enhancement in the presence of this anion was attributed to an interaction that blocks the PET from the amide -NH to the indole units. As described above, probe **58** generally bound guests more strongly relative to probe **57** and **59**. This was ascribed to its more rigid structure and the presence of more hydrogen bonding groups.

The same group also reported tryptophan decorated calix[4]arenes **60A-D**[134] (Figure 13), which not only exhibit excellent enantioselective recognition of *R*-phenylglycinol, but also discriminated it from phenylalaninol. The addition of 6 equivalents of *R*-phenylglycinol to a solution of **60D** ($\lambda_{ex.}$= 368 nm) in MeCN lead to an 800% fluorescence enhancement at 456 nm (excimer emission). The corresponding value for *R*-phenylalaninol was only 35%. The large difference in optical properties was also reflected in their 1:1 K_a values, which were calculated to be 565 M^{-1} for *R*-phenylglycinol and 91 M^{-1} for *R*-phenylalaninol. The fluorescence enhancement was attributed to π-π stacking between the indole moieties of the receptor and the aromatic ring of *R*-phenylalaninol, which ultimately favors an energy transfer from the excited state of the fluorophore to the ground state. Similar behavior was observed for other derivatives **60A-C**. However, **60C** and **60D** showed a better fluorescence response compared with **60A** and **60B**, presumably because they possess more flexible structures that enable the two indole moieties to more easily approach one another.

An indicator displacement assay (IDA) in which a fluorophore is displaced from the host pocket by analyte anion binding has been investigated in a number of cases.[135,136]

Using an amalgamation of IDA and PET, Pischel *et al*.[137] devised water-soluble non-covalent supramolecular complex **61** (Figure 13) for the selective sensing of citrate. In this complex an intramolecular PET process strongly quenched fluorescence of the naphthalimide dicarboxylate dye. However, in the presence of citrate ions the corresponding ternary complex was formed. This resulted in a shift in the p*K*a of free amine groups of the imidazoliums of the calixarene, partial protonation, and fluorescence enhancement as PET is attenuated.

Thus, controlling the directionality and preorganization of hydrogen bonds groups allow for the recognitions of specific shaped anions of different size, geometry and hydrogen bonding preferences. For instance, fine tuning of spacer length in probes **57**-**59** bearing L-tryptophan allowed the discriminated detection of L- and D-isomers of alanine, mandelate and phenylalaninol. Following similar changes, probes **60A-D** enantioselectively discriminated *R*-phenylglycinol from phenylalaninol. Again, the fluorescence outcomes depend upon the binding events and type of fluorophore. An IDA approach highlights the importance of non-covalent strategy for selective detection of anion.

2.2.4 Detection of amino acids and nucleotides

Beyond their fundamental role as components in proteins, amino acids are also involved in cell signaling, for example in the protein phosphorylation cascade and in gene expression.[138] For example, aspartic acid (Asp) and glutamic acid (Glu) are important excitatory neurotransmitters.[139] Moreover, altered glutamatergic neurotransmission appears to be closely related to the pathophysiology of Parkinson's disease (PD).[140,141] For these and many other reasons, the selective recognition of amino acids in an aqueous has garnered increased recent attention.

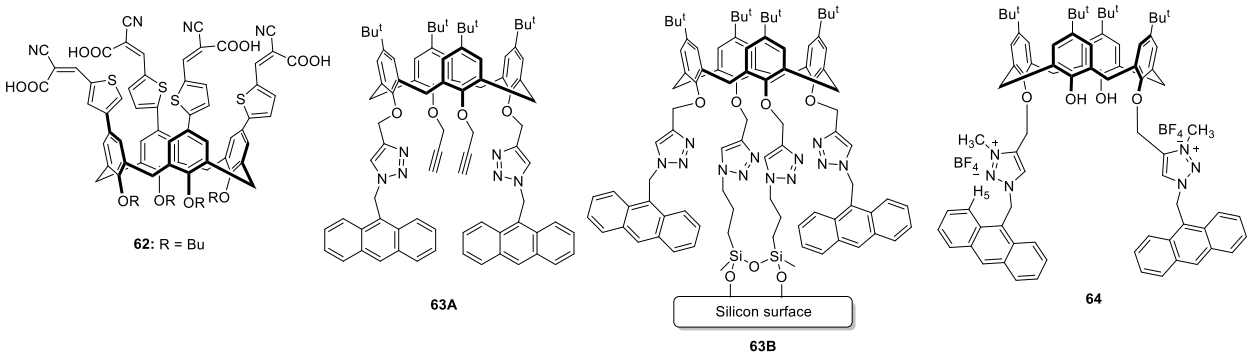

Figure 14. Molecular structures of calix[4]arene derivatives **62**-**64** for recognition of amino acids and nucleotides.

Su *et al*.[142] reported water-soluble calix[4]arene derivative **62** (Figure 14) conjugated with four thiophene-cyanoacrylic acid groups as fluorescent ‘‘turn-off’’ probes for the detection of Asp and Glu. Probe **62** showed about 90% and 85% fluorescence quenching at 540 nm (λ_{ex} = 370 nm) upon the addition of 200 equivalents of Asp and Glu respectively, with a slight (8 nm) bathochromic shift in both cases. The fluorescence quenching of **62** was tentatively attributed to the excitation energy or charge transfer from the probe to the Asp/Glu guest, whilst the bathochromic shift of both the fluorescence and absorption bands were attributed to the fact that the binding of Asp/Glu provides a better stabilization of the excited state of **62** than that of the ground state. No significant change was observed with other amino acids, demonstrating the selective nature of probe **62** towards acidic amino acids.

Another fluorescent probe for amino acids, calixarene **63B**, was designed by Li *et al*.[143] They coupled anthracene units to a calix[4]arene scaffold to form **63A**, and then covalently attached to the adduct to a silica surface *via* click chemistry to give a self-assembled monolayer for tryptophan recognition. Material **63B** is a wettable functional surface, *i.e.,* it can change its character from hydrophilic to hydrophobic (or vice versa) in response to an added guest or change in solute. Such materials find wide applications in electronic devices and in microfluidics systems.[144-146] The selective recognition ability of **63A** itself was first investigated by fluorescence microscopy. The addition of tryptophan to **63A** in DMSO greatly reduced its fluorescence intensity at 419 nm, indicating the formation of a **63A**-tryptophan complex. This was further confirmed by ESI-MS. AFM imaging showed that, upon guest binding, particles of **63A** increased in size from 30-80 to 60-200 nm. The binding stoichiometry was found to be 1:1 by Job plot.

The wettability of silica-modified **63B** was then investigated by water contact angle (CA) measurements and fluorescence spectroscopy. After the covalent attachment of **63A** onto the silica surface, the surface became superhydrophobic (CA changed from 71.5° to 151.7°). To evaluate its wettability response, **63B** was immersed into solutions of different amino acids, revealing that the surface became highly hydrophilic (CA 13.5°) only in the presence tryptophan. An anticipated effect considering the expected reversibility of binding, this value reverted to its original value (151°) upon washing with water.

The key role of nucleoside triphosphates (NTPs) – adenosine triphosphate (ATP), guanosine triphosphate (GTP), cytidine triphosphate (CTP), thymidine triphosphate (TTP), and uridine triphosphate (UTP) – in all living systems have also made them attractive targets for sensor designers. In this regard, triazolium-anthracenyl calix[4]arene conjugate **64** (Figure 14) was reported by Rao *et al*.[147] for the fluorescent detection NTPs. Probe **64** was found to be selective for NTPs, but not selective for specific NTPs; it responds to all five NTPs with enhancement in the fluorescence emission. Previous fluorescent probes showed similar response but to only one or two NTPs.[148,149] Moreover, NMR and fluorescence spectroscopy revealed that probe **64** can differentiate between mono and di-phosphates NTPs. The fluorescence enhancement of **64** upon binding analyte binding followed the order: ATP ≈ UTP > CTP ≈ TTP > GTP (K_a = 40,000 ± 900, 21,665 ± 550, 19,000 ± 440, 17,000 ± 250, and 9,316 ± 120 M^{-1} respectively). The higher selectivity of **64** for NTPs over other phosphates was attributed to electrostatic interactions between the anionic phosphates and the cationic triazolium moieties. The selective binding of **64** to NTPs was also confirmed by absorption spectroscopy, where an increase in the absorption band corresponding to the anthracenyl moiety was observed only in the presence of NTPs. The NTP-induced change in the microstructure of solid **64** was studied by AFM, showing that addition of NTPs to a solution of **64** induced the formation of aggregates whose size varies depending upon the type of NTP added. The fluorescence enhancement of **64** with NTPs was attributed to aggregation-induce emission (AIE). However, no such aggregation behavior was observed with mono or di-phosphate analogues. Similarly, scanning electron microscopy (SEM) also showed unique morphological structural changes in the presence of NTPs such as compressed spheres, flower-like and chain-like structures.

Thus, ditopic receptors such as **62** are capable of recognizing the zwitterionic structure of amino acids. Developing ditopic, wettable probe **63B** by its binding to silica-surface is an interesting approach for detection of amino acids. Alternatively, electrostatic interactions between the cationic triazolium moieties of **64** and the anionic phosphates of NTPs offers another strategy over a covalent approach.

2.3 Bifunctional fluorescent receptors

The applicability of fluorescent receptors can be maximized if a single molecular probe can be designed for multi-ion detection. This strategy can be realized by incorporating different binding sites into the artificial receptor. In this regard, both the upper and lower rims, as well as the different conformations of calixarenes, have been utilized for the concurrent detection of anions, cations, and biomolecules. This section highlights the usefulness of multifunctional calixarene receptors. Table 3 lists the binding stoichiometries, binding constants and detection limits of various calixarene probes toward cationic and anionic guests.

2.3.1 Bifunctional fluorescent receptors for different cations

Chung *et al.* reported a ditopic receptor **65** (Figure 15) for Pb^{2+} and K^{+} ions.[150] In this 1,3-alternate calixarene two anthracene groups were incorporated into one rim, whist a crown[4]-ring occupied the other. Probe **65** exhibited a strong quenching of the fluorescence emission of anthracene at 415 nm (λ_{ex} = 367 nm) upon binding Pb^{2+}. This was attributed to both a reverse PET process from the anthracene unit to the triazole group and the heavy metal ion effect. The fluorescence emission at 415 nm was revived upon further titration with K^{+}, which was attributed to a combination of electrostatic repulsion and negative heterotropic allostery. Similarly, a ditopic fluorescence behavior was also observed between Hg^{2+}, Cu^{2+} and Cr^{3+}, and K^{+} ions. Such cation exchange in the two different binding sites resulted into a switchable “on-off” optical sensor.

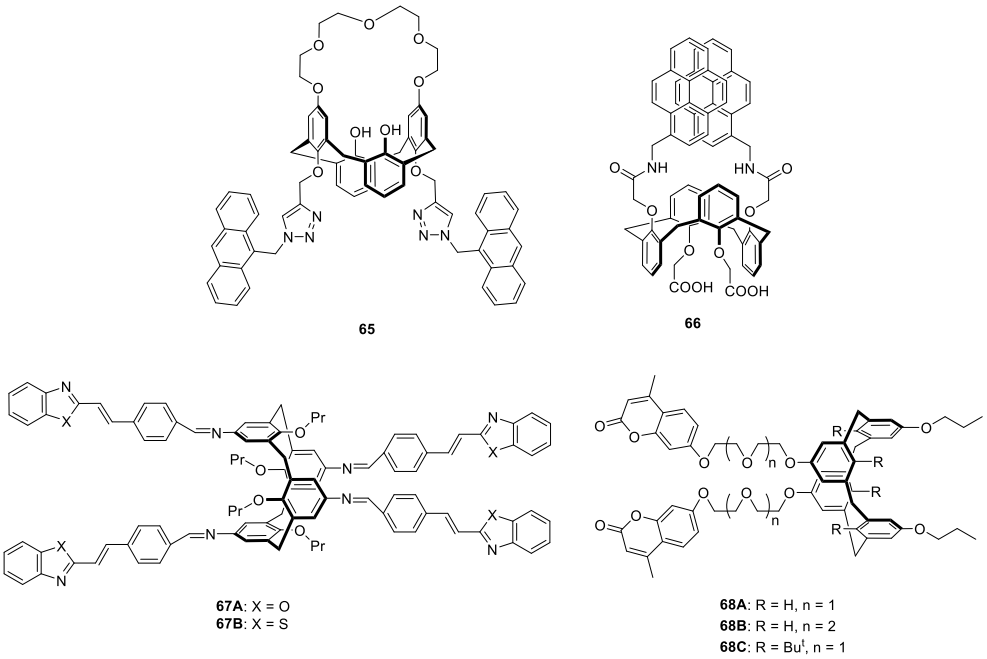

Figure 15. (A) Structure and binding modes of probe **65** with Pb^{2+} and K^+ ions. (B) Molecular structures of bifunctional calix[4]arene receptors **66**-**68**.

Kim *et al.* reported a calix[4]arene dicarboxylate derivative **66** (Figure 15), which exhibited selective binding towards Ca^{2+} and Pb^{2+} among other tested monovalent (Ag^+, Cs^+, K^+, Li^+, Na^+) and divalent (Zn^{2+}) ions.[151] Screening assays revealed that Ca^{2+} binding enhanced pyrene monomeric emission and resulted in a shorter wavelength excimer emission band. This was attributed to less effective HOMO-LUMO interactions of the **66**·Ca^{2+} complex in the excited state as compared to the ground state. On the other hand, in the presence of Pb^{2+} quenching of both monomer and excimer emission bands occurred. The latter was attributed to conformational changes induced by coordination of Pb^{2+} to the amide carbonyls and a resulting enhanced separation of the pyrene groups.[152,153] Furthermore, the addition of Ca^{2+} to the **66**·Pb^{2+} complex resulted in the reappearance of both monomer and excimer emission bands. However, such behavior was not observed with the corresponding ester analogue of **66**. This suggested that the carboxylates of **66** can strongly bind to Ca^{2+} ion, displace the Pb^{2+} in the **66**·Pb^{2+} complex, and as a result greatly alter the fluorescence properties of the probe.

Xue and co-workers designed and prepared chemosensors **67A** and **67B** (Figure 15) containing benzoxazole and benzothiazole ionophores linked through imino

groups.[154] Compounds **67A** and **67B** exhibited weak fluorescent emission in solution (455 nm and 460 nm respectively) due to PET from the imine to the benzoxazole and benzothiazole units respectively. However, upon incubation with various metal ions a selectivity for Fe^{3+} and Cr^{3+} was observed with a remarkable fluorescence enhancement *via* PET inhibition. This was attributed to efficient electron transfer from the imine nitrogen to the vacant orbitals of Fe^{3+} and Cr^{3+}.

Paul and co-worker reported a series of 1,3-alternate calix[4]arene derivatives **68A-C** (Figure 15) bearing ethylene glycol units as binding sites and a pair of fluorescent coumarin reporters.[155] Owing to the flexible ethylene glycol units, these derivatives exhibit ion responsive behavior. Thus, out of sixteen metal ions Fe^{3+} induced 70-85% fluorescence quenching at 390 nm (coumarin, λ_{ex} = 317 nm) in all derivatives, whilst Cu^{2+} exhibited about moderate to strong (60-75%) quenching in **68B** and **68C**. Quenching of fluorescence emission probes **68A-C** was attributed to metal-induced intramolecular charge transfer from the coumarin moiety to the metal ions, leading to fluorescence quenching.[156,157] In contrast, Ca^{2+} induced a 20-35% fluorescence enhancement for the three hosts *via* CHEF.[158]

These studies illustrate the key strategy of bifunctional receptors for this area. Depending upon the type and number of binding site (hard such as O atom, or soft such as N/S atom) and the conformation of calix[4]arene, the designed probe can complex a variety of metal cations. While in the complexed form, the bound metal cation can induce electrostatic effects upon the other metal cation guests.

Table 3. Various bifunctional receptors **65**-**84** and their binding stoichiometries and constants, and detection limits toward various cations and anions.

Probe number (L)	Guest species (G)	Stoichiometry ratio (L: G)	Binding constant	Detection limit	Reference
65	Pb^{2+}	1:1	$K = 3.71 \times 10^4\ M^{-1}$ [a]	- [b]	150
	K^+	1:1	- [b]	- [b]	
66	Ca^{2+}	1:1	- [b]	- [b]	151
	Pb^{2+}	1:1	$K = 2.1 \times 10^5\ M^{-1}$ [a]	- [b]	
67A	Fe^{3+}	1:1	$K = 1.53 \times 10^5\ M^{-1}$ [a]	- [b]	154
	Cr^{3+}	1:1	$K = 4.53 \times 10^5\ M^{-1}$ [a]	- [b]	
67B	Fe^{3+}	1:1	$K = 1.39 \times 10^5\ M^{-1}$ [a]	- [b]	
	Cr^{3+}	1:1	$K = 7.80 \times 10^4\ M^{-1}$ [a]	- [b]	
68A	Fe^{3+}	1:1	$K = 5.34 \times 10^3\ M^{-1}$ [a]	- [b]	155
	Cu^{2+}	1:1	- [b]	- [b]	
	Ca^{2+}	1:1	$K = 4.79 \times 10^3\ M^{-1}$ [a]	- [b]	

68B	Fe^{3+}	1:1	$K = 3.85 \times 10^3\ M^{-1}$ [a]	- [b]	
	Cu^{2+}	1:1	$K = 5.62 \times 10^4\ M^{-1}$ [a]	- [b]	
	Ca^{2+}	1:1	$K = 3.12 \times 10^3\ M^{-1}$ [a]	- [b]	
68C	Fe^{3+}	1:1	$K = 7.31 \times 10^3\ M^{-1}$ [a]	- [b]	
	Cu^{2+}	1:1	$K = 5.54 \times 10^4\ M^{-1}$ [a]	- [b]	
	Ca^{2+}	1:1	$K = 6.41 \times 10^3\ M^{-1}$ [a]	- [b]	
69	Cs^{+}	1:1	$K = 5.4 \times 10^2\ M^{-1}$ [a]	- [b]	159
	F^{-}	1:1	$K = 1.9 \times 10^3\ M^{-1}$ [a]	- [b]	
70	Cu^{2+}	1:1	$K = 1.72 \times 10^4\ M^{-1}$ [a]	- [b]	161
	AcO^{-}	1:1	$K = 1.59 \times 10^5\ M^{-1}$ [a]	- [b]	
	F^{-}	1:1	$K = 5.99 \times 10^4\ M^{-1}$ [a]	- [b]	
71	Cu^{2+}	1:1	$K = 2.38 \times 10^5\ M^{-1}$ [a]	- [b]	163
	NO_3^{-}	1:1	$K = 1.64 \times 10^5\ M^{-1}$ [a]	- [b]	
72	Cu^{2+}	1:1	$K = 6.1 \times 10^4\ M^{-1}$ [a]	- [b]	164
	F^{-}	1:1	$K = 1.1 \times 10^4\ M^{-1}$ [a]	- [b]	
73	Cu^{2+}	1:1	$K = 53303\ M^{-1}$ [a]	4.51 ppm	166
	Fe^{2+}	1:1	$K = 26844\ M^{-1}$ [a]	3.96 ppm	
	Zn^{2+}	1:1	$K = 41341\ M^{-1}$ [a]	45 ppb	
74A	Cu^{2+}	1:1	$K = 1.24 \times 10^5\ M^{-1}$ [a]	- [b]	167
	F^{-}	1:1	$K = 2.10 \times 10^3\ M^{-1}$ [a]	- [b]	
74B	Cu^{2+}	1:1	log K = 5.09 [a]	- [b]	173
	F^{-}	1:1	log K = 5.30 [a]	- [b]	
75A	Cu^{2+}	1:1	$K = 14.0 \times 10^8\ M^{-1}$ [a]	4.16 nM	174
	F^{-}	1:1	$K = 12.18 \times 10^8\ M^{-1}$ [a]	2.15 nM	
75B	Fe^{3+}	1:1	$K = 9.73 \times 10^8\ M^{-1}$ [a]	0.88 pM	175
	$H_2PO_4^{-}$	1:1	$K = 9.73 \times 10^8\ M^{-1}$ [a]	1.11 pM	
76	Sr^{2+}	1:1	$K = 9.46 \times 10^6\ M^{-1}$ [a]	1.04 pM	176
	Cd^{2+}	1:1	$K = 9.65 \times 10^6\ M^{-1}$ [a]	0.94 pM	
77	Hg^{2+}	1:1	$K = 7.52 \times 10^4\ M^{-1}$ [a]	- [b]	177
	F^{-}	1:2	- [b]	- [b]	
78A	F^{-}	1:1	$K = 3.54 \times 10^4\ M^{-1}$ [a]	- [b]	178
	AcO^{-}	1:1	$K = 6.36 \times 10^4\ M^{-1}$ [a]	- [b]	
78B	F^{-}	1:1	$K = 4.66 \times 10^4\ M^{-1}$ [a]	- [b]	178
	AcO^{-}	1:1	$K = 1.99 \times 10^4\ M^{-1}$ [a]	- [b]	
79	Cu^{2+}	1:1	$K = 7.38 \times 10^5\ M^{-1}$ [a]	- [b]	179
80	Cd^{2+}	1:1	- [b]	- [b]	180
	$H_2PO_4^{-}$	1:1	- [b]	- [b]	
81	Hg^{2+}	1:1	$K = 1.06 \times 10^4\ M^{-1}$ [a]	1.87 ppm	181
82	Ag^{+}	1:1	$K = 1.06 \times 10^4\ M^{-1}$ [a]	450 ppb	182
	Cu^{2+}	1:1	$K = 3.02 \times 10^4\ M^{-1}$ [a]	- [b]	
83A	Zn^{2+}	1:1	$K = 9.2 \times 10^4\ M^{-1}$ [a]	47 ppb	185
83B	Cd^{2+}	1:1	- [b]	58 ppb (Cys)	189
83C	Zn^{2+}	1:2	- [b]	0.53 ppm (His)	190
83D	Zn^{2+}	2:1	$K = 7.2 \times 10^4\ M^{-1}$ [a]	278 ppb ($P_2O_7^{4-}$)	191
84	Mg^{2+}	1:1	- [b]	- [b]	192

[a] Calculated using fluorescence titrations, and [b] not reported by the original article.

2.3.2 Bifunctional fluorescent receptors for cation and anion

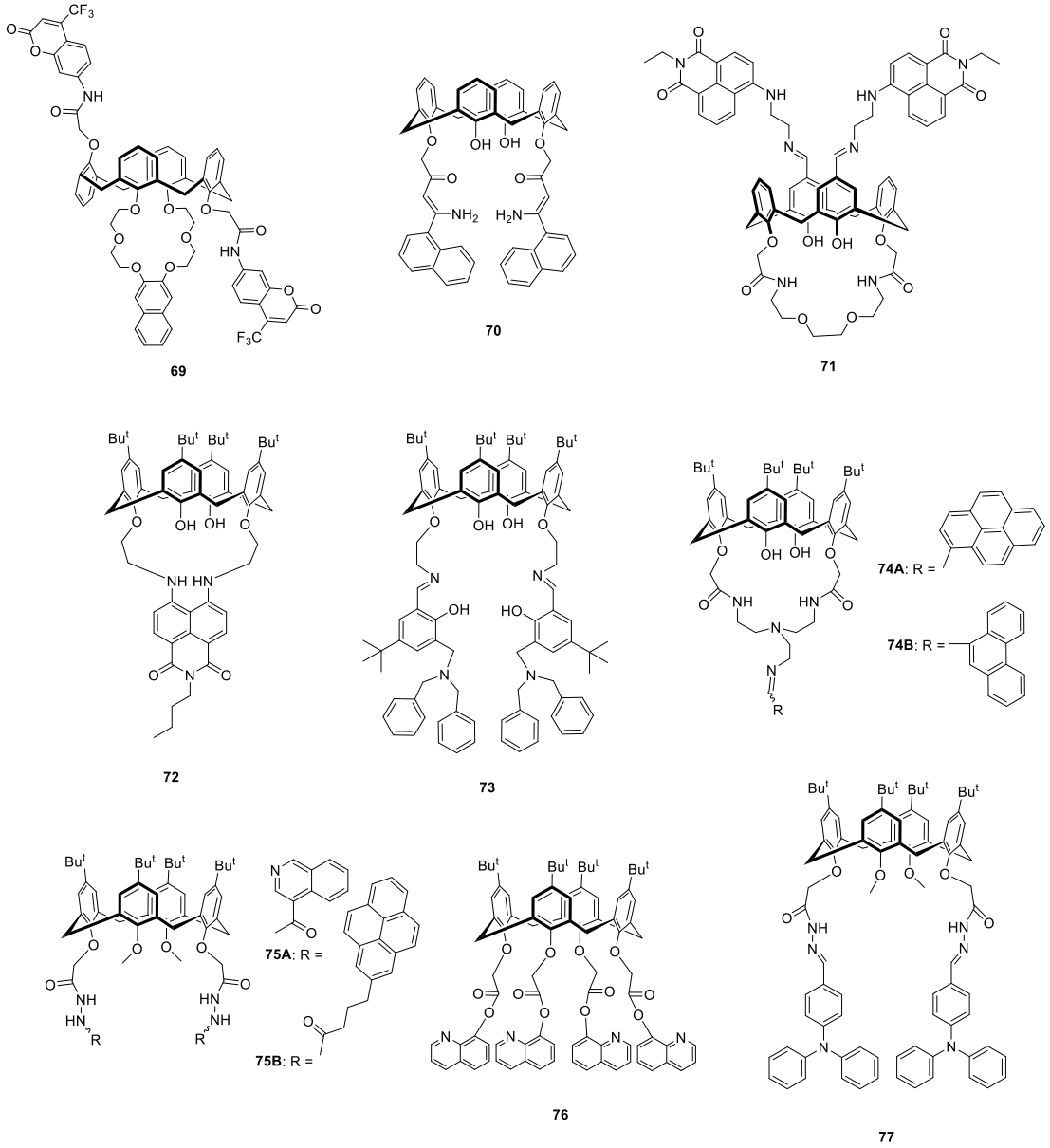

Figure 16. Chemical structure of bifunctional receptors **69**-**77**.

Kim and co-workers developed a novel chemosensor **69** containing one 2,3-napthocrown[6] unit and two coumarin fluorophores in calix[4]arene locked in a partial cone conformation (Figure 16).[159] Chemosensor **69** containing the crown[6] loop and two coumarin amide groups as binding sites exhibited both colorimetric and FRET-based fluorometric response towards Cs^+ and F^- respectively. In the free state, **69** exhibited an intramolecular FRET between the naphthalene unit (emission) and coumarin unit

(absorption). Addition of F^- to a solution **69** induced a significant bathochromic shift in coumarin absorption (344 nm to 435 nm, $K_a = 1.9 \times 10^3\ M^{-1}$). However, a larger excess of F^- (1000 equiv.) resulted in coumarin emission quenching (536 nm), probably due to PET from F^- to the coumarin unit. Likewise, **69** displayed preferential selectivity for Cs^+ ion over K^+ ion ($K_a = 5.4 \times 10^2\ M^{-1}$ versus $1.6 \times 10^2\ M^{-1}$) due to size-complementary with the crown ether ring and additional cation–π interactions.[160] This was accompanied by the suppression of PET from the oxygen atoms of the crown ether to the naphthalene unit, and hence a significant emission enhancement of the coumarin.

Chung and co-workers synthesized calix[4]arene derivative **70** functionalized with β-amino-α,β-unsaturated ketone moieties at the lower rim (Figure 16).[161] Out of ten tested metal ions (Li^+, Na^+, K^+, Ag^+, Ca^{2+}, Pb^{2+}, Hg^{2+}, Ni^{2+} and Cr^{3+}), **70** displayed selectivity towards Cu^{2+} ion (1:1 complex, $K_a = 1.72 \times 10^4\ M^{-1}$) with both chromogenic and fluorogenic responses. The monomeric emission of **70** at 343 nm increased with Cu^{2+} ion concentration, presumably due to a CHEF process induced by Cu^{2+} ion locking the free movement of the β-amino-α,β-unsaturated ketone moieties. This was also accompanied by the formation of a new band at 438 nm due to an MLCT between Cu^+ and the phenolic OH groups of **70**.[162] Cyclic voltammetry analyses further confirmed the reduction of Cu^{2+} to Cu^+ by the phenolic OH groups on the lower rim. The **70**·Cu^+ complex was further used for the detection of AcO^- and F^- ions and showed ditopic behavior with monomer emission enhancement (438 nm) upon complexation with AcO^- and F^- ($K_a = 1.59 \times 10^5$ and $K_a = 5.99 \times 10^4\ M^{-1}$ respectively).

Another bifunctional receptor is calix[4]arene probe **71** (Figure 16), bearing two naphthalimide moieties on the upper rim conjugated *via* imine units, and an amide-containing crown on the lower rim.[163] Testing of a series of metal perchlorates revealed that only Cu^{2+} bound to the imine groups of **71** and brought the naphthalimide groups together in such a manner as to cause quenching in the fluorescence emission at 510 nm *via* an electron transfer process. On the other hand, probe **71** showed non-selective quenching in optical emission in the presence of F^-, Cl^-, Br^-, $H_2PO_4^-$, NO_3^-, I^-, and HSO_4^-. The disappearance of amide NH proton signal from the NMR spectrum of probe **71** with NO_3^- indicated that the amide groups acted as an anion binding site.

Another napthalimide-calix[4]arene chemosensor, **72**, has been developed as a bifunctional receptor for F^- and Cu^{2+} (Figure 16).[164] Chemosensor **72** displayed a strong emission band at 480 nm (λ_{ex} = 435 nm) which was quenched upon addition of $Cu(ClO_4)_2$. Concomitantly, the appearance of a weak bathochromic-shifted emission band due to the deprotonation of the napthalimide NH units of **72** was also observed.[165] The authors demonstrated a 1:1 complex between **72** and Cu^{2+} (K_a = 6.1 ± 0.61 × 10^4 M^{-1}). Likewise, a fluorescence titration assay revealed that **72** also formed a stable, selective 1:1 complex with F^- (K_a = 1.1 ± 0.11 × 10^4 M^{-1}). Compared to the other ions tested, F^- ion was sufficiently basic to deprotonate both the OH and NH groups of **72**. Thus, the observed selectivity for CuF_2 arose through a combination of electrostatic interactions between the NH groups of **72** and Cu^{2+} ions, and the basicity of F^- and its hydrogen bonding interactions with the OH and NH groups of the probe.

Rao and co-workers synthesized bifunctional sensor **73** possessing salicylimine moieties (Figure 16).[166] Out of the eight divalent metal ions tested conjugate **73** exhibited a colorimetric response for Cu^{2+} (4.51 ± 0.53 ppm) and Fe^{2+} (3.96 ± 0.42 ppm) at low concentration, whilst Zn^{2+} ion was detected by fluorescence spectroscopy at a minimum concentration of 45 ± 4 ppb. A methanolic solution of conjugate **73** displayed weak fluorescence at 380-620 nm (λ_{ex} = 360 nm); however, a concentration-dependent fluorescence enhancement (22-25 fold) was observed with the addition of Zn^{2+}. This was attributed to the binding of Zn^{2+} to the imine and phenolic groups in **73** (1:1 complex) and its blocking of PET from the imine nitrogen to the salicyl group. The **73**·Zn^{2+} complex was further tested for its anion binding properties. Treatment with $H_2PO_4^-$, HPO_4^{2-}, and $P_2O_7^{4-}$ resulted in large quenching effects due to direct interaction between the anions and the Zn^{2+} and hence enhanced PET.

In 2013, Sahin developed pyrene-based chemosensor **74A** (Figure 16) and described its potential for recognizing metal ions and anions.[167] Compound **74A** showed a distinct fluorescence response at 392 nm (λ_{ex} = 325 nm) towards different metal ions. Upon titration with Cu^{2+} ion, a significant fluorescence quenching (56%) was observed due to the coordination of the paramagnetic Cu^{2+}.[168] Titration with Zn^{2+}, however, resulted in fluorescence enhancement presumably due to CHEF or PET in the complex.[169-172] Furthermore, **74A** selectively exhibited fluorescence quenching due to a PET process

brought about by deprotonation of the amide-NH groups upon titration with F^- ion. Replacement of the pyrene reporters in **74A** by phenanthrenes resulted in sensor **74B** (Figure 16) which also showed selectivity towards Cu^{2+}.[173] Likewise, a similar fluorescence quenching at 325 nm (λ_{ex} = 250 nm) was observed upon titration with F^-.

Menon and co-worker synthesized quinolone bearing calix[4]arene sensor **75A** (Figure 16) for the selective recognition of Cu^{2+} and F^-.[174] Chemosensor **75A** showed a weak fluorescence emission band at 476 nm (λ_{ex} = 410 nm), which upon Cu^{2+} ion titration resulted in a fluorescence enhancement (limit of detection = 4.16 nM, K_a = 14.00 × 10^8 M^{-1}) due to PET from the 4-isoquinolinoyl groups to the guest, and ICT from the diamido moieties to the guest. In contrast, fluorescence quenching was observed upon titration with F^- anion (limit of detection = 2.15 nM, K_a = 12.18 × 10^8 M^{-1}). Further, **75A** was successfully demonstrated as a sensitive and cost-effective fluorometric tool for the detection of Cu^{2+} in blood serum and F^- in waste water samples.

Replacing the 4-isoquinolinoyl fluorophore with pyrene resulted in chemosensor **75B** (Figure 16).[175] Sensor **75B** exhibited a fluorescence turn-off response towards Fe^{3+} (limit of detection = 0.88 pM) with an association constant K_a = 9.73 × 10^8 M^{-1}. A similar response was observed for $H_2PO_4^-$ (limit of detection = 1.11 pM) which bound strongly to the host (K_a = 9.73 × 10^8 M^{-1}). The selective fluorescence quenching towards these ions was attributed to electron transfer from the receptor to the guest species upon complexation. The same group also developed **76** (Figure 16), bearing the same calixarene core and 8-hydroxylquinoline reporters linked *via* esters.[176] This chemosensor exhibited selective fluorescence enhancement and quenching towards Sr^{2+} (limit of detection = 1.04 pM, K_a = 9.46 × 10^6 M^{-1}) and Cd^{2+} (limit of detection = 0.94 pM, K_a = 9.65 × 10^6 M^{-1}). Furthermore, chemosensor **76** was successfully tested for the detection of these metal ions in industrial wastewater samples with excellent recovery percentages.

Calix **77** bearing triphenylamine units was developed by Erdemir and co-workers (Figure 16).[177] Out of eleven tested metal ions of biological relevance, chemosensor **77** exhibited both a colorimetric (yellow) and fluorescence turn-off response in the presence of Hg^{2+}. Host **77** formed a 1:2 complex with Hg^{2+} (K_a = 7.52 × 10^4 M^{-2}). Fluorescence quenching for the triphenylamine group arose through FRET inhibition. Likewise, a

similar fluorescence turn-off response was observed for F^- anion *via* deprotonation of the phenolic and amidic protons of **77**.

Liu *et al*.[178] synthesized calix **78A** and its ruthenium complex **78B** to investigate the effect of metal coordination on anion selectivity (Figure 17). Probe **78A** showed a strong emission band at 460 nm in DMF which underwent quenching exclusively upon the addition of F^- and AcO^- ions. Concomitantly, these anions induced the formation of bathochromically-shifted bands at 537 and 525 nm respectively. No significant fluorescence changes were observed with other anions. The bathochromically shifted bands were attributed to the deprotonation of the NH group of the imidazo[4,5-*f*]-1,10-phenanthroline groups. Furthermore, the intramolecular charge distribution as a result of NH deprotonation resulted in **78A** acting as a colorimetric sensor for the naked-eye detection of F^- and AcO^-. Interestingly, ruthenium complex **78B** showed a different fluorescence response. In this case, the addition of F^- and AcO^- ions induced fluorescence quenching but without formation of any bathochromically-shifted bands, whilst other anions such as Cl^-, Br^-, I^-, and HSO_4^- led to fluorescence enhancement. One possible explanation for this anomalous behavior is that other anions partially neutralized the charge on the ruthenium center, thereby weakening the PET from the NH group of imidazo[4,5-*f*]-1,10-phenanthroline to the ruthenium center. However, in the case of F^- and AcO^-, quenching is favored by efficient PET from the deprotonated NH group to the ruthenium center. For the formation of 1:1 complex with **78A**, the association constants for F^- and AcO^- were found to be 3.54×10^4 and 6.36×10^4 M^{-1} respectively. For **78B**, these values were respectively 4.66×10^4 and 1.99×10^4 M^{-1}.

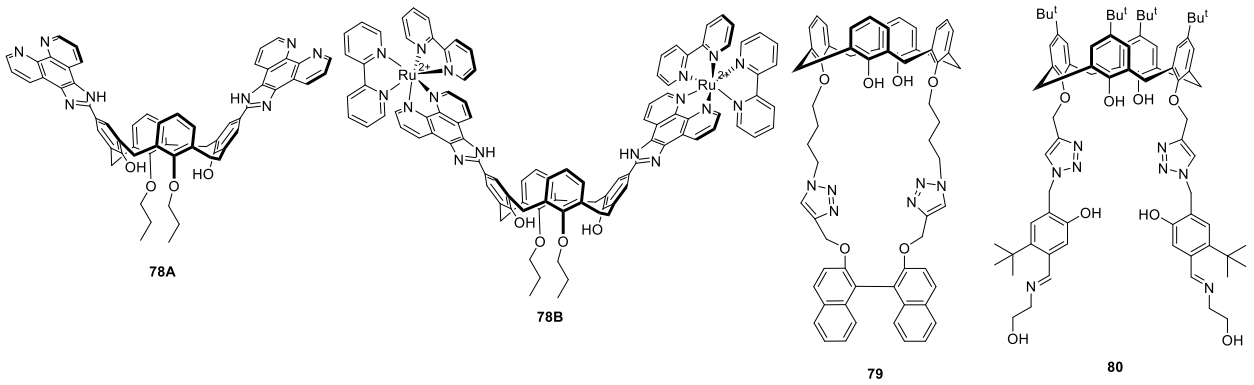

Figure 17. Structure of bifunctional calix[4]arene derivative **78-80**.

Li *et al*.[179] functionalized the lower rim of a calix[4]arene scaffold with chiral 1,1'-bi(2-naphthol) (BINOL) groups to give **79** (Figure 17). Fluorescence quenching in the presence of Cu^{2+} revealed that this host formed a strong 1:1 complex (K_a = 7.38 × 10^5 M^{-1}) with Cu^{2+} ions. Subsequently, this copper complex was utilized as a fluorescence ''turn-on'' sensor for the enantioselective recognition of mandelic acid. A 6.34-fold fluorescence enhancement with *R*-mandelic acid was observed, in contrast to a 4.87-fold enhancement in the presence of the *S*-isomer. As this fluorescence difference was quite small (limit of detection = 20 μM) AFM and DLS were also employed to improve the sensitivity of detection methods. AFM images showed that the addition of *R*-mandelic acid significantly increased the size of particles of the Cu^{2+} complex from 25-35 nm to 447-572 nm. There were also morphological changes from spherical to non-spherical. However, upon treatment with *S*-mandelic acid the particle size only increased to 149-233 nm and there were no morphological changes. DLS revealed the diameter of particles of **79** increased by 6.74-fold and 2.79-fold upon the addition of *R*- and *S*-mandelic acid respectively. The detection limit of enantioselectivity calculated from the plot of size distributions of nanoparticles versus concentration of mandelic acid was found to be 0.2 μM, indicating that DLS analysis was 100-fold more sensitive for chiral recognition than fluorescence.

Calix sensor **80** (Figure 17) was developed as a bifunctional receptor for Cd^{2+} and $H_2PO_4^-$.[180] The structure elucidation of the Cd^{2+} complex by single crystal X-ray diffraction suggested that two Cd^{2+} ions are bound by a N_2O_4 core furnished by the triazole-linked hydroxyethylimino moiety. The binding ligands in the coordination spheres around each Cd^{2+} were comprised of two phenolic oxygens, two ethanolic hydroxyl groups, and two imine nitrogens. As demonstrated by various techniques, *viz.*, UV-Vis. fluorescence spectroscopy, ^{1}H NMR spectroscopy, ESI-MS, among others, the isolated [**80**·Cd^{2+}]$_2$ complex displayed strong binding affinity particularly to inorganic phosphate ($H_2PO_4^-$). The complex [**80**·Cd^{2+}]$_2$ also displayed complete fluorescence quenching at a concentration of four equivalents of $H_2PO_4^-$, whereas other anions induced much smaller changes. Among all the phosphates studied, the order of quenching was $H_2PO_4^-$ > ATP^{2-} ~ HPO_4^{2-} ~ ADP^{2-} > AMP^{2-} ≫ $P_2O_7^{4-}$. Very low concentrations (20 ppb) of $H_2PO_4^-$ showed considerable quenching, whilst other anions required concentrations of between 50-580 ppb to show similar quenching efficiencies. Thus, an absorption spectrum

showed a decrease in absorption at 370 nm with the formation of two new bands at 326 nm and 430 nm. The fluorescence quenching and color change of the [**80**·Cd^{2+}]$_2$ complex upon $H_2PO_4^-$ binding was attributed to decomplexation to form free **80**, which was confirmed by ^{1}H NMR studies. The practical utility of this system was evaluated for the detection of $H_2PO_4^-$ in HeLa cells using confocal microscopy. Thus when **80** and Cd^{2+}/pyrithione-incubated HeLa cells were treated with $H_2PO_4^-$ for 20 minutes at 37 °C, confocal images showed decreased fluorescence intensity within the cells.

In summary, there are two general types of bifunctional receptors for cation and anion. The first type contains two binding sites, one for cation and another for anion, such as in probes **69**, **71**, **74**, **75**, **77** and **78**. The cation binding sites include O atom (hydroxy/carbonyl) and N atom (amide/amine/imine) groups, whereas the corresponding anion binding sites are “NH protons (amide/ amine) and OH (hydroxyl). The fluorescence output of these probes depends upon the mechanism of cation and anion binding such as FRET, PET, CHEF and ICT. On the other hand, the second type of bifunctional receptors, such as **70**, **73**, **79** and **80,** include metal-complexes for probeing specific anions. In these systems the strong binding affinity of anion to the specific metal cation resulted in its decomplexation from the probe and therefore a reversing the fluorescence output signal.

2.3.3 Bifunctional fluorescent receptors for cation and biomolecules

Chemosensor **81** (Figure 21) bearing two 1,3-di(4-antipyrine)amide groups as the binding site at the lower rim of a calix[4]arene was developed for duel binding of cations and neutrals.[181] Out of the fourteen biological mono- and divalent metal ions tested, **81** exhibited high selectivity for Hg^{2+}. Titration with Hg^{2+} led to a decrease in the absorbance at 280 nm and an increase in absorbance bands at 256 and 315 nm of **81**. In the fluorescence spectra of **81**, significant quenching at 400 nm (λ_{ex} = 280 nm) was observed with addition of Hg^{2+} as a 1:1 complex was formed (K_a = 1.06 × 10^4 ± 700 M^{-1}). Based on a fluorescence titration assay, the minimum detection limit for Hg^{2+} ion was found to be 1.87 ± 0.1 ppm. Similar fluorescence quenching effects were observed for conjugate **81** in the presence of pyrimidine bases (cytosine, uracil, and thymine), presumably *via* coordination by the antipyrine groups.

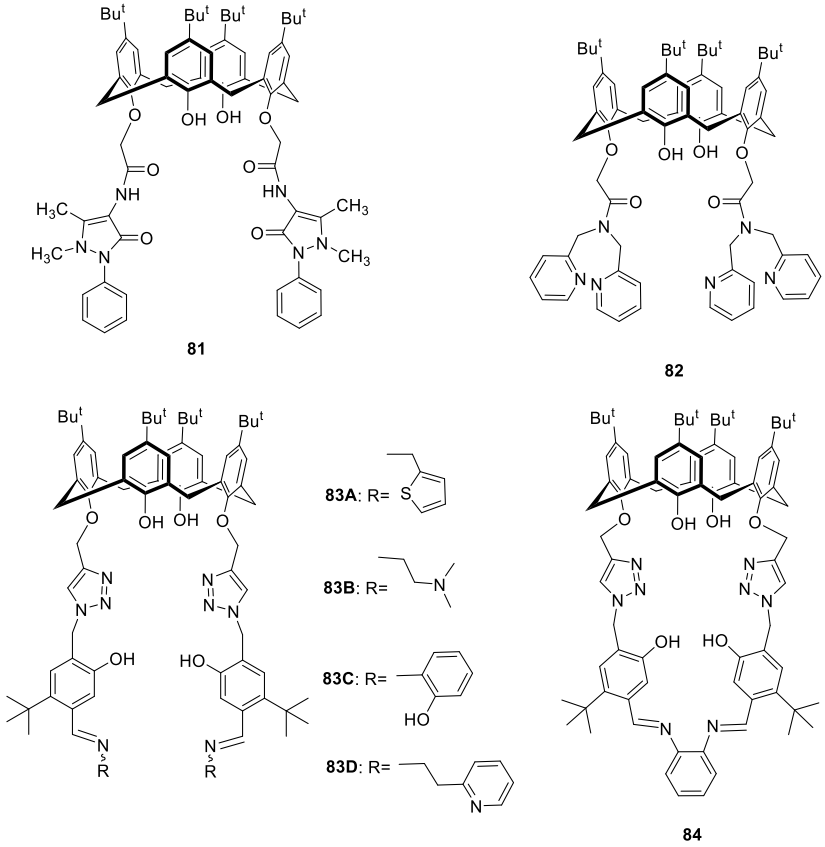

Figure 18. Structure of bifunctional calix[4]arene receptors **81-84**.

Introduction of two bis-(2-picolyl)amine units on the lower rim of a calix[4]arene scaffold resulted in the formation of chemosensor **82** (Figure 18).[182] Treatment with Ag^+ resulted in the emission band of **82** at 315 nm being quenched, and a concomitant enhancement at 445 nm due to the formation of an excimer from the pyridyl units.[183] The binding constant was $K_a = 1.06 \times 10^4 \pm 190\ M^{-1}$. This study also revealed that **82** bound Cu^{2+} ion ($K_a = 3.02 \times 10^4 \pm 1600\ M^{-1}$) with a turn-on fluorescence response.[184] As expected, the fluorescent response was completely reversed upon treatment of the complex with cysteine (Cys) as Ag^+ was released from the complex. Thus, probe **82** served as a bifunctional chemosensor showing a selective primary response towards Ag^+ and a secondary response to Cys, and presumably other thiols.

Rao *et al*. observed how the fine-tuning of receptor binding sites can lead to a significant change in their selectivity. Consider, for example, imine-based conjugate **83A** (Figure 18).[185] Conjugate **83A** possessed weak fluorescence (λ_{em} = 454 nm, λ_{ex} = 390 nm, 1:2 v/v HEPES buffer–EtOH) due to PET between the imine nitrogens and the two

salicyl groups. Out of twelve mono- and divalent metal ions tested **83A** exhibited a turn-on fluorescence response only upon treatment with Zn^{2+} ion. In this complex (K_a = 9.2 × 10^{-4} M^{-1}) the PET was blocked by the bound Zn^{2+}. The resulting complex served as a secondary chemosensor for the detection of thiol-containing mimics of metallothioneins (cysteine/dithiothreitol)[186] and pyrophosphate.[187] With the addition of thiols, Zn^{2+} is displaced from the complex resulting in restoration of PET and the fluorescence attenuation. The potential of the **83A**·Zn^{2+} complex to recognize thiol-containing cysteine was also demonstrated in HeLa cells.[188]

The same research group developed a *N,N'*-dimethylamine ethylimino-bearing triazole linked chemosensor, **83B**, which exhibited a turn-on fluorescence response at 456 nm (λ_{ex} = 380 nm) upon complexation with Cd^{2+} (Figure 18).[189] This **83B**·Cd^{2+} complex was further utilized for recognition of Cys among the 20 biologically important amino acids. In the case of Cys the complex fluorescence was attenuated and there was a color change from fluorescent blue to non-fluorescent (limit of detection = 58 ppb). During the addition of Cys to a methanolic solution of **83B**·Cd^{2+}, a fluorescence enhancement was initially observed, followed by gradual quenching until saturation. This was attributed to binding between the thiol of Cys with Cd^{2+}, followed by its removal from the coordination sphere. The chemosensor **83B**·Cd^{2+} exhibited good reversibility and was further utilized for sensing Cys in biological environments. *In vitro* studies performed on MCF-7 cells demonstrated the potential of **83B** for sensing Cd^{2+} and Cys.

Replacing the *N,N'*-dimethylamine ethylimino functionality in **83B** with *o*-iminophenol groups furnished chemosensor **83C** (Figure 18). This sensor exhibited the recognition of Zn^{2+} amongst other tested metal ions, with a hypsochromically-shifted fluorescence response (535 nm to 495 nm) upon the formation of the 1:2 complex.[190] This complex displayed selectivity towards histidine (His), with a turn-off response at 495 nm (λ_{ex} = 360 nm), induced by decomplexation Zn^{2+}. Similarly, the same group developed chemosensor **83D** bearing pyridyl functionality[191] which exhibited a turn-on fluorescence response at 455 nm (λ_{ex} = 390 nm) upon titration with Zn^{2+} ion (K_a = 7.2 ±0.09 × 10^4 M^{-1}). The **83D·Zn^{2+}** complex was also shown to show to function as a selective turn-off response towards $P_2O_7^{4-}$ (278 ± 10 ppb).

Rao and co-workers have also developed phenylenediamine-capped chemosensor **84** (Figure 18).[192] Compound **84** exhibited a selective turn-on fluorescence response at 510 nm (λ_{ex} = 339 nm) with visual green color upon complexation with Mg^{2+}. Fitting the fluorescence data revealed a 1:1 complex, which was confirmed by absorption and mass analysis data.[193] The **84**·Mg^{2+} complex was isolated and further tested for the detection of various phosphates. Out of the six tested phosphates, titration with HPO_4^{2-}, AMP^{2-}, and $P_2O_7^{4-}$ resulted in initial fluorescence enhancement followed by quenching at higher guest concentrations. Fluorescence enhancement was attributed to the formation of a ternary complex between the coordinated **84**·Mg^{2+} complex and the phosphate, while quenching at higher guest concentration was due to de-complexation of Mg^{2+} from **84**. The remaining three anions, $H_2PO_4^-$, ATP^{2-}, and ADP^{2-} showed only quenching upon binding.

2.4 Fluorescent receptors for nitro-aromatics and explosives

Lee *et al.* reported the first calix[4]arene-pyrene conjugated system for the fluorescence-based detection of nitro-aromatic species such as trinitrotoluene (TNT).[194] The sensing properties of 1,3-alternate calix[4]arene **85** (Figure 19) were assessed in acetonitrile where it was found to detect TNT down to the 1.1 ppb level. Interestingly, the X-ray structure of the host-guest complex revealed that the pyrene substituents in **85** are splayed outwards and interact with the guest in a host-donor guest-acceptor arrangement. ^{1}H NMR and DFT calculations supported the conclusion that sensing relies primarily on charge-transfer.

Kandpal *et al.* have added a new tool to the growing list of micro-cantilever sensors for detecting explosives.[195] Excitation of upper-rim modified calix[4]arene **86** (Figure 19) at 310 nm lead to emission at 345, 360, and 395 nm. Monitoring these bands in the presence of different guests revealed selectivity for TNT (K_a = 3 × 10^4 M^{-1}). MD simulations of the binding of TNT to **86** revealed that up to three molecules could associate with the host, two of which could simultaneously bind within the pocket. When coated on a cantilever, host **86** was shown to be able to detect trace explosives in moist air. The sensor was selective for TNT over 1,3,5-trinitro-1,3,5-triazinane (RDX) and pentaerythritol tetranitrate (PETN).

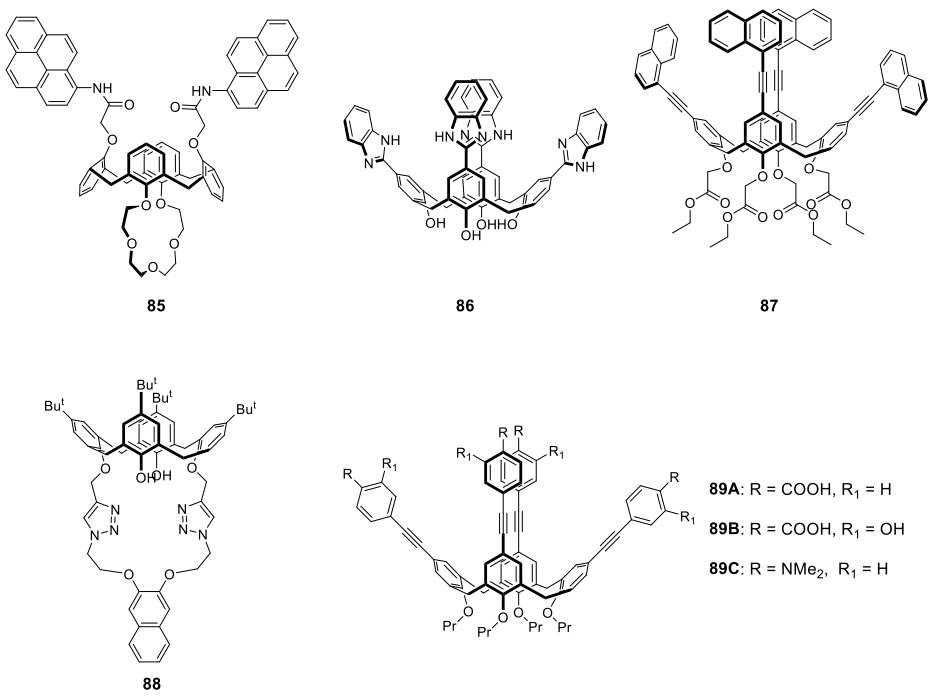

Figure 19. Structure of calix[4]arene receptors **85-89** for detection of nitro-explosives.

The Li group used Sonogashira coupling to synthesize tetranaphthylcalix[4]arene **87** (Figure 19).[196] ^{1}H NMR spectroscopy revealed that this host selectively bound *p*-nitrophenol over other nitro-aromatic guests. Fluorescence spectroscopy demonstrated the expected fluorescence quenching of **87** as the electron deficient *p*-nitrophenol bound to its cavity. NMR, IR and simulations revealed a 1:1 stoichiometry and a complexation dominated by π-π interactions.

A fluorescent calix[4]arene bridged at the 1,3-positions of the lower rim was synthesized using click chemistry (**88**, Figure 19).[197] Fluorescence spectroscopy revealed **88** bound nitro-benzenes, and in particular, 4-nitroaniline. Fluorescence titrations and MALDI-MS confirmed that the complexations were of 1:1 stoichiometry. Further, NMR spectral data suggest that the binding of 4-nitroaniline was driven by the possibility of hydrogen bonding between the aniline NH and the free OH of **88**.

Towards field detection of TNT and other nitro-derivatives, the Sukwattanasinitt group has reported on the synthesis and properties of fluorescent arylethynyl calix[4]arenes **89A-C** (Figure 19).[198] The calixarene cones were deepened with tolane moieties on the upper rim using Sonogashira coupling. Fluorescence quenching experiments with a variety of guests demonstrated that calixarene **89C** was the most

responsive to the binding of TNT and dinitrotoluene. Stern–Volmer plots revealed a good linear response of **89C** to TNT between 1-10 μM, with a limit of detection of 0.3 μM (68 ppb). NMR revealed a 1:1 complex between **89C** and TNT, and suggested complexation of the guest in the upper section of the pocket. The authors also demonstrated paper strips coated with **89C** could be used for the detection of TNT.

In summary, the design of fluorescent probes for nitro-aromatics depends strongly on donor-acceptor energy transfer. The detection ability of the probe is further enhanced by the calix[4]arene cavity that provide facile hydrophobic interactions for both donor and acceptor.

2.5 Miscellaneous fluorescent receptors

The Swager group have built a chemiresistor from single-walled carbon nanotubes (SWCNT) and a calix[4]arene-substituted polythiophene **90** (Figure 20).[199] The polymer itself was shown to selectively sequester xylenes from the gas phase, with a selectivity of *p*- > *m*- > *o*-xylene. When fabricated into a sensor by spin-coating a mixture of the polymer and SWCNTs onto gold electrodes, it was found that each xylene isomer induced a unique reduction in conductance. In contrast, the same type of device devoid of the calix[4]arene displayed a weaker and uniform response to the three isomers. Quartz crystal microbalance studies confirmed the selectivity of the SWCNT-calix[4]arene-polythiophene material. Correspondingly, fluorescence spectroscopy data revealed that the fluorescent polymer was closely associated with the SWCNTs and therefore underwent partial quenching. Moreover, guest binding led to a characteristic fluorescence increase for the xylene isomers, suggesting that binding weakened the polymer-SWCNT interactions. Field effect transistor and passivation studies suggested that xylene transduction was the result of both charge transfer and polymer conformational changes producing greater inter-SWCNT separations.

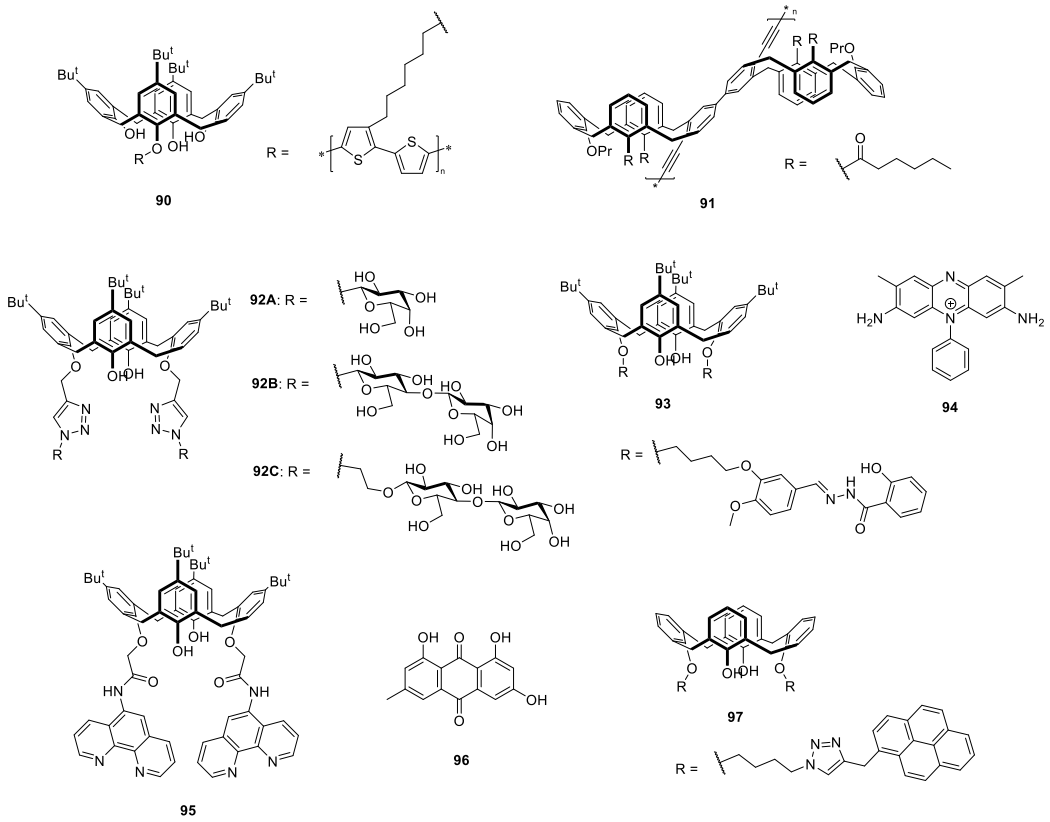

Figure 20. Structure of calix[4]arene receptors **90-97**.

The Vigalok group used Sonogashira and Glaser coupling to synthesize a tubular conjugated polymer **91** (Figure 20) based on a 5,5'-bicalixarene. The requisite 5,5'-bicalixarene was itself synthesized *via* an iron(III)-mediated oxidative coupling of two calix[4]arenes.[200] The fluorescence properties of polymer **91** were profoundly affected by its conjugation, such that it exhibited a 30 nm Stokes shift relative to its absorption. This intrinsically hollow polymer was measured to be approximately 1 nm in diameter and therefore capacious enough to bind small guests. Nitric oxide (NO), with its importance in human physiology, was chosen as a guest. Though normal detection for NO relies on the formation of NO^+, quenching of the fluorescence of the conjugated polymer was observed upon complexation of neutral NO. Moreover, the complex could be reversed by application of a low vacuum. The fluorescence of the corresponding monomer was insensitive to NO. On exposure to NO^+ and higher nitrogen oxides it was found that the observed fluorescence quenching was irreversible; however, the presence of atmospheric oxygen and CO did not affect NO detection.

Lower rim glycosyl-appended 1,3-calix[4]arenes such as lactose conjugates **92A-C** (Figure 20) have been studied for the binding to amino acids and the galactose-specific lectin, jacalin.[201] For the latter studies the authors focused on fluorescence spectroscopy and circular dichroism (CD). CD spectroscopy revealed that the binding of **92C** induced the greatest changes to the secondary structure of the lectin. Zhu and co-workers synthesized a fluorescent calixarene substituted with a 1,3-diacyl hydrazone **93** (Figure 23).[202] This calixarene was sensitized using sodium dodecyl sulfate and was shown to bind the biological strain safranin T (**94**) in a 1:1 manner.

In a separate study, Zhu and Ma reported a bis-phenanthroline-substituted calix[4]arene **95** which, used in combination with amphiphilic sensitizers, can detect emodin **96** (Figure 20).[203] The authors used fluorescence spectroscopy to determine 1:1 complex formation in water. Surfactants such as sodium dodecyl sulfate (SDS), cetyl trimethylammonium bromide (CTAB), and Triton-X, were tested, with the highest fluorescence quenching value achieved with a 1% CTAB solution.

The sensing properties of fluorescent bis-(triazole-linked pyrene) calix[4]arene **97** (Figure 20) have also been investigated.[204] Fluorescence spectroscopy revealed that **97** is capable of recognizing the insecticide carbaryl in the presence of other structurally similar carbamates. A binding constant of $K_a = 4.2 \times 10^5$ M^{-1} was determined. NMR spectroscopy and computational methods demonstrated that the guest bound into the calix pocket and not between the pendent pyrenyl groups. Subsequently, the receptor was non-covalently attached to a graphene oxide layer; AFM, X-ray photoelectron spectroscopy (XPS), and static contact angle measurements confirmed a surface layer of the receptor. Having successfully functionalized the graphene oxide, the investigators then demonstrated how the receptor could function as an impedimetric sensor in electrochemical measurements on glassy carbon electrodes. This work showed that the sensor could selectively detect a 0.1 mM carbaryl concentration. Extending this idea, the authors also demonstrated that the presence of 10^{-9} M carbaryl in serum solution could be detected with high selectivity.

Highly luminescent, layered nano-particles consisting of CdTe nano-crystals (quantum dots, QDs) coated sequentially with silica and calix[n]arenes (n = 4, 7) have been prepared, and their sensitivity to polyaromatic hydrocarbons reported (Figure 21,

98).[205] The UV-Vis spectra of the QDs and the two different coated particles showed that the coating process conserved the absorption properties of the nano-crystals. In contrast, the fluorescence spectra of the different nano-crystals and nano-particles revealed that the calixarene coatings have significant impact on their fluorescence enhancement; a phenomenon attributed to the inhibition of photo-oxidation/photo-bleaching of the quantum dots. With higher amount of calix loaded onto the surface of the particle, significantly enhanced fluorescence relative to the silica coated particle was observed. With these findings, the authors examined the fluorescence response of the different particles to a range of polyaromatic hydrocarbons (PAHs). Their data revealed that the greatest fluorescence enhancement was observed from the calix-coated particles, and that the greatest enhancements were observed when the calix and PAHs were complementary. Thus, for the calix[4] coated particle the ideal guest was anthracene, whilst for the calix[7] particle it was found to be pyrene. The respective detection limits were 2.45 × 6 10^{-8} M and 2.94 × 6 10^{-8} M.

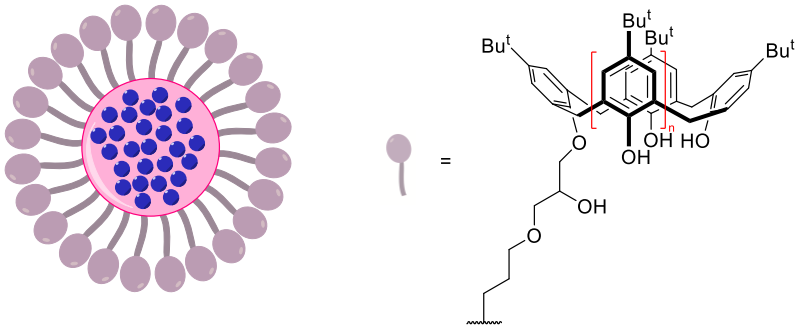

98

Figure 21. CdTe nanoparticles (blue spheres) encased in silica (pink shell) coated with calix[n]arenes (mauve structures, n = 1 or 4) **98**.

2.6 Biomedical applications of fluorescent calix[4]arenes

Living systems are comprised of regulated networks of both supramolecular interactions, and catalytic pathways whose individual processes can be either under kinetic or thermodynamic control. The diversity of calixarenes – their derivatization and incorporation of different functional groups furnishing multivalent architectures – are ideal for targeting such complex biological systems, and hence for designing new pharmaceutical applications. Multivalent calixarenes bearing fluorophores, biocompatible moieties, and cell targeting units are known to elicit stronger binding affinities for

biomolecules compared to monovalent analogues. Additionally, the dynamic reciprocity and stimulus responsiveness of these materials can also pave the way to improved selectivity and selectivity. In this regard, numerous modifications have been carried out on the calixarene scaffold to generate biocompatible fluorescent biosensors, amphiphilic systems, and gene and drug delivery vectors. In this section, we discuss interesting applications of calixarene scaffolds as potential biomaterials.

2.6.1 Fluorescent calix[4]arenes as biosensors

The recent literature has revealed the exploration of calixarenes in biological systems, particularly as ion channel mimics,[206,207] as magnetic resonance imaging (MRI) agents,[208,209] in protein recognition at cell surfaces,[210] and as drug delivery systems (DDS).[211,212] However, a comprehensive understanding of their cellular uptake and localization has not yet been attained. Towards this, fluorescent conjugates **99**[213] and **100**[214] bearing NBD fluorophores have been developed (Figure 22). The conjugate **99** bearing four ammonium groups exhibited fast cellular uptake in Chinese Hamster Ovary (CHO) cells. Moreover, the cellular uptake was not affected by various endocytosis inhibitors such as filpin, sucrose, and β-cyclodextrin, suggesting a different mechanism of uptake. Further, the conjugate **99** was found preferentially in the cell cytoplasm and exhibited low toxicity towards CHO (IC_{50} = 82 nM) and HL-60 (IC_{50} = 8 mM) cells. Conjugate **100** bearing folic acid, on the other hand, exhibited cellular uptake *via* folate-mediated endocytosis. The folate positive HeLa cells showed better cellular uptake for **100** as compared to normal fibroblast NIH3T3 cells, with endo-lysosomal accumulation as confirmed by co-localization studies.

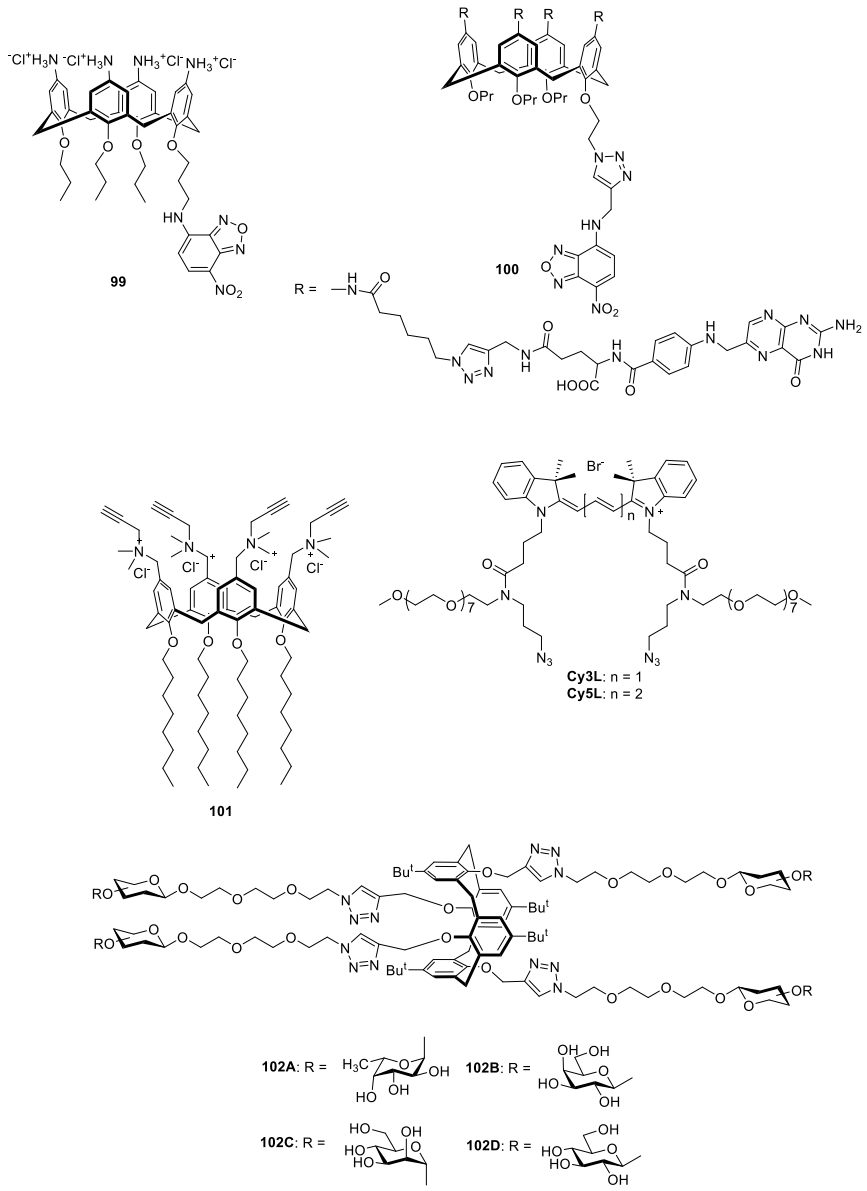

Figure 22. Chemical structure of calix[4]arene conjugates **99**-**102.**

In another investigation, Klymchenko and co-workers explored the possibility of developing calix[4]arene-based protein-sized fluorescent nano-particles (NPs) by tagging cyanines (**Cy3L**, **Cy5L**) onto the calixarene **101** core through a Cu(I)-mediated click reaction (Figure 22).[215] The resulting micelles **101**-**Cy3**L/**Cy5L**, exhibited a homogeneous particle size of approximately 7 nm, and a relatively broad bathochromically-shifted emission band. The fluorescent quantum yield of the micelles was found to be dependent upon the viscosity of the media that was lower relative to free **Cy3L** and **Cy5L**. This was ascribed to the aggregation-induced quenching effect.[216]

Furthermore, the microscopic imaging in HeLa cells showed that the brightness of **101**-**Cy3L**/**Cy5L** NPs was twice that of commercially available quantum dots (QD-585) (λ_{exc} = 532 nm). Although the resulting NPs possessed lower brightness in the microscopic images as compared to conjugated polymer nanoparticles (NPs),[217] their additional advantages such as stability in both aqueous and organic media, preferential cellular uptake, minimal leakage, and high signal to noise ratio with such a small size, suggest many potential future applications.

Vidal *et al.* developed a series of calix[4]arene glycoclusters **102A-D** (Figure 22), by tagging the calixarene scaffold with galactosidase or fucoside units through an azide-alkyne click reaction.[218] The binding affinities of these conjugates were tested towards two major soluble lectins (*i.e.,* LecA and LecB) of *Pseudomonas aeruginosa*, a pathogen known for the major cause of pulmonary infections. The conjugates **102A-D** exhibited significant bacterial clumping in a LecA-dependent manner only and induced antibiofilm-formation properties with significant antiadhesive activities. Confocal microscopic studies using conjugates **102A**-**D** and 4′,6′-diamidino-2-phenylindole (DAPI) indicate that bacterial cells were found close to the host cell membrane. The authors also tested the potential of these conjugates in mouse pulmonary lung infection models. Although compared to the cell-based studies with nanomolar activities, the comparable activity found in animal models was in millimolar range. This may be due to several unidentified adhesions, proteins or lectins that may compete with the target sites.

2.6.2 Gene delivery systems using fluorescent calix[4]arenes

Calixarenes have also been utilized successfully for gene delivery into cells. Ungaro and co-workers reported calix[4]arene derivatives **103**-**108** (Figure 23) bearing guanidinium groups and hydrophobic tails at the upper and lower rims, respectively and demonstrated their ability to interact, and transport DNA across the cell membranes.[219] It was observed that small, rigid calix[4]arene derivatives in the cone conformation formed strong complexes with the phosphodiester backbone of DNA. This was in part driven by the hydrophobic effect inducing non-polar group associations, resulting in compact, collapsed DNA plasmids. In contrast, the larger, conformationally flexible calix[6]- and calix[8]arene derivatives resulted in extended inter-strand aggregates with no observed

DNA collapse. Interestingly, only calix[4]arene derivatives **103A**, **103B** and **105** exhibited efficient transfection attributed to both electrostatic and non-polar interactions.

A new class of calix[4]arene-based cytofectins **109A-C** (Figure 23) bearing alkyl guanidinium moieties at the phenolic oxygen atoms have been developed.[220,221] They compacted DNA and served as efficient transfection agents with 2,3-di(oleolyoxy)propyl phosphatidyl ethanolamine (DOPE) as a helper lipid. Compared with the commercially available lipofectamine, these macrocyclic vectors exhibited better transfection efficiency. Additionally, the overall cell cytotoxicity was found to be negligible in this case.

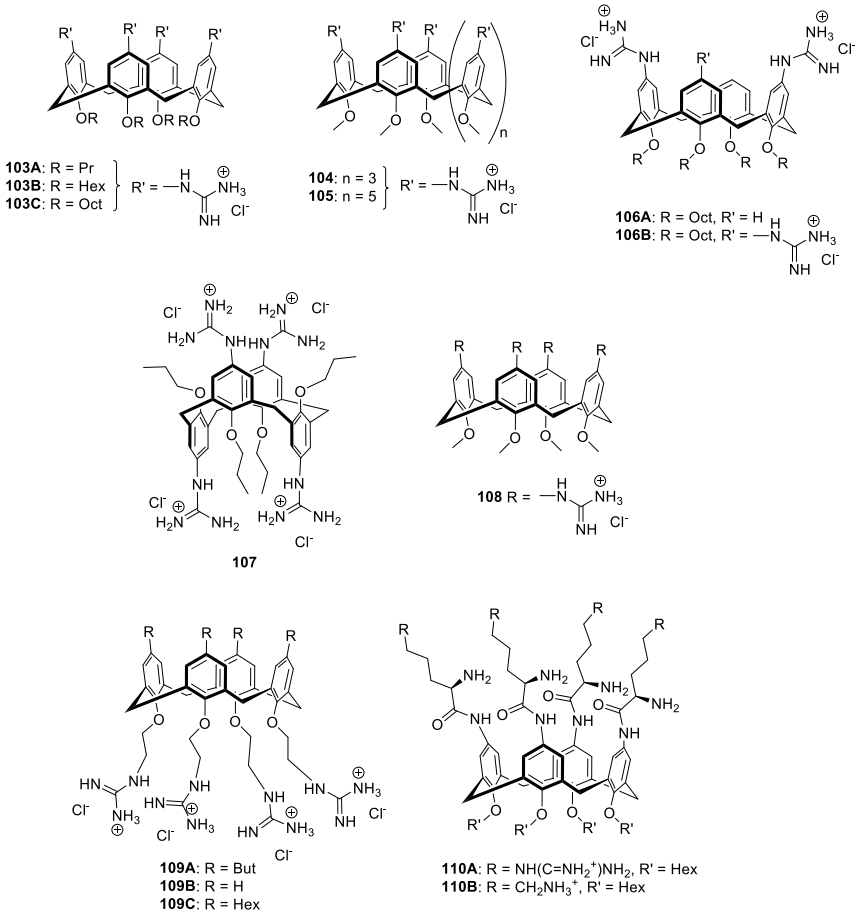

Figure 23. Chemical structure of guanidinium based calix[n]arene conjugates **103-110**.

In another report, the Ungaro research group synthesized calix[4]arene derivatives **110A-B** (Figure 23) with pendent arginine units with amino groups at both upper and lower rims.[222] Both derivatives were found to enhance the cell penetration of oligoarginine

fragments. In particular, the presence of unprotected α-amine groups was found to be responsible for protecting the vector-DNA complex from lysosomal degradation, resulting in the release of cargo into the cytosol.

More recently, Fernandez *et al*. reported calix[4]arene derivative **111** (Figure 24),[223] which was found to self-assemble in the presence of plasmid DNA. A new mechanistic model involving initial electrostatic interaction, followed by subsequent calix[4]arene bilayer formation with DNA, was revealed by various experimental analyses (DLS, TEM, and AFM). The higher expression of green fluorescent protein (GFP)-encoded plasmid pEGFP-C1 in COS-7 cells in the presence of **111,** as monitored using fluorescence microscopy, was attributed to greater effective transfection efficiency.

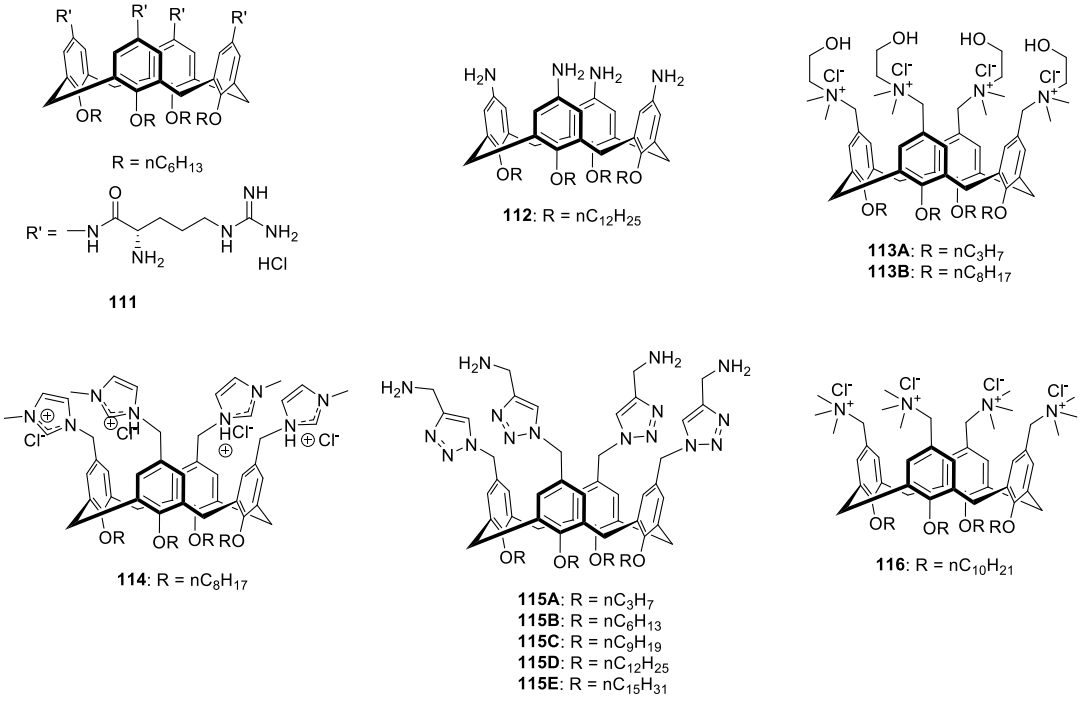

Figure 24. Chemical structure of calix[4]arene conjugates **111-116.**

Shahgaldian and co-workers investigated the ability of polycationic calixarene-based solid-lipid NPs derived from macrocycle **112** (Figure 24) to transfect mammalian cells.[224] Loading **112** with plasmid DNA and chitosan (a complementary polycationic polymer) in a layer-by-layer method led to a vector that could efficiently transfer DNA into Madin-Darby canine kidney (MDCK) cell cytoplasm. To visualize cellular uptake and the transfection process the dye tetramethylrhodamine was coupled with the chitosan; the

incubation of MDCK cells with **112**-DNA-chitosan NPs resulted in the appearance of the red fluorescence in the cytoplasm of MDCK cells indicative of cellular uptake.

In another investigation, Klymchenko and co-workers developed an amphiphilic cationic calixarenes **113A-B** and **114** (Figure 24) capable of forming two-step hierarchical assemblies with DNA for gene delivery applications.[225] A combination of DLS and fluorescence correlation spectroscopy techniques confirmed that the macrocycle **113A** bearing choline head groups was capable of forming micelles with a diameter of between 3-4 nm. On the other hand, **113B** and **114** formed micelles of 6 nm diameter. The authors found that all three macrocycles complex efficiently with DNA but *via* different interactions. Whilst the interactions in the case of **113A** were purely electrostatic, it was found to be both electrostatic and non-polar interactions driven together by the hydrophobic effect were key in **113B** and **114** bearing longer alkyl chains (octyl). The micelles formed by **113B** and **114** were found to condense DNA, thereby increase their average size to 65 and 55 nm respectively. As a model, calf thymus DNA (CT-DNA) was selected for gene delivery. Relative to NPs formed from **113A** and CT-DNA, both **113B** and **114**-CTDNA NPs exhibited low toxicity and high transfection efficiency in COS-7 and HeLa cells. This was attributed to their positive zeta potential leading to efficient endocytosis. Furthermore, the possibility for the optimization of larger calixarene-DNA based NPs was investigated.[226] The presence of longer alkyl chains resulted in small NPs possessing low polydispersity with minimal cytotoxicity and enhanced gene transfection. In contrast, the incorporation of additional amine head groups was found to alter the calix-DNA complex stoichiometry only.

Sakurai and co-workers synthesized a series of tetracationic, amphiphilic calix[4]arene-based conjugates **115A-E** (Figure 24) bearing alkyl chains with different lengths (C3-C15) at the lower rim. These derivatives were shown to form NP carriers for the transfection of pDNA.[227] The conjugate derived from calix[4]arene **115B** bearing C6 alkyl chains furnished maximum transfection efficiency, whilst **115E** conjugates hardly exhibited any favorable results due to poor pDNA condensation.

Similarly, the Junquera research group have highlighted the fact that polycationic calixarene-based **116** only forms successful vectors when combined with the zwitterionic lipid DOPE (Figure 24).[228] Strikingly, the transfection efficiency of **116**:DOPE based

lipoplexes was correlated to their ratio used and their interactions with biological membrane.

As the purely ionic-based interactions between the cationic groups in NPs and phosphate-carrying nucleic acid backbones are relatively non-specific, the combination with other non-covalent interactions such as hydrogen bonding or π stacking, present an opportunity to differentiate between base pairs, and the helical grooves of duplex D(R)NA. Shahgaldian and co-workers found that simple dodecyl bearing tetraguanidinium-based calix[4]arene derivatives exhibited a preference for binding poly-adenine-thymine (AT) sequences.[229] Likewise, the Alzvijeh group have reported that calix[4]arene conjugates **117A-B** (Figure 25) bearing arginine peptides at the lower rim exhibited sequence-specific minor groove recognition;[230] strong fluorescence enhancement was observed for 5′-fluorescein-labeled DNA upon interacting with **117A-B**. Peptidocalix[4]arene **117B** exhibited strong binding (K_a = 3.6 × 10^7 M^{-1}) towards well-matched DNA. Conversely, **117A** showed 27-fold stronger binding toward mis-matched DNA (K_a = 2.1 × 10^8 M^{-1}) compared to well-matched DNA (K_a = 7.8 × 10^6 M^{-1}), which was attributed to minor groove binding.

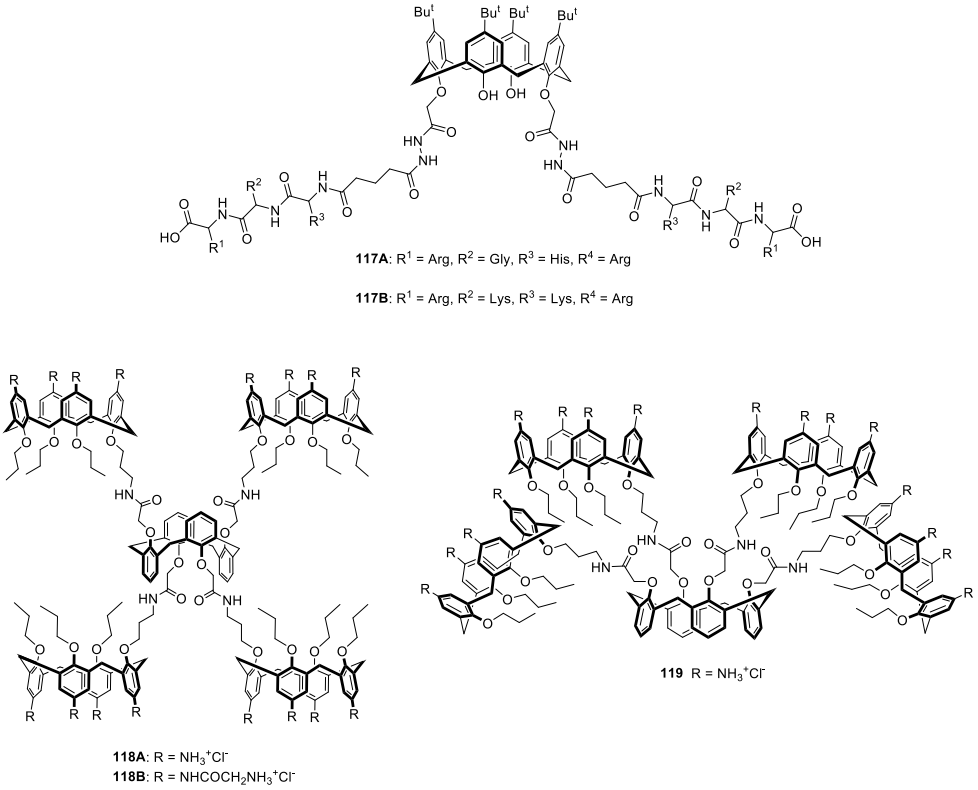

Figure 25. Chemical structures of calix[4]arene constructs **117-119**.

Matthews and co-workers developed amine functionalized multi-calixarene derivatives **118A-B** and **119** (Figure 25) to understand the cooperative role of pre-oriented functional groups in transfection studies.[231] These dendritic like calixarene conjugates were terminated with either free amine groups or glycyl moieties. Binding of DNA was only observed at low concentrations, while at high concentrations the calixarenes underwent self-assembly. Gene transfection was tested in CHO cells, revealed efficient delivery with no significant cell toxicity.

2.6.3 Drug delivery systems based on calix[4]arenes

Imatinib is an FDA-approved tyrosine kinase III inhibitor used as a chemotherapeutic agent for the treatment of chronic myeloid leukemia and gastrointestinal stromal tumors.[232-234] It is highly soluble, with more than 95% bioavailability. However, its strong interaction with plasma proteins such as albumin and α1-acid glycoprotein make it less available at the target site.[235-237] Additionally, patients undergoing treatment with the drug are prone to develop drug resistance due to various genetic mutations.[238,239]

Schramm *et al.* investigated the possibility of calix-mediated drugs and neurotransmitter transport.[240] Thus calix[4]arene **120A** bearing four phosphonic acid groups, homologs **120B** and larger calix[5] **121** and calix[6] **122** were targeted (Figure 33). It was found that **120A** and **120B** efficiently transported dopamine and serotonin under neutral and acidic conditions. Conjugate **120A** enhanced the transportation of calcein indicated by its enhanced fluorescence emission in the aqueous layer. Furthermore, it was observed that incorporation of trimethylammonium ethylene group to various lipophilic drugs such as ibuprofen, acetaminophen, and tamoxifen, enhanced their transportation efficiency with hosts **120A** and **120B**.

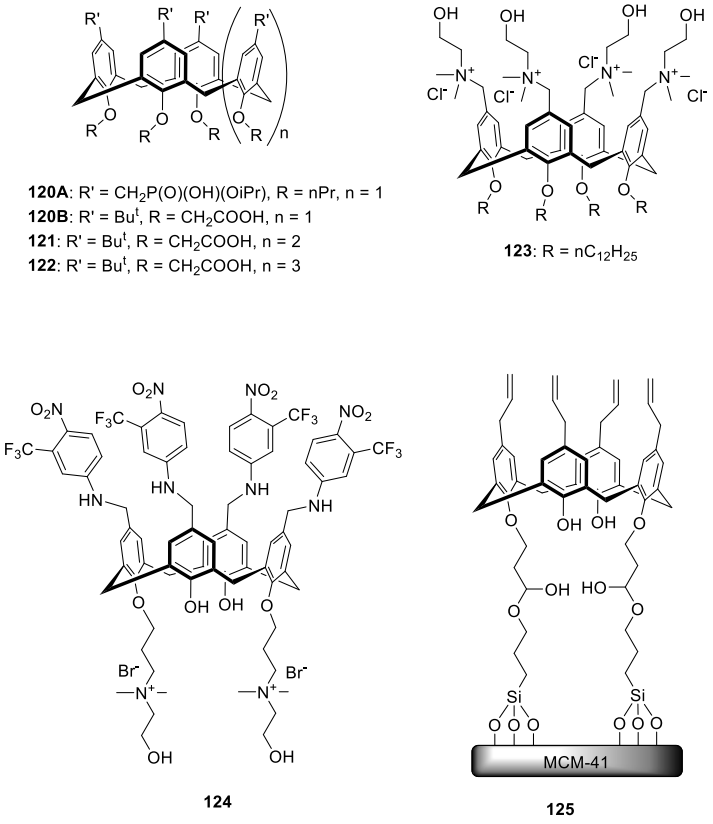

Figure 26. Chemical structure of calixarene derivatives **120-125**.

Consoli *et al.* reported on amphiphilic calix[4]arene **123** (Figure 26) as a carrier to deliver curcumin for ocular applications *in vitro* and *in vivo*.[241] Curcumin, a natural polyphenol, possesses multiple therapeutic properties including antimicrobial, anti-inflammatory, and antitumor activities.[242-244] However, its chemical instability, low water solubility, and its limited bioavailability due to its plasma protein interactions, and rapid clearance limits its clinical benefits.[245] Polycation **123** formed a clear colloidal assembly with curcumin having the appropriate size, stability, surface charge, and loading efficiency suitable for topical ocular delivery. Curcumin encapsulation within these assembled aggregates was strongly supported by a red shift in fluorescence emission from 540 nm in the free state to 610 nm in the bound. The choline groups in the assembly served to facilitate its passage through the cornea *via* both diffusion and choline transporters located in the iris. Without sacrificing viability, the assembly exhibited significant reduction in lipopolysaccharide (LPS) stimulated pro-inflammatory markers (I-kappa B kinase degradation, COX-2 and iNOS expression, nitrosative stress, and NF-κB p65

nuclear translocation) in J774A.1 macrophages compared to free curcumin. The assembly also significantly reduced the clinical inflammation in LPS-induced uveitis in rat models with good recovery signs.

Sortino *et al*. reported polycationic calixarene derivative **124** (Figure 26), decorated with 3-(trifluoromethyl)-4-nitrobenzenamines as a nitric oxide (NO) photodonor.[246] The quaternary ammonium linker at the lower rim provided sufficient aqueous solubility for the amphiphile to allow self-assembly into nano-aggregates. Further, light-triggered NO-induced bactericidal activity of these assemblies was shown against *Escherichia coli* ATCC 10536 (Gram-negative) and *Staphylococcus aureus* ATCC 6538 (Gram-positive).

Rao *et al*. developed an inorganic-organic hybrid-based material **125** (Figure 26), consisting of a mesoporous material MCM-41 (Mobil Composition of Matter-41) surface modified with a calixarene to deliver the anticancer drug doxorubicin (Dox).[247] The higher Dox loading capability of **125** (300% relative to the parent MCM-41) was ascribed to the hydrophobic core of the calixarene. Hybrid **125** exhibited a higher drug release profile at pH 5.0 than at pH 7.4, but a slow and sustained release of DOX relative to the parent material. These points suggest that **125** is ideal for sustained release of DOX in the acidic environment of many cancer cells. There was a slight preference for the Dox-loaded hybrid materials to be taken up by MCF7 cancer cells relative to HeLa and MDA-MB231 cancer cells. Thus, the internalization of Dox-loaded materials, as evaluated by fluorescence-activated cell sorting, revealed enhanced fluorescence and ~150% higher internalization into MCF7 cells compared to HeLa cells.

2.6.4 Sulfonatocalix[4]arene based receptors and their applications

Because they are both straightforward to synthesis and water-soluble, sulfonatocalix[4]arenes represent a significant sector of the calix[4]arene field.[248] Here we summarize recent developments with sulfonatocalix[4]arenes.

2.6.4.1 Sulfonatocalix[4]arene for self-assembly

Self-assembled fluorescent organic NPs have received increasing attention in chemo-and bio-sensing applications such as biomolecule and cell labeling,[249-252] memory devices, and logic gates.[253] The tetraphenylethene (TPE) moiety has been a prime target

in this regard; TPE is known to exhibit aggregate-induced emission (AIE) in which molecules are non-fluorescent when solubilized but emit strongly when they aggregate due to the restricted intramolecular rotation of the phenyl rings.

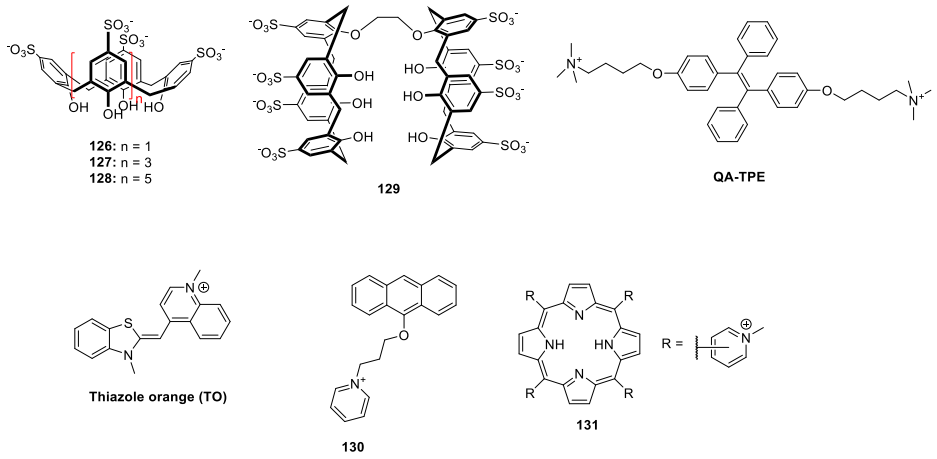

Figure 27. (A) Chemical structures of **128-133**, QA-TPE, and thiazole orange.

Liu *et al*.[254] reported a strategy for the construction of supramolecular assemblies *via* calixarene-induced aggregation (Figure 27). Quaternary ammonium-modified TPE (**QA-TPE**) was unable to aggregate because of unfavorable repulsive forces between terminal ammoniums that offset favorable π-π interactions. However, in the presence of sulfonatocalixarene derivatives **126** and **129**, strong AIE fluorescence was observed with a pronounced decrease in critical aggregation concentration.[255-259] From the fluorescence titration curve, the molar ratios of **126** and **129** to **QA-TPE** were found to be 0.5 and 0.25, respectively. These values respectively correspond to 1:2 (**QA-TPE**·**126**) and 1:4 (**QA-TPE**·**129**) stoichiometries. Aggregation was found to occur in two steps: (1) **QA-TPE** forms inclusion complexes where its ammoniums are encapsulated into the cavities of two **126** host molecules forming a 1:2 complex; and (2) electrostatic interactions between sulfonate groups of calix[4]arene and the positively charged groups of **QA-TPE**. SEM and DLS results suggested that both **126**·**QA-TPE** and **129**·**QA-TPE** formed spherical aggregates with an average diameter of 30 nm and 90 nm, respectively. Additionally, AFM images demonstrated that within the spherical morphology, **126**·**QA-TPE** formed multi-layered stacks, whilst regular linear arrays extending away from sphere were observed in the case of **129**·**QA-TPE**. Furthermore, photo-modulation of free **QA-**

TPE and its complex **126**·**QA-TPE** was examined. Upon UV irradiation, non-fluorescent **QA-TPE** cyclized to fluorescent diphenylphenanthrene. This photocyclization rate was significantly enhanced in the presence of **126**, which was attributed to the restriction of intramolecular rotation of the phenyl groups of **QA-TPE**.

Heyne *et al*.[260] observed an unexpected interaction between thiazole orange (**TO**) and calix[4]arene sulfonate **126** (Figure 27), whereby the calixarene acts as template for the formation of H-aggregates exhibiting side-by-side orientations of **TO**. The binding of **TO** into **126** was accompanied by fluorescence enhancement with a slight bathochromic shift of the emission band from 635 nm to 641 nm. Although the fluorescence enhancement was justified by the confinement of the **TO** dye into the calix[4]arene cavity, the bathochromic shift was unexpected since literature reports suggest that monomers of **TO** intercalate into DNA and undergo a hypsochromic shift.[261,262] Thus the observed fluorescence enhancement and bathochromic shift can't be attributed to **TO** binding with **126** in the monomeric form. To confirm this, the absorption spectra of **TO** was recorded in the presence of **126**. The absorption bands at 500 nm and 472 nm that correspond to monomeric and dimeric **TO** disappear completely upon addition of **126**, with the concomitant formation of new a band at 429 nm. Based on literature precedence,[263] this was ascribed to the formation of H-aggregates of **TO**. The fluorescence enhancement can be rationalized by the fact that the non-radiative decay of excited-state **TO** brought about by photoisomerization is reduced by the overall rigidity of the H-aggregates.

A pyridinium-substituted anthracene **130** (Figure 27) was found to bind in a 1:1 stoichiometry to upper-rim sulfonated calix[4]arene **126** to form a supramolecular amphiphilic assembly in water.[264] A K_a value of 4.22×10^5 M^{-1} was ascertained from fluorescence spectroscopy. DLS and TEM analysis revealed the size and morphology of the assemblies. The enhanced fluorescence emission of the complex was ascribed to a regulated intramolecular PET process, whereby the electron-rich cavity of the calixarene acted as the donor and the pyridinium as the acceptor. UV irradiation of the complex induced an accelerated photo-decomposition of the bound guest. Thus, after irradiation at 365 nm for 15 minutes, 52% of the bound guest decomposed in the presence of singlet oxygen ($^1O_2$), whilst less than 20% decomposed in the absence of **126**. Photolysis was expected to break the well-defined aggregate, and DLS confirmed a larger size

distribution indicative of the precipitation of insoluble anthraquinone produced. The photolysis of the complex was also possible using visible light and an exogenous photosensitizer such as eosin Y. The absorption spectra showed evidence of π-π stacking between eosin Y and the anthranyl group, although DLS data showed no size increase during the interaction between eosin and the complex. Degradation was more efficient upon irradiation at 520 nm.

Kubát *et al.* have studied the supramolecular interactions between sulfonated calix[n]arenes **126** (n = 1), **127** (n = 3), and **128** (n = 5) and various *N*-methylpyridinium *meso*-substituted porphyrins **131** (Figure 27) *via* transient absorption spectroscopy, cyclic voltammetry (CV), and DFT.[265] On its own, porphyrin **131** has a sub-150 fs $S_2 \rightarrow S_1$ relaxation time-scale, but upon complexation, there is a bathochromic shift in the Soret band, a decrease in quantum yields of the triplet states, and a shortening of fluorescence lifetimes. These changes were associated with PET within both the host-guest complex and porphyrin aggregates. The free energy associated with the electron transfer was obtained by using CV to determine the oxidation and reduction potentials of the donor calix[n]arene and the porphyrin acceptor. The oxidation of the calix[n]arene phenolates was complicated by an irreversible oxidation step. In contrast, the reduction of the porphyrin was reportedly a two-step process whereby the formed, unstable π-radical anion disproportionated to phlorin or chlorin. The electron transfer was shown to be an energetically downhill process. Though a comparison between the transient absorption spectra of the free and the bound porphyrins did not indicate any spectral changes in the S_1 state, there was a clear trend in an increase of fluorescence quenching as a function of increasing calixarene size. The authors also showed that fluorescence quenching of the S_1 state was more efficient at higher pH, suggesting that electron transfer emanates mostly from the ionized phenolate groups. DFT calculations suggested that the binding motif of the porphyrin to the calixarene was not “side-on”, where the pendant *meso*-groups reside inside the pocket of the calixarene. Rather, a “face-to-pocket” binding was proposed. Calculations also show that electron transfer occurred mostly in the pendant *meso*- groups of **131** in both the ground and excited states.

2.6.4.2 Sulfonatocalix[4]arene for enzymatic assays

As mentioned in the previous sections, the inclusion/displacement of guest species into/from a fluorescent macrocyclic reporter pair, can be exploited to assess both the concentration of a target as well as its relative change over time. This latter strategy has also been employed for monitoring enzymatic activity in a biological media through a product-selective assay.

Ammonium groups play many important roles in biology, and their ability to form inclusion complexes with sulfonatocalixarenes make them prime targets. Nau and co-workers reported a series of indicator displacement assays for monitoring the cationic by-products formed in amino acid decarboxylase-catalyzed reactions.[266] The host in question, *p*-sulfonatocalix[4]arene **126** (Figure 28), interacts strongly with fluorescent aminomethyl-substituted 2,3-diazabicyclo[2.2.2]oct-2-ene (**DBO**) to form a weakly fluorescent complex **DBO-126** (K_a = 2.3 ± 0.5 × 10^4 M^{-1}). However, this complex exhibited strong affinity for cationic alkylammonium products produced from decarboxylase-catalyzed reactions of amino acids that resulted in the displacement of DBO with enhanced fluorescence emission (Figure 28).

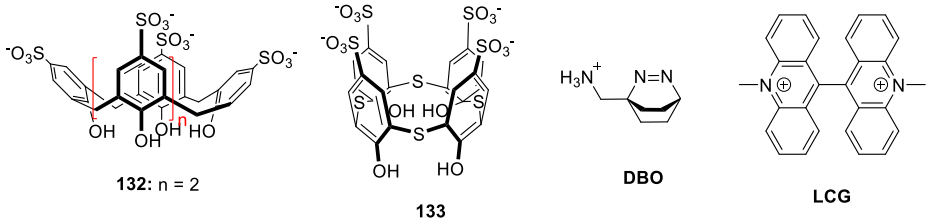

Figure 28. Chemical structures of calix[n]arene derivatives **132**, **133**, **DBO** and **LCG**.

Nau *et al*.[267] have introduced a label-free, economic, and convenient approach called substrate-selective tandem assay, in which a macrocycle has a higher affinity for a substrate than the corresponding product of an enzyme. In this approach, as the substrate is depleted so a fluorescent dye is able to form a complex with the macrocycle and produce the desired optical signal. Thus, enzyme activity can be monitored by observing the difference in fluorescence intensity of a dye before and after enzymatic reaction. Consider for example arginase, an enzyme that hydrolyses arginine to ornithine and urea in the last step of the urea cycle. The *p*-sulfonatocalix[4]arene **126** exhibited stronger binding of the substrate arginine than the ornithine (K_a = 6,400 and 550 M^{-1}

respectively). In contrast, **126** displayed an even stronger affinity for DBO (K_a = 6 × 10^4 M^{-1}) compared to arginine and ornithine, and showed strong fluorescence when free and weak fluorescence complex to **126**. Addition of arginase to a solution of **126**, arginine, and DBO led to the hydrolysis of arginine to ornithine and urea. This therefore allowed the DBO to form a complex with **126** resulting in an overall decrease in fluorescence intensity. The same authors also investigated enzyme inhibition by using known arginase inhibitors *S*-(2-boronoethyl)-L-cysteine (BEC) and 2-(*S*)-amino-6-boronohexanoic acid (ABH).[268] The reduction of arginase activity was signaled by a suppressed fluorescence response of the dye upon the addition of either of the two inhibitors. From the dose–enzyme activity plot, the IC_{50} values were found to be 3.7 ± 0.7 μM for BEC and 0.22 ± 0.04 μM for ABH.

The practical utility of such systems can be realized if the supramolecular host-dye pair has sufficient aqueous water solubility, is operational over a wide pH range, and the fluorescent dye exhibits a large fluorescence change in response to its binding or extrusion from the host cavity. For example, Nau *et al*.[269] have reported novel host-dye reporter pairs, consisting of one of three hosts, **126**, **132**, and **133** (Figure 28), and the fluorescent agent lucigenin (**LCG**, N,N'-dimethyl-9,9'-biacridinium dinitrate). Fluorescence spectroscopy, UV-Vis. spectroscopy, and isothermal titration calorimetry (ITC) revealed that **LCG** formed strong 1:1 complexes with each calixarenes **126, 132**, and **133**, and that fluorescence was quenched upon guest binding. The quenching efficiency followed the order: **126** (98%) > **132** (75 %) > **133** (70%). Charge transfer from the calixarene (electron donor)[270] to **LCG** (electron acceptor)[271] was assumed to be the mechanism for quenching.

These calixarene–**LCG** complexes have been used as reporter pairs to monitor choline oxidase activity of acetylcholinesterase (AChE) in an approach called substrate-selective enzyme-coupled tandem assay.[267] Butyrylcholinesterase (BChE) is an enzyme belonging to the family of serine enzymes that ubiquitously co-exist with AChE throughout the body[272] and acts as a scavenger to detoxify anticholinesterase compounds. In a number of reports, BChE has been used as an activator for converting prodrugs into active forms.[273] More importantly, an impaired function of BChE in humans is implicated in many disorders such as Alzheimer's and Parkinson's diseases, and has proved to be

important diagnostic biomarker for progression of these diseases.[274] With these points in mind, Liu *et al*. [275] developed a supramolecular tandem assay approach for monitoring the activity of BChE, and screening of inhibitors. Calixarene derivatives **126**, **132, 134**, and **135** (Figure 29) were used as hosts because of their strong binding affinity with cations.[276] Succinylcholine, a clinical neuromuscular relaxant, was employed as a substrate that could be hydrolyzed by BChE but not by AChE.[277] In the presence of BChE, the calixarene–**LCG** reporter pair showed fluorescence quenching as the reaction proceeds. Since BChE is highly specific for hydrolysis of succinylcholine this approach readily discriminated BChE in the presence of AChE.

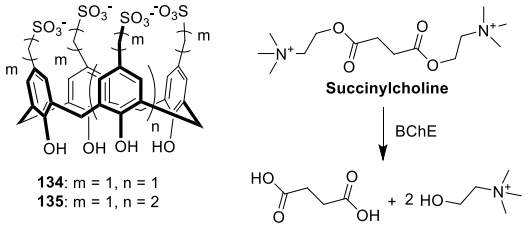

Figure 29. Chemical structure of calix[n]arene derivatives **134**, and **135**, and an enzymatic catalyzed reaction by butyrylchloinesterase BChE.

2.6.4.3 Sulfonatocalix[4]arenes as drug delivery carriers

Drug encapsulation within nanocarriers is achieved either by covalent or non-covalent interactions. However, both approaches have their own limitations. In the first approach, the drug loading efficiency is typically less than 10%, whilst the second typically requires a complicated synthetic procedure wherein the drug molecule must first be conjugated with a hydrophilic synthetic block, which then self-assembles to form drug-loaded nanoparticles. Liu *et al*.[278] proposed an alternative strategy wherein the drug-loaded carrier (drug chaperone) was fabricated by direct co-assembly of amphiphilic calixarene derivative **136** and the drugs irinotecan HCl (**IRC**) and mitoxantrone HCl (**MTZ**) (Figure 30). Their results suggested that the calix-drug assemblies were driven by a combination of electrostatic interactions between oppositely charged host and guests, and π-π interaction between the aromatic cores of the drug molecules. Since the hydrophilic groups of **136** are localized at the surface of each assembly, they further decorated the assemblies with biotin-pyridinium (BtPy) and hyaluronic-pyridinium (HAPy) ligands to

enhance cancer cell targeting. After treating with the ligating groups, the zeta potential of the surface of the **136**·**MTZ** complex decreased from -35 mV to -21 mV, indicating successful incorporation of the targeting ligands. The *in vitro* cytotoxicity of these assemblies was evaluated against MCF-7 cells (human breast cancer cells that over-express both biotin[279] and hyaluronic acid[280] receptors). Both assemblies were easily internalized into the cell *via* receptor-mediated endocytosis. The viability of cells treated with **136**+MTZ+BtPy assembly was significantly reduced (18%) relative to free MTZ (34%). Similar results were obtained with **136**+IRC assembly decorated with HAPy ligand.

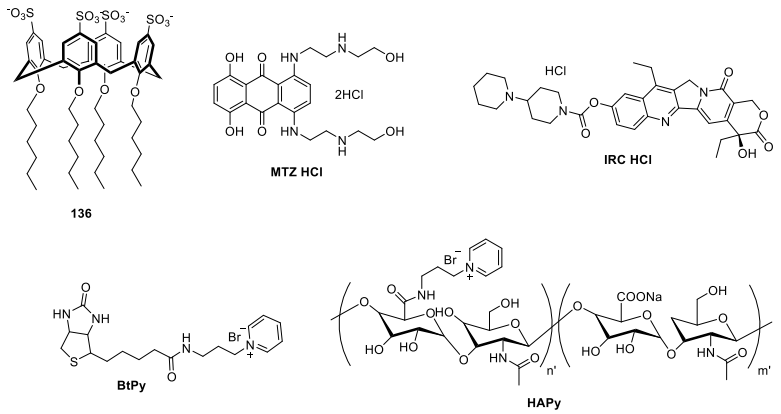

Figure 30. Chemical structures of anticancer drugs (**IRC** and **MTZ**), **136** and targeting ligands (**HAPy** and **BtPy**).

In another investigation, Liu *et al*.[281] fabricated calixarene coated liposomes by embedding amphiphilic calixarenes **137** (Figure 31) and **136** (Figure 30) into dipalmitoylphosphatidyl choline (**DPPC**) liposomes. The negatively charged outer surface furnished by the sulfonate groups provided the liposome enhanced stability in aqueous media. Thus, it was found that both **136**·**DPPC** and **137**·**DPPC** were highly stable at room temperature for 6 months, whereas simple **DPPC** liposomes precipitated after 7 days even after storing at 0 °C. This stability was attributed to the incorporation of charge-dense **136**/**137** into the surface of the liposomes maximizing electrostatic repulsions between liposomes. The incorporated calixarenes also allowed further surface modifications of the liposomes with suitably (pyridinium) appended molecules. For example, the incorporation of fluorescent tags such as **FITCPy**, or cancer targeting moieties such as **BtPy**) was readily established.

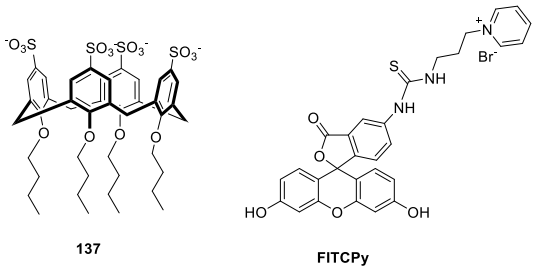

Figure 31. Chemical structure of calix[n]arene derivative **137**, and **FITCPy**.

2.7 Fluorescent calixarenes materials

The last few decades have witnessed a large and rapid development of smart functional materials such as organic electronics, light emitting devices, photovoltaics, and stimulus-triggered architectures. Calixarene conjugates have been intensively investigated and utilized for the role they have played in the development of these materials, particularly when incorporated into covalent or supramolecular polymeric systems. This section summarizes the role and utility of fluorescent calixarenes in these advances.

2.7.1 Fundamental photophysical and photochemical properties

The chromophoric properties of perylene bis-imide (PBI) units **138** (Figure 32) have been exploited by the Würthner group to build an extensive array of photoactive calixarene derivatives. The *bay* substituents of PBIs (X and Y in **138**) provide a convenient site for modulating the chromophoric properties, and the Würthner group have focused on three examples: an orange PBI (X, Y = H; R = $CH(C_5H_{11})_2$), a green analogue (X = H, Y = pyrrolidin-1-yl; R = cyclohexyl), and a red chromophore (X = Y = 4-*t*-butylphenoxy; R = butyl).

They have examined the photophysical properties of PBI-calixarene conjugates **139** and **140** (Figure 32, X, Y = H; R = $CH(C_5H_{11})_2$).[282] Both calixarene derivatives **139** and **142**, as well as model PBI derivative without calixarene substituents, were studied by UV-Vis absorption and steady-state fluorescence spectroscopy. In contrast to the strongly fluorescent PBI reference compound, solutions of **139** and **140** exhibit almost no fluorescence. Furthermore, although on the edge of instrumental limitations, the bis-calixarene **140** clearly showed weaker emission than **139**. Fluorescence lifetime

experiments revealed that the reference compound possessed a lifetime (τ) of between 3.9 and 4.9 ns depending on the solvent. However, in both calixarene derivatives, τ was less than 150 ps. CV of mono-calixarene **139** revealed two reversible reduction bands attributed to the radical mono-anion and di-anion of the PBI chromophore and an irreversible oxidation wave assigned to the oxidation of the calix[4]arene moiety. Building on this, the authors estimated the Gibbs free energy for the intramolecular charge separated state (ΔG_{CS}) of **2** to be –0.418 eV. That is, the electron transfer from the calix[4]arene moiety to the photo-excited PBI core is exergonic, and that the creation of a charge-separated state in **139** explains the very low fluorescence of **139** (and **140**). Femtosecond transient absorption spectroscopy identified an intense bleaching due to the $S_0 \rightarrow S_1$ transitions of the PBI chromophore, as well as an intense negative signal attributed to the stimulated emission of the chromophore; these features were accompanied by a strong positive absorption band for **139** and **140** assigned to the $S_1 \rightarrow S_n$ absorption of the orange perylene. For definitive proof, the authors turned to global and target analysis that avoided the inherent problem of fitting measured kinetic profiles at single wavelengths when several processes are occurring simultaneously. These more complex analyses provided clear evidence of the formation of a charge-separated and a PBI mono-anion and demonstrated that the lifetime of bis-calixarene **140** was approximately half that of the mono-calix **139**.

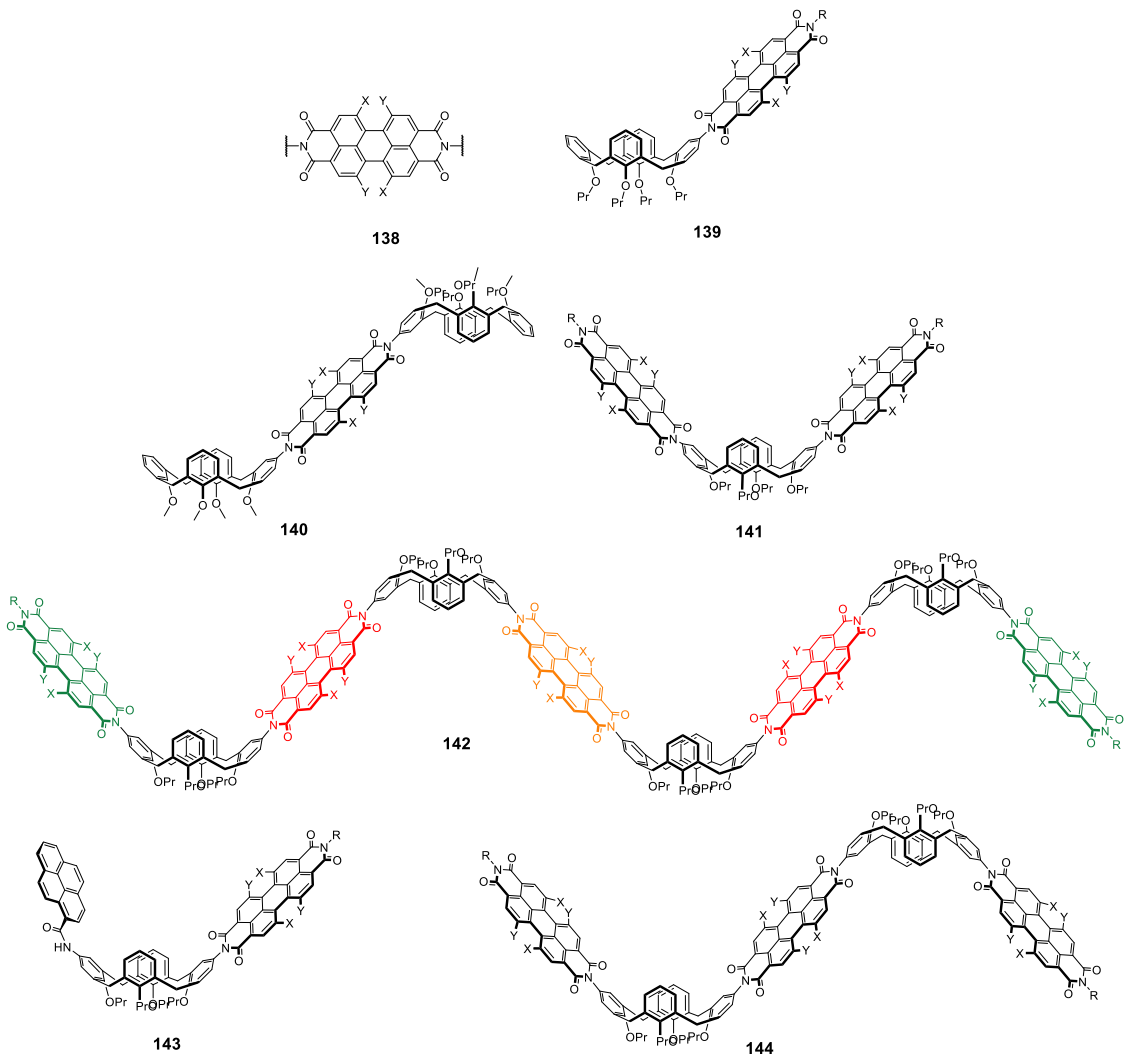

Figure 32. Perylene bisimide (PBI) moiety **138** with variable substituents X and Y at the *bay* positions. Calix[4]arene-PBI conjugates **139-144**. (a) For **139** and **140**: X, Y = H; R = $CH(C_5H_{11})_2$); (b) For **141** and **142**: Green: X = H, Y = pyrrolidin-1-yl, R = cyclohexyl; Orange: X, Y = H, R = $CH(C_5H_{11})_2$; Red: X, Y = 4-t-butylphenoxy, R = butyl; (c) For **143**: X, Y = H, R = $CH(C_5H_{11})_2$; (d) For **144**: X,Y = 4-*t*-butylphenoxy; R = butyl.

The same group have studied the effect of coupling different PBI units to calixarenes to form zig-zag arrays.[283] "Dimer" **141** and "pentamer" **142** are two such examples (Figure 32). The bis-PBI calixarene can exist in two pinched cone conformations: where the opposing PBI moieties are either stacked, or not stacked. Molecular modelling and VT ^{1}H NMR data supported the idea that the pinched cone conformation with outward oriented PBI groups predominates. UV-Vis absorption and steady-state fluorescence emission also supported this. Thus, relative to simple PBI dye models, none of the investigated arrays displayed new absorption or emission bands; there was little, if any,

ground state interaction between the chromophores of each calixarene. As a result, the absorption properties of any arrays were simple combinations of the individual absorption patterns of the model chromophores. By examining energy transfer and fluorescence quantum yields, efficient energy transfer between proximal orange and red (and proximal red and green) PBI units was determined. However, only limited energy transfer between proximal orange and green subunits was observed. This was attributed to energy transfer from the excited orange to the green PBI chromophore, and concomitant electron transfer from the calix[4]arene core to the orange PBI moiety. Femtosecond transient absorption spectroscopy confirmed an efficient energy transfer process from the orange and the red PBI unit to the green. However, it was global and target analysis of femtosecond transient absorption data-matrices that provided the most detailed information; the lifetimes and the true spectra of the individual excited state species. Thus, in good agreement with Förster theory, the excellent spectral overlap of orange/red and red/green chromophores allowed trimers to display very fast and directional energy transfer (*e.g.* 4 ps and 89% efficiency), whereas if a red "mediator" chromophore was absent, transfer between orange and green was slower and less efficient (7 ps, 62%).

To probe in more detail the preferred orientation of PBI units is these derivatives, the Würthner group has examined the photophysical behavior of six PBI calix[4]arenes: the "monomers" **139** and the "dimer" bis-1,3-calixarenes **141** (Figure 32).[284] This work took advantage of the fact that the different bay substituents not only affect the chromophoric properties, but also the overall steric hindrance of the PBI moiety. As alluded to above, each bis-PBI calixarene can exist in two pinched cone conformations: where the opposing PBI moieties are either stacked or not stacked. The photophysical behavior of all six calixarene derivatives of **139** and **141** was referenced to the three corresponding PBI dyes devoid of calixarene moieties. Analysis of the ^{1}H NMR data for dimers **141** confirmed their dynamism but could not unequivocally differentiate between the stacked-non-stacked equilibrium being fast on the NMR timescale, or slow on the NMR timescale but biased towards one conformer. Moreover, VT NMR work revealed other conformational equilibrium in operation. UV-Vis absorption in a variety of solvents showed that in non-polar solvents dimers **141** ("green" and "orange") primarily existed as their intramolecular π-stacked form. However, there was very little evidence of solvent-

induced π-stacking of bulky "red" dimer **141**. This preference for solvent-induced stacking in the dimers was also revealed by steady-state fluorescence emission spectroscopy. Thus, whereas monomer **139** and its reference PBI dye showed typical emission spectra, "orange" dimer **141** exhibited a solvent-dependent excimer emission band. Fluorescence quantum yield data further supported this picture, as did molecular modeling and potential of mean force calculations. Going further, time-resolved emission spectroscopy showed that the fluorescence lifetimes of the reference dyes showed no dependence on solvent polarity, whereas the monomer **139** and dimer **141** possessed drastically shortened lifetimes; phenomenon induced by the very efficient photo-induced electron transfer process from the electron-rich calix[4]arene substituent to the electron-poor orange PBI unit. Finally, femtosecond transient absorption spectroscopy and global and target analysis provided exquisite detail of the dynamics of the PBI dimers, including the lifetimes and true spectra of the individual excited-state species. This data unequivocally showed that the π-stacked conformations of dimers decay *via* an excimer state, whereas the non-stacked conformers decay through a charge separation process involving electron donation from the calix[4]arene.

In related work, the groups of Würthner and Williams have appended an electron-donating pyrene and a PBI acceptor onto a calix[4]arene scaffold (Figure 32, **143**).[285] Both UV-Vis absorption and fluorescence spectroscopy indicate a strong interaction between the donor and acceptor. Femtosecond transient absorption spectroscopy revealed a fast, charge separation phenomenon to form the radical cationic pyrene and radical anion PBI moiety. Formation of this charge transfer complex was observed in all solvents investigated, suggesting that **143** has a predisposition to form a π-stacked conformation. Unique to the solvents investigated, in THF calix **143** possessed two excited-state decay channels. These were attributed to a dominating π-stacked conformation showing fast charge transfer (< 0.1 ps), and a non-stacked conformation possessing a slower photo-induced electron transfer. When **143** was irradiated at 350 nm in this solvent, pyrene excitation led to a fast, competitive charge separation process from the non-stacked conformation in which the pyrene acted as an electron acceptor, and the calixarene moiety acted as an electron donor.

With the idea of using fluorescent calixarenes to sense strain and hence detect inhomogeneities in polymer films, Würthner, Brouwer and co-workers have used probe **139** as a single molecule reporter for the glass transition temperature (T_g) of a polymer.[286] This approach exploited the sensitivity of PET processes involving PBIs to their surroundings. The UV absorption of **139** was similar to that of the parent PBI **138**, with a fluorescence emission spectrum the mirror image of the absorption spectrum. However, the emission intensity was largely diminished due to electron transfer from the electron-rich calixarene core to the electron-poor PBI moiety. Reporter **139** was embedded into different polymer films, including those of polystyrene, poly(methyl acrylate), and poly(vinyl acetate). Using variable-temperature fluorescence measurements it was shown that the observed fluorescence intensity change correlated with the T_g of the polymeric medium. Wide-field microscopy imaging showed that the number of individual molecules that could be counted was highest around T_g, and the intensity of the fluorescence of individual molecules decreased as a function of increasing temperature. This indicated that above the T_g, there is enough free volume in the polymer matrix which promotes PET and hence fluorescence quenching. It was also shown that the fluorescence could be switched on and off multiple times by switching the environment of the probe.

The Köhler and Würthner groups have carried out detailed single-molecule studies on the calix[4]arene-PBI dimer **141** (X,Y 4-*t*-butylphenoxy; R = cyclohexyl) embedded in a polystyrene matrix.[287] The authors distinguished three kinds of blinking arising from three distinct intensity levels: 1) a high-intensity level attributed to a dimer described as two independent emitters; 2) an intermediate intensity level attributed to the emission from one of the PBI moieties in a dimer whilst the other one is either reversibly in a non-fluorescent state or irreversibly photo-bleached; and 3) a background level corresponding to a doubly photo-bleached calixarene. The charged dark-state of **141** was assumed to form in one of two ways: charge tunneling between the PBI and the embedding polystyrene matrix, or photo-excitation of an electron from the calixarene to the PBI moiety and reduction of the cationic calix. Although it was not possible to distinguish between these two options, the subsequent neutralization process was determined to arise by charge tunneling between the PBI and the surrounding matrix. The different types

of blinking were themselves attributed to: 1) a molecule of **141** located within a large polymer cavity in which reversible reduction of one of the PBI units forms the radical anion and there is a subsequent efficient excitation energy transfer; 2) a dynamic, time-dependent PBI → $PBI^{-\cdot}$ energy transfer from a molecule of **141** within a smaller polymer cavity; in this situation the charge on one of the PBI units is assumed to reside on the most distant carbonyl oxygen with respect to the neutral PBI; 3) a blinking process induced by a relatively slow PBI → $PBI^{-\cdot}$ excitation energy transfer. This last process was attributed to the situation whereby charge resides on the carbonyl oxygen closest to the neutral PBI unit, inducing a strong local electrostatic field and inducing a Coulomb blockade.

In more recent work studying the fluorescence of PBI-calixarene conjugates as a function of time, it was demonstrated that the common conclusion that stepwise decreases in emission intensity from multi-chromophoric systems arises from sequential photo-bleaching of individual subunits may not necessarily be true.[288]

Consider for example PBI conjugate **144** (Figure 32, X,Y = 4-*t*-butylphenoxy; R = butyl) and model **140** (Figure 32, X,Y = 4-*t*-butylphenoxy; R = butyl). Ensemble experiments were as anticipated. Thus, the absorption spectra of **140** and **144** were very similar, with a maximum at 573 nm and a shoulder at 533 nm corresponding respectively to the electronic $S_0 \rightarrow S_1$ transition and the transitions in the vibrational levels of S_1. Additionally, a band at 400–475 nm was attributed to the transition into a higher excited singlet state ($S_0 \rightarrow S_2$). In the fluorescence spectra, a 3 nm red-shift from the model **140** to the trimer **144** emission was attributed to perturbation induced by the calix moiety. These results reveal a weak electronic interaction between the PBI subunits within **144**, both in the ground state and in the electronically excited states.

Complementary single molecule experiments examined three different molecules of **144**. In the first, the total intensity as a function of time showed three intensity steps that potentially could be interpreted as arising from the sequential bleaching of the individual PBI groups. However, additional information from the polarization resolved trajectories and spectra revealed that this was not the case. Rather, the authors showed that the best model consisted of three different scenarios for the relative orientations of the transition-dipole moments and the relative site energies of the emitting subunits. The

second and third single-molecule targets were described within a similar framework, but their unique intensity trajectories required different scenarios of transition dipole orientations and relative energy levels. In combination, this data revealed that changes in fluorescence intensity as a function of time is best described by a combination of photo-bleaching, fluctuations of absorption cross-sections and/or quantum yield, and temporal variations of energy transfer pathways. More importantly, perhaps the data revealed that in multi-chromophoric systems such as **144** it is not possible to neglect the competition between downhill energy transfer and thermally activated, uphill energy transfer processes.

2.7.2 Materials applications

2.7.2.1 Nonlinear, OLED and multi-photon materials

A collaborative effort has investigated the geometry and second-order nonlinear optical properties of alkynyl expanded donor–acceptor calixarenes.[289] Sonogashira coupling was used to functionalize either the upper or lower rim of a calix[4]arene core with three different ethynylphenyl substituents (4-NO_2, 4-CF_3, and H). Three families were synthesized (Figure 33), those with two or four substituents at the upper rim (**145** and **146**) and those with two at the lower rim (**147**). A comparison of the absorption spectra of these calixarenes with tolane models revealed small spectral shifts. Thus, to a first approximation the chromophores of the calixarenes did not electronically communicate. That stated, data for the calixarenes functionalized at the lower rim suggest some weak interactions between adjacent subunits. The authors also used hyper-Rayleigh scattering to probe the second-order nonlinear optical properties of the calixarenes, specifically the wavelength dependent hyper-polarizability (β) and the wavelength-independent hyper-polarizability (β_0). This data, in conjunction with X-ray structures, revealed the opening angle θ between the chromophoric tolane subunits. Thus, in the cases studied, consistently larger opening angles were found for the upper rim disubstituted calixarenes than for the lower rim disubstituted analogies, with the largest angles observed in the tetra-substituted calixarenes.

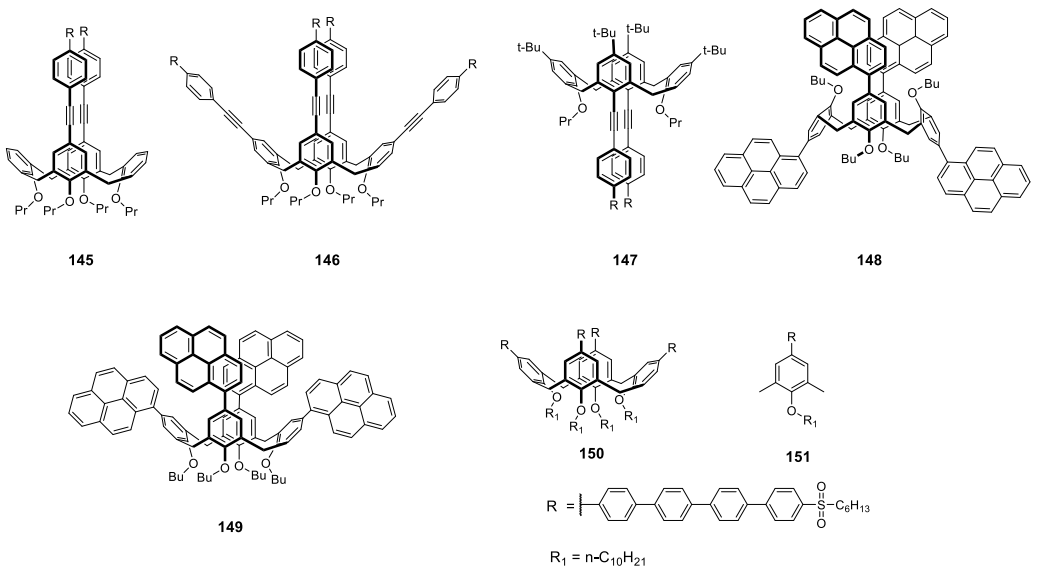

Figure 33. Structures of calix[4]arene based materials **145-151**. For **145**-**147**: R = NO_2, or CF_3, or H.

In 2012 the Sellinger group reported a *tetra*-pyrenyl 1,3-alt-calix[4]arene **148** as a solution processable, non-doped, and blue fluorescent OLED.[290] The photophysical properties of both **148** and its corresponding cone conformer calixarene **149** were examined in both dilute chloroform solutions and in thin films. This latter work revealed that aggregation of either hosts was minimal in the solid state. Moreover, spin-coating solutions of these two calixarenes (as well as a model pyrene derivative) on an indium tin oxide/poly(3,4-ethylenedioxythiophene):polystyrene sulfonate surface led to materials with excellent blue emission. The electroluminescence profile of each material was very similar to their photoluminescence properties, however the device from the 1,3-alternate **148** performed more efficiently than the corresponding device built with the cone calixarene **149**. Specifically, the former showed a maximum current efficiency of 10.5 cd A^{-1} at 14 mA cm^{-2} (external quantum efficiency = 6.4%) and a maximum luminous efficacy of 4 lm W^{-1} at 6.1 mA cm^{-2}. Moreover, even at high brightness the current efficiency remained high.

Kok Wai Cheah and co-workers have reported the multi-photon absorption properties of a strongly violet emissive calix[4]arene substituted at the upper rim with terphenyl groups.[291] Calix **150** (Figure 33) was composed of a decyloxyaryl donor, quaterphenylene core and hexylsulfonyl as acceptor. When compared to a model quinquephenylene **151**, both compounds showed a broad absorption band at 319 nm,

i.e., in the electronic ground state, little chromophoric interactions between donor–acceptor chromophores were observed. In contrast, excitation at this absorption maximum led to strong violet-light emission for both **150** and **151** between 407-425 nm, but with the emission maxima of **150** red-shifted by 18 nm relative to **151**. Thus, excitonic interactions between the quaterphenylene groups of **150** do occur. Furthermore, the authors showed that although the array of four dipolar units in **150** possessed a similar, high, fluorescence quantum yield to **151** (Φ_{PL} = 0.79), **150** had a longer excited state. Finally, the effect of these chromophoric interactions in **150** on its nonlinear optical properties was examined utilizing femtosecond pulsed laser. These studies revealed that **150** showed strong multi-photon induced photoluminescence upon excitation at 650, 960, 1250 and 1450 nm, correspond to the two-, three-, four- and five-photon absorption. The authors also examined the two-photon absorption cross-sections (σ_2) of **150** and **151**, determining that σ_2 of **150** was a synergistic 5.4 times that of **151**. This enhancement was observed throughout the measured spectrum and was ascribed to the excitonic coupling of the proximate donor–acceptor.

2.7.2.2 Tuneable self-assembled fluorescent aggregates

The Hirsch group have synthesized a water-soluble, fluorescent calix[4]arene with an overall amphiphilic structure: water-solubilizing G1 dendrons at the 1,3-positions on the lower rim, and PBI units at the 2,4-positions on the upper rim (**152**, Figure 34).[292] The upper-rim substitution provides a large surface for π-π stacking resulting in a preferred closed “pinched-cone” conformation. In a $CHCl_3$/TFA solvent system three well-resolved vibronic bands were observed in the UV spectrum corresponding to the 2–0, 1–0, and 0–0 transitions of the $S_0 \rightarrow S_1$ band of the perylene chromophore polarized along the molecular axis. The fluorescence spectrum of **152** was stokes-shifted relative to a PBI model. In both cases, in polar organic solvents, the 0–0 transition band was the highest intensity, characteristic of non-aggregated PBI units. In water, however, the absorbance and fluorescence intensities change drastically; the 1–0 transition band becomes the most prominent, characteristic of aggregated PBI moieties. Furthermore, the intensities were also reduced to 20% relative to the non-aggregated system. Dilution studies in water showed that the absorption and fluorescence emission bands did not shift as a

function of concentration, pointing to an intramolecular PBI dimerization and closed pinched-cone conformation. Cryo-TEM revealed **152** formed rigid, tube-like aggregates with lengths ranging from 8-100 nm and diameters from 8- 20 nm. Changing the dielectric of the solvent by incrementally adding THF unsurprisingly changed the fluorescence signature of the molecule. Starting from pure water, the 0–0 and the 1–0 transition bands hypsochromically shifted up to a ratio of 30% THF (v/v). Complementary to the fluorescence data, cryo-TEM shows aggregates that formed within days of titration of up to 30% THF. These aggregates had a polymorphous appearance with lengths of several hundred nm and diameters of ~5 nm. Within 4 weeks, however, the dense fibrous aggregates were replaced with long striated fibers. In contrast, dissolution of **152** directly in 30% THF in water resulted in hollow, fibrous aggregates, with outer diameters of 8 nm, and inner diameters of 2 nm. Molecular dynamics (MD) simulations suggest that this swelling occurred due to the tubular hydrophobic cavity accommodating THF molecules.

The Hirsch group has used fluorescence to probe the assembly of amphiphilic calixarenes.[293] The chromophoric benzamide groups of **153** (Figure 34) allow fluorescence spectroscopic probing of micelle formation. Dissolution of **153** in water containing twelve equivalents of NaOH and monitoring the intensity of the benzamide band at 490 nm revealed a critical micelle concentration (CMC) of 2.2×10^{-5} M, a result confirmed by conductance measurements. Analogous experiments buffered to pH 7 and 9 revealed higher CMC values, whilst cryo-TEM revealed a pH-dependent aggregation. Thus, pure **153** forms predominantly rod-like and spherical micellar aggregates at pH 7, and mostly uniform spherical micelles at pH 9. At pH = 7.2, TEM image-averaging revealed twelve molecules in each assembly and an overall D_2-symmetry. Moreover, at pH = 4 calix **153** formed very large and wrinkled membrane sheets of micrometer size possessing a regular pattern of uniform pores of 5.0 nm diameter. Pyrene guests were found to complex with the assemblies and were noted to alter their properties. Monitoring the intensity ratio between the first and third vibronic bands I_1 and I_3 of pyrene guests revealed that under basic conditions the guests in the micellar aggregates were predominantly exposed to the more polar-regions at the upper rim of the calixarenes. The lack of excimer emission confirmed that in this situation pyrene was itself not aggregating.

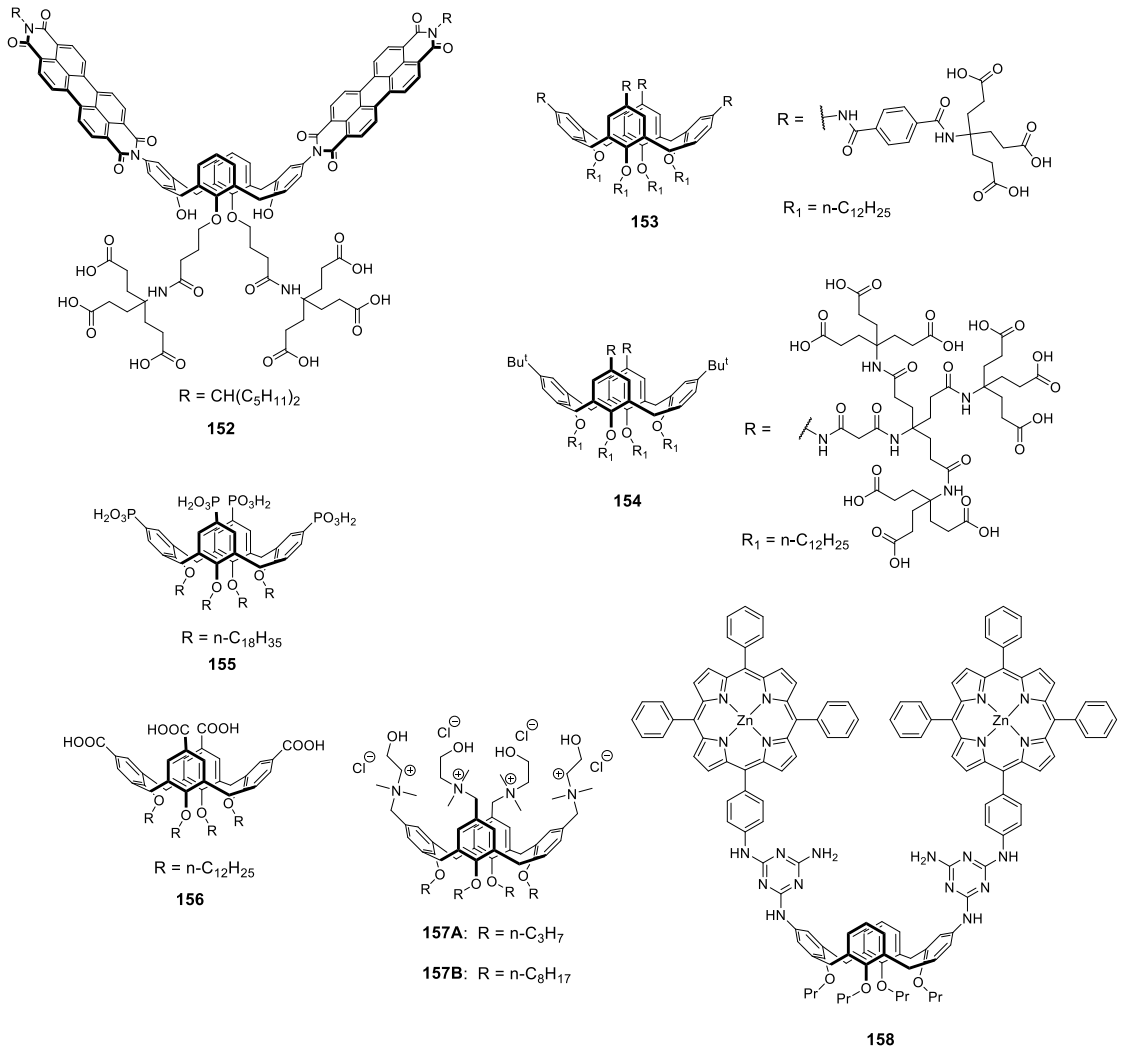

Figure 34. Structures of calix[4]arene based self-aggregated materials **152-158**.

Amphiphilic dendro-calixarene **154** (Figure 34) has been found to persist in aqueous media and have a CMC lower than 40 μm.[294] Fluorescence data show that pyrene is solubilized by the calixarene in aqueous media. However, the first and third vibronic bands of pyrene (I_1 and I_3) suggest that there is incomplete shielding of pyrene by the calixarene.

The Raston group have synthesized a *p*-phosphonic acid calix[4]arenes with lower rim C18 pendent groups (**155**, Figure 34), and shown with AFM that it assembles from toluene into a mat of interwoven fibers of uniform diameter of 6 nm.[295] Molecular modeling suggested that these fibers are composed of self-assembled discs, each of which is comprised of sixteen calixarene subunits oriented with their polar lead groups around the

circumference of the disc. Modeling also suggested the embedding of toluene molecules within the assembly. The interwoven fibers of **155** underwent dramatic expansion upon exposure to 7-nitro-4-(prop-2-ynylamino)benzofurazan. Thus, deposition of the material from toluene in the presence of this fluorescent guest resulted in nano-fibers of approximately 125 nm diameter.

The amphiphilic *p*-carboxycalix[4]arene **156** (Figure 34) has been found to self-assemble at the air-water interface to form monolayers that responded to the presence of divalent 4th-series transition elements Ni^{2+}, Cu^{2+}, Co^{2+}, and Mn^{2+}.[296] Changes in the assembly were examined with Langmuir compression isotherms, Brewster angle microscopy, and surface sensitive X-ray scattering. This revealed that the presence of Cu^{2+} ions were the most affecting. A number of X-ray techniques, including X-ray near-total-reflection fluorescence, showed that the polar rims of the calixarenes bound the copper ions relatively strongly, and the presence of $Cu(OH_2)_2$ clusters below the monolayer.

The aggregation properties of two cationic calixarenes with propyloxy **157A** or octyloxy **157B** chains on their lower rim have been investigated by the encapsulation of fluorescein dyes (Figure 34).[297] Both calixarenes form positively charged aggregates with similar ζ-potentials. The octyloxy calixarene **157B** was found to have a substantially lower critical aggregation concentration value and formed aggregates 1.5 times larger than **157A**. More interestingly, the nature of the aggregates was noted to affect the fluorescence spectra of each encapsulated dye by perturbing the equilibria relating their different tautomers and constitutional isomers. This allowed the authors to conclude that only aggregates of octyloxy **157A** closely resemble the micelles of common cationic surfactants.

Towards the formation of non-covalent assemblies comprised of porphyrin arrays, Bisht *et al.* have reported the synthesis of 1,3-melamine-porphyrin disubstituted calix[4]arene **158** (Figure 34).[298] This calixarene assembles into a D_3 symmetric trimer or “rosette” in the presence of barbituric acid derivatives. The authors noted that, relative to earlier pioneering work from the Whitesides group, these 3:6 host/guest assemblies were stable in concentrations as low as 10^{-4} M. The assemblies where characterized by ^{1}H NMR, MALDI MS, and UV-Vis and fluorescence spectroscopy. Regarding the last of

these techniques, assembly resulted in a red-shift of the characteristic porphyrin emission to 700 nm, as well as a 20-fold increase in emission intensity.

2.7.3 Calixarene conjugated polymers

The Prata group have reported the synthesis of a novel fluorescent (*p*-phenylene ethynylene)-calix[4]arene-based polymer **159** (Figure 35) using the cross-coupling polymerization of the corresponding bis-calix[4]arene and 1,4-diethynylbenzene.[299] GPC revealed that the number-average molecular weight of the polymer was 23,300 g mol^{-1}. A model polymer devoid of the calixarene groups was also synthesized for comparison. IR, NMR, and GPC spectroscopy were used to characterize the polymers, with the consensus of data identifying a length of eleven repeat units in the case of **159**. Absorption and fluorescence analyses of **159** and the model revealed that they shared similar absorption and HOMO–LUMO energy gaps, suggesting that they have analogous conjugation lengths despite the higher degree of polymerization in calix-polymer **159**. Similarly, both polymers possessed nearly identical fluorescence spectra and calculated solution quantum yield (Φ_{162} = 0.43 versus Φ_{model} = 0.51). New fluorescent calix[4]arene–carbazole-containing polymers have been synthesized and their photophysical properties determined.[300] Both 2,7- and 3,6-substituted 9*H*-carbazoles formed the basis of these polymers, linked through phenylene-*alt*-ethynylene linkers appended with *bis*-calix[4]arenes (**160** and **161** respectively, Figure 35). NMR experiments revealed the expected structures, suggested a degree of polymerization for **160** and **161** to be six and three to four respectively, and highlighted that the cone conformation of the calixarene was maintained in each. Gel Permeation Chromatography (GPC) revealed that the 2,7-substituted polymer had approximately 3-4 times the mass average molar mass of the 3,6-isomeric polymer. The UV-Vis and fluorescence spectra for solutions of the two polymers confirmed a number of key points. First, the large, distinct molar absorptions in the UV-Vis spectra revealed fully spin-allowed π-π electronic transitions reflective of the conjugation within each polymer. Relatedly, drop-casted films showed absorption similar features, suggesting limited aggregation within the film. As expected, of the two materials the solution luminescence of the 2,7-polymer **160** was the higher of the two materials, and its emission shifted to lower energies. The stokes shifts of 36–42 nm for the two

polymers relative to the monomers indicated that a sizeable conformational reorganization accompanied excited-state relaxation. Both polymers were also emissive in the solid state and were only slightly red-shifted relative to solution.

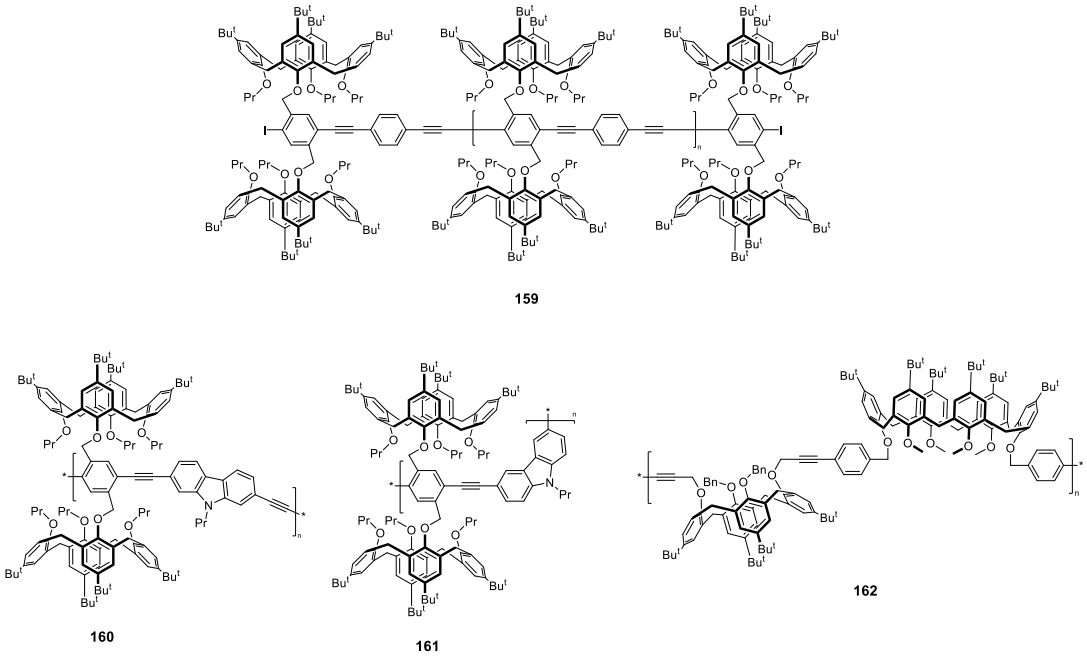

Figure 35. Structures of calix[4]arene based polymers **159-162**.

The Ogoshi and Nakamoto groups have synthesized the first copolymer comprised of alternating calix[4] and calix[6] groups (**162**, Figure 35).[301] To examine the binding properties of **162**, the authors used fluorescence spectroscopy to compare it to the two monomeric calixarenes. Fluoranthene, which shows strong emission at 450–470 nm when excited at 360 nm, was selected as a guest. Upon addition of fluoranthene to a solution of **162**, the emission was largely quenched. In contrast, the control experiments showed little fluorescence quenching. Analogous titration experiments quantified this difference. Thus, whilst there was no evidence of binding to the controls, a K_a value of 2,700 M^{-1} for fluoranthene binding to polymer **162** was determined.

2.7.4 Calix[4]arene based gels

Recent developments of soft materials such as hydrogels or organogels has been intense because of their potential for myriad applications,[302] including the controlled release of drugs,[303] tissue regeneration,[304] and energy storage.[305] Typically, gels are

formed by the crosslinking of a gelator through chemical or physical interactions. Chemical gels are formed due to strong crosslinking of gelators, whilst physical gels are maintained mainly *via* intermolecular non-covalent interactions; physical gels have the advantage of reversibility. Thus, such gels can be responsive to external stimuli such as light,[306] pH, temperature, and stress.[307] Low molecular-weight gelators (LMWGs)[308] comprised of calixarenes have gained interest due to the versatility of functionalizing their lower and upper rims to incorporate groups capable of tunable non-covalent interactions. After the first report of calix[4]arene-based gel bearing long alkyl chains,[309] many investigations have been carried out exploring the general utility of calix scaffold in this area. This section will focus on these developments.

2.7.4.1 Cholesterol based gel

Rao *et al.* reported a thermoreversible gel based on mono-cholesteryl-appended calixarene **163** (Figure 36).[310] Calix **163** formed stable gels in THF–MeCN (1:1 v/v) at a concentration of 0.6 weight percent. An observed bathochromic shift in absorption from 298 nm to 320 nm suggested J-aggregation in the gel, in which the molecules are arranged in lateral or slipped manner.[311] In the emission spectra of the calixarene, an increase in fluorescence emission was observed owing to AIE. SEM and TEM analyses showed that the gel was composed of intertwined nano-bundles whose diameters (~12 nm) varied with gelation concentration. DFT calculations pointed to head-to-tail packing of the cholesterol units in the gel. In contrast, the sol state contained spherical aggregates. Absorption and emission spectra, and SEM images revealed a gel-to-sol transition temperature of ~48 °C. The reversible binding properties of the gels was demonstrated by encapsulating different fluorescent dyes and drugs in the calix cavity, and their subsequent release over a 2-hour period by the addition of excess water. The guest-entrapped gels had slightly different textures and nano-bundle diameters, and the sol-gel transition temperature also increased to ~55 °C. The addition of water did not affect the gel structure.

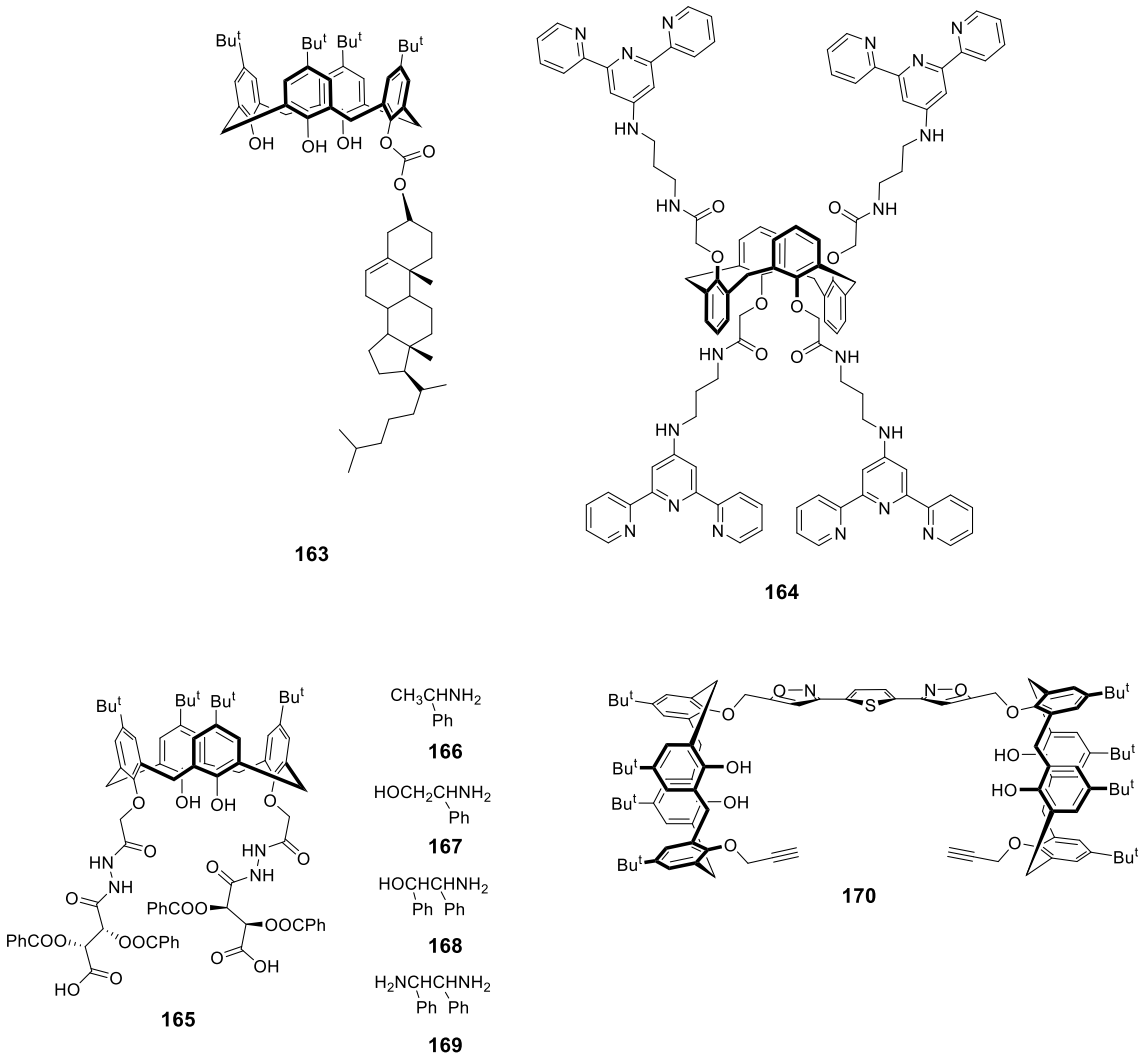

Figure 36. (A) Structures of calix[4]arene conjugates **163-165** and **170**.

2.7.4.2 Guest induced calix gels

Jung *et al*. investigated the gelation and luminescence properties of terpyridine-bearing calixarene in the 1,3-alternate conformation **164** (Figure 36) in the presence of Pt^{2+} under different solvent ratios of DMSO/H_2O.[312] It was observed that **164** required 4 equivalents of Pt^{2+} to form the metallogel (**164**-$[PtCl]_4^{4+}$), a finding that was further confirmed by the ESI mass spectrum of the complex. The gel was strong in 7:3 H_2O-DMSO compared to other solvent ratios. SEM analysis of the metallogel indicated the formation of spherical aggregates of 1.8−2.1 μm diameter. With an increase in the amount of added water, the luminescence emission of the metallogel changed from 570 nm to 660 nm, attributable to the triplet metal−metal-to-ligand charge transfer of the

aggregated species. Decreasing the concentration resulted in the solubilization of **164**·$[PtCl]_4^{4+}$. The luminescence lifetimes (τ_1 and τ_2) of **164**·$[PtCl]_4^{4+}$ complex in solution were found to be relatively long: 71.22 and 199.57 ns. In the gel phase, luminescence lifetimes (τ_1 and τ_2) increased further and was found to be dependent on concentration: 82.39 ns and 201.25 ns for 0.5 wt %, and 143.20 ns and 250.90 ns for 1.0 wt %. The G′ value was found to be five to seven times higher than G″ over the frequency range of 0.1−100 rad s^{-}, indicating the moderate tolerance of the metallogel to external mechanical stress.

Reports on enantioselective recognition by chiral gels are rare. In this regard, Zheng *et al*.[313] reported chiral calix[4]arene derivative **165** substituted with L-2,3-dibenzoyltartaric acid groups at the lower rim (Figure 36). In 1,2-dichloroethane, enantiopure **165** formed a gel with *R*-α-methylbenzylamine **166**, whilst the corresponding *S*-isomer led to a clear solution. With other chiral amines **167-169**, however, enantioselective discrimination was observed only in a 1,2-dichloroethane–cyclohexane solvent system. Compound **165** exhibited strong fluorescence emission at 308 nm (λ_{ex} = 280 nm). Upon interactions with **167**-**169**, a quenching in the fluorescence emission of **165** was observed. The stoichiometry of **165** with **166** or **167** was found to be 1:2, whilst with **168** or **169**, it was 1:1. The morphological investigation of gels obtained from **165** and both (*R*)-**166** and (*S*)-**167** by FE-SEM revealed a nano-fibrous structure which had length and breadth in the range of 10-50 μm and 100-500 nm. However, a web-like morphology was observed from the suspension obtained from **165** with either (*R*)-**166** or (*S*)-**167**. Contrastingly, the suspension obtained from **165** with (1*R*,2*S*)-**168** or (1*S*,2*S*)-**169** showed a spherical morphology with respective diameters of 200 nm and 500 nm. This spherical morphology was further confirmed by TEM.

Chung *et al.* reported a biscalixarene-based gel that acts as highly selective phase gelator for recovery of oil spills.[314] Biscalixarene **170** (Figure 36), bearing two isoxazole group connecting two mono-propargylated calixarenes, showed gelation in alcoholic solvents, and mixtures of EtOAc and hexane. A minimum gelation concentration range of 0.05 to 0.13% (w/v) was observed. At 10 mM concentration **170** exhibited excellent and selective gelation in a mixture of seawater and non-polar liquids (1:1 v/v) such as pump oil, diesel, and silicone oil. This phenomenon was not however observed in

gasoline (petrol). The selective gelation behavior of **170** was attributed to the phenolic hydroxyls, isoxazole, and *tert*-butyl groups which provide intermolecular H-bonding, dipole-dipole interactions, and van der Waals interactions. SEM images of the gel showed the formation of a fibrous network having variable width (30-70 nm). At higher concentrations of **170**, a three-dimensional network formed that was capable of oil entrapment. Variable temperature ^{1}H NMR studies were performed to evaluate the type of interactions involved in the sol-gel transition. Decreasing temperatures led to a downfield shift of the isoxazole and phenolic-OH signals and an upfield shift of the *tert*-butyl proton resonances, suggesting the involvement of dipole-dipole interactions, H-bonding, and van der Waals interactions. An increase in the fluorescence emission of **170** at 352 nm was observed with decrease in temperature from 363 K to 273 K attributed to self-assembled aggregates involving π-π interactions between isoxazole-thienyl groups.

2.7.4.3 UV-light responsive gel

Jung *et al*. reported gels from calixarene **171** and stilbene **172** whose mechanical, fluorescent, and physico-chemical properties could be tuned upon exposure to UV-light and changes in temperature (Figure 37).[315] The stilbene units of the gel exhibit blue fluorescence due to formation of H-aggregates upon excitation with 340-380 nm light (Figure 37a). Upon heating the gels at 60 °C, the partial H-aggregation (blue fluorescence) changed to a J-aggregation (green emission, Figure 37b). This was attributed to increased solvent movement within the gel network modulating the stacking pattern. The UV irradiation of H-aggregates resulted in a [2+2] cycloaddition between stilbene units, yielding a partial cyclobutane-conjugated gel, whose blue fluorescence was attenuated (Figure 37c). The authors also noted that the addition of DMSO led to the disappearance of green emission, *i.e.,* the disassembly of J-aggregates (Figure 37d). Tuning the proportion of H- (blue fluorescence) and J-aggregates (green emission) by heating, and further controlling the H-aggregates cross-linking by UV irradiation lets variable fluorescence photopatterning. It was observed that upon exposure of UV light, the mechanical strength of the gel (>3) was enhanced (>1300-fold increase in storage and loss moduli) compared to without irradiation. This was attributed to the formation of

cyclobutane units which increase the gel's tolerance to shear stress. The stiffness of gel was found to be in the range of ~100 to 450 kPa.

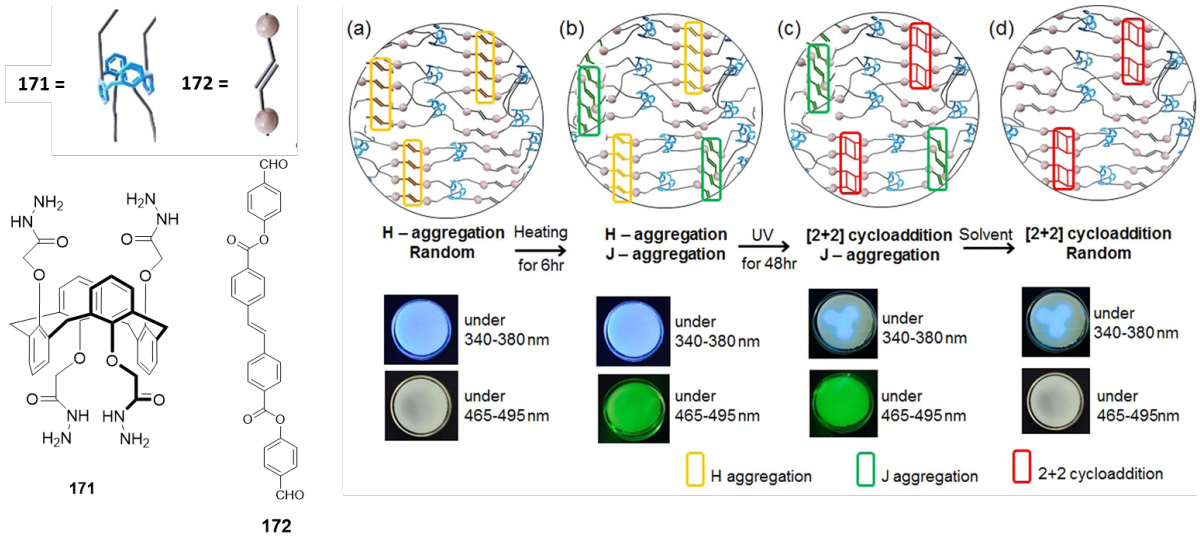

Figure 37. Illustration of gel formation by compound **171** with stilbene aldehyde **172**. (a) Before and (b) after heating at 60 °C for 1 h, (c) after UV irradiation, and (d) after immersion in DMSO. (Reprinted from Ref. 315. Copyright @2017 American Chemical Society).

2.7.5 Miscellaneous applications

Wong and co-workers have synthesized tetraoligothiophene-substituted calix[4]arene **173** (Figure 38) using palladium-catalyzed Kumada coupling.[316] The calixarene adopts a pinched-cone conformation in the solid state, typical of arylene-substituted calixarenes. In addition to band broadening, the absorption and emission spectra of the mono- to tetra-substituted calixarenes showed a stepwise hypsochromic shift in the absorption, a bathochromic shift in the emission, and an overall quenching of the emission intensity with each additional thiophene unit. Slightly longer fluorescence lifetimes were also noted (in the order of 1.8 ns) relative to the non-calixarene-conjugated counterparts (ca. 1.3 ns). These were ultimately attributed to the through-space intramolecular interaction between the proximate oligomers. In addition, CV data suggested a decrease in the HOMO–LUMO gap, contributing to the observed lowering of the first oxidation potential that stabilizes the radical cation and higher oxidation states of the oligothiophene.

With a long-term goal of developing new calix-based dyes, the Nolan group developed phthalocyanine derivative **174** (Figure 38) in the partial cone conformation.[317]

NMR showed that this dye had a reduced propensity to aggregate, whilst fluorescence studies (excitation at 650 nm) resulted in the strong fluorescence at 715 nm with a Stokes shift of 7 nm relative to phthalocyanine itself. Similarly, excitation at 614 nm resulted in the same fluorescence spectrum as that of phthalocyanine, indicating that the phthalocyanine group in **174** was unaffected by the calix moiety.

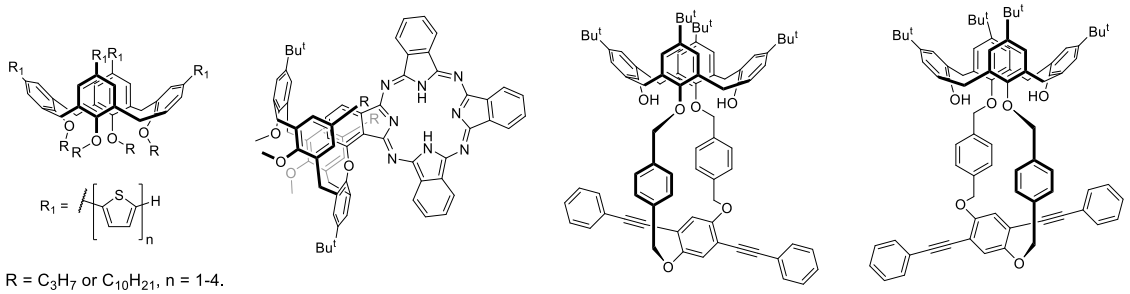

Figure 38. Structures of calix[4]arene conjugates **173-175**.

An inherently chiral calixarene **175A-B** (Figure 38) with planar chirality (*pS* and *pR*) was successfully synthesized and the enantiomers resolved.[318] The identity of these enantiomers was elucidated using a chiral NMR shift reagent, NOESY, and Circular Dichroism (CD). The separated enantiomers displayed similar absorption spectra, in addition to mirror-image CD spectra indicative of enantiomeric pairs.

The size-tunable optical properties and narrow emission bands of quantum dots (QDs) have made them prime tools for biological and medical applications. For example, zinc sulfide-based QDs have been widely used in many applications due to their affordable, facile synthesis, good photocatalytic properties, and relatively low toxicity. In an attempt to preserve and enhance the optical properties of zinc QDs, Menon *et al*.[319] coated poly(vinylpyrrolidone) capped zinc sulfide-based WDs with calix **126** (Figure 27). The resulting complex assumed a ‘‘cup-like’’ assembly,[320] with the OH groups at the lower rim of **126** interacting with the QDs through hydrogen bonding. Upon the addition of **126**, the emission intensity of the QDs increased up to 80%. The capping process resulted in the reduction of both hanging bonds and surface defects, and consequently higher stability and higher fluorescence intensity. TEM and DLS measurements showed an increase in size of the **QDs** from 2.0 nm to 30 nm, thereby confirming the successful

surface coating with **126**. Furthermore, **126-QDs** were applied for the detection of vitamin K3, a synthetic vitamin utilized in the bone mineralization and blood coagulation processes. Significant quenching in the fluorescence emission (95%) at 482 nm of **126-QDs** was observed with addition of 50 µL of vitamin K3, with the detection limit of 80 nM.

3. Higher Calixarenes

Compared to calix[4]arenes higher calix[*n*]arene (n = 5, 6, and 8) have been less explored. This is primarily because of limited regioselective synthetic transformations, low synthetic yield, and their complex conformational options. Despite these limitations, higher calixarenes have been successfully utilized in the development of various applications.[321] The large dimensions of higher calix[*n*]arenes make them exquisite hosts for the inclusion of larger guests,[322] and in this section we discuss recent advances pertaining to higher calixarenes in the context of fluorescence spectroscopy.

3.1 Applications of calix[5]arene derivatives

Because of their many potential applications, the fabrication of smart polymeric materials whose macroscopic properties can be tuned by external stimuli has received considerable attention in the polymer sciences. These materials can be constructed by employing non-covalent interactions such as hydrogen bonding,[323] metal-ligand interactions,[324] or salt bridges.[325] However, reports employing host-guest interactions to drive cross-linked polymers are very limited. Haino *et al*.[326] constructed a supramolecular polymeric array by using host-guest interactions between [60]fullerene-tagged poly(phenylacetylene)-poly(**A**) and calix[5]arene derivative **176** (Figure 39). Each calix unit can encapsulate a C_{60} moiety from the polymer, as evidenced by ^{1}H NMR spectroscopy. Specifically, upon complexation with the C_{60} moiety, the bridging methylene protons of the calix[5]arene unit, which otherwise give very broad signals due to intermediate time-scale ring-flipping, show a well-resolved quartet resonance signal indicating restricted flipping induced by guest complexation. C_{60} is known to be a good energy acceptor,[327] and as expected, the addition of poly(**A)** leads to the fluorescence quenching of **176**. Based upon the 2:1 **176**–poly(**A**) model, the association constants for two binding sites of host **176** were found to be K_{a11} = 4.36 ± 0.58 × 10^4 M^{-1} and K_{a12} = 7.50 ± 1.70 × 10^4 M^{-1}. The complex showed a solvent-dependent stability from high in

toluene, to very weak in chloroform or *o*-dichlorobenzene. As suggested by AFM, the macroscopic solid-state morphologies of poly(**A**) showed drastic change before and after complexation with host **176**. Because of the limited solubility of C_{60}, poly-**A** randomly aggregates. In contrast, upon complexation with **176**, the assumes a more ordered morphology in the form of fibrils.

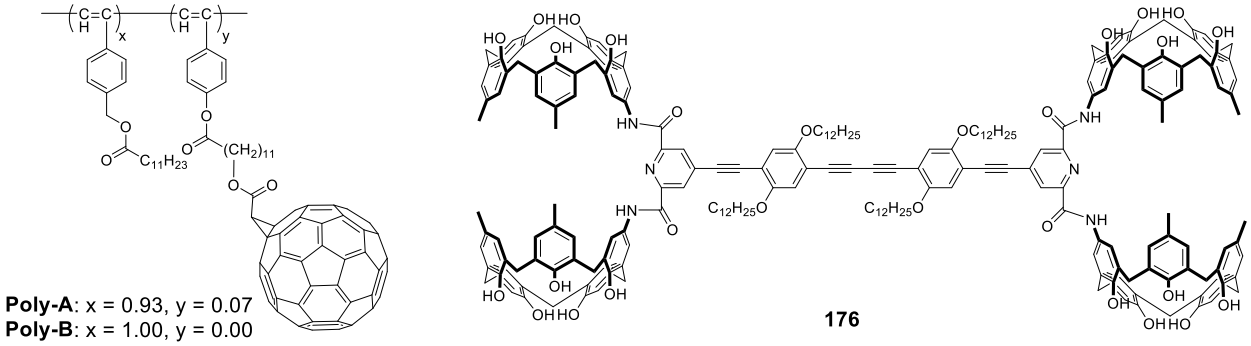

Figure 39. Molecular structure of homoditopic host **176** and **poly-A** and **poly-B**.

Placing C_{60} on a polymeric chain is very challenging, and the supramolecular host-guest complexes of C_{60} and the calix[5]arene derivative has insufficient solubility in organic solvents for detailed analysis of their macroscopic properties. Thus, a new class of linear and network fullerene polymers were synthesized and their complexation behavior with calix[5]arene derivatives **177** and **178** (Figure 40) investigated.[328] Long alkyl chains were introduced into dumbbell-fullerenes **G3a** and **G3b** in order to increase their solubility. **G3b** formed complexes with calixarene hosts **177** and **178**, where each C_{60} moiety is encapsulated into a cavity formed by the calixarene framework, resulting in the formation of linear and network supramolecular polymers, respectively. The identity of these linear and network were examined by NMR studies, UV-Vis and fluorescence spectroscopy, and SEM analysis. Hosts **177** and **178** showed strong fluorescence emissions at 451 nm and 464 nm, respectively. Significant quenching in the fluorescence emissions were observed upon binding with the C_{60} moiety. Job plots gave stoichiometries of 1:1 for **177** and **G3b** and 2:3 for **178** and **G3b**. Furthermore, the nature and dimension of supramolecular complexes were determined by viscometry. These results suggested that the viscosity of solution of **178** is greatly affected by the addition of **G3b** compared to that of **177**, implying that supramolecular complex of **178** and **G3b** are dimensionally extended to form cross-linked network structures. The macroscopic

properties of these complexes were studies by SEM analysis which demonstrated a fibrillar structure for the 1:1 complex of **177** and **G3a** with a diameter of 180 ± 50 nm. In contrast, the 2:3 complex of **178** and **G3a** gave a sheet-like morphology. The large morphological difference further validated the formation of linear and networked polymers by **177** and **178** respectively. The detailed insight into the supramolecular structures at the nanoscale, as evaluated by AFM imaging, suggested that **178** and **G3a** form well-defined honeycomb-like structures.

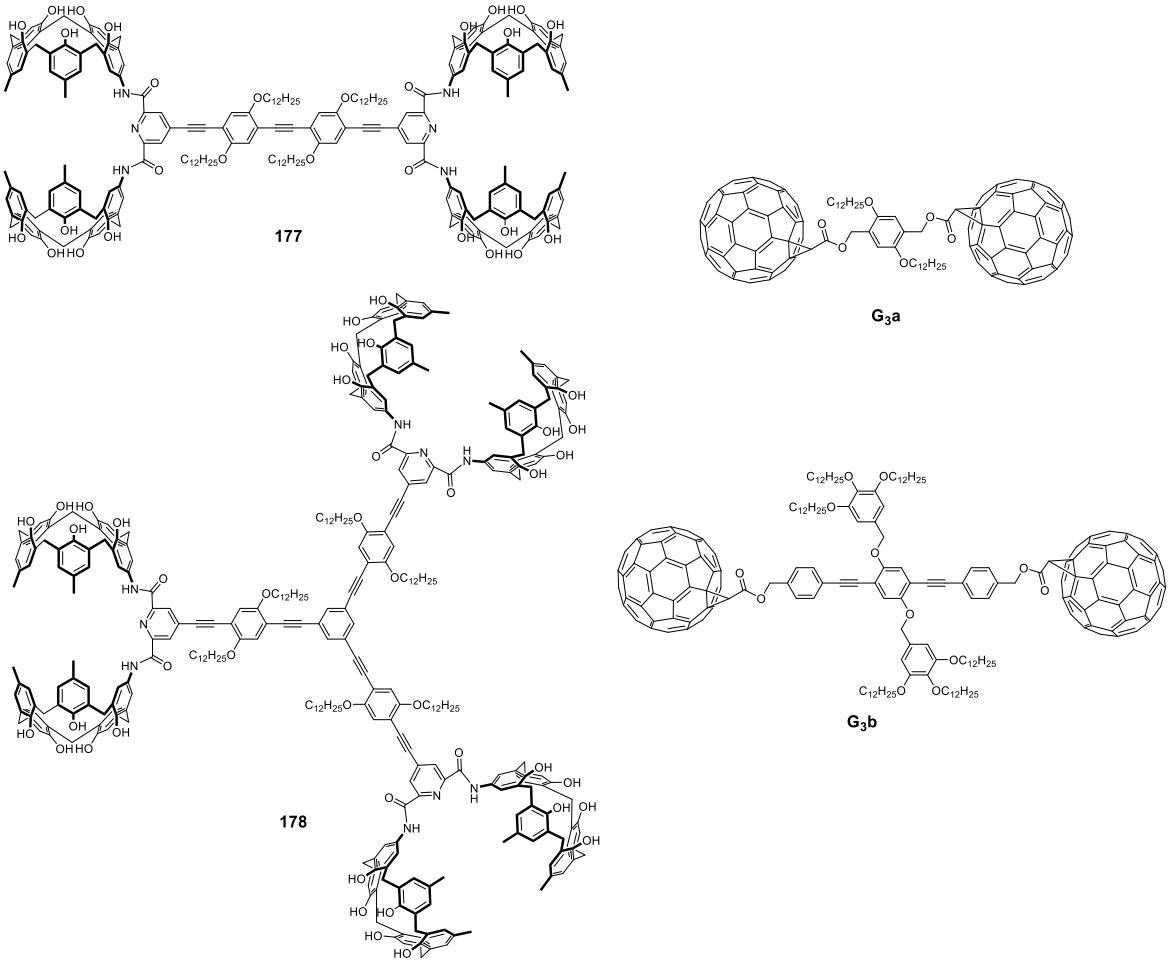

Figure 40. Molecular structures of calix[5]arene-based host **177** and **178,** and dumbbell-shped fullerene **G3a** and **G3b**.

Gou *et al.* developed an IDA for the ultrasensitive detection of lysophosphatidic acid (LPA), a phospholipid marker for the early-stage ovarian and other gynecologic cancers.[329] For this they used water-soluble guanidinium-decorated calixarene host **179** (Figure 41), and either fluorescein (FI) or Al(III) phthalocyanine chloride tetra-sulfonic acid

($AlPcS_4$) as reporters dyes. The phosphate head and long-chain fatty acid tail of LPA was shown to have a greater affinity for **179** ($K_a = 1.6 \pm 0.1 \times 10^8\ M^{-1}$) over FI ($K_a = 5.0 \pm 1.0 \times 10^6\ M^{-1}$) resulting in displacement of FI with a turn-on fluorescence response. The limit of detection of LPA was found to be 1.7 μM. An observed interference from adenosine triphosphate (ATP) over LPA was resolved by using the **179**–$AlPcS_4$ reporter pair *via* a differential sensing technique. The authors also tested the scope of assay for detection of LPA as a diagnostic marker in biological serum samples.

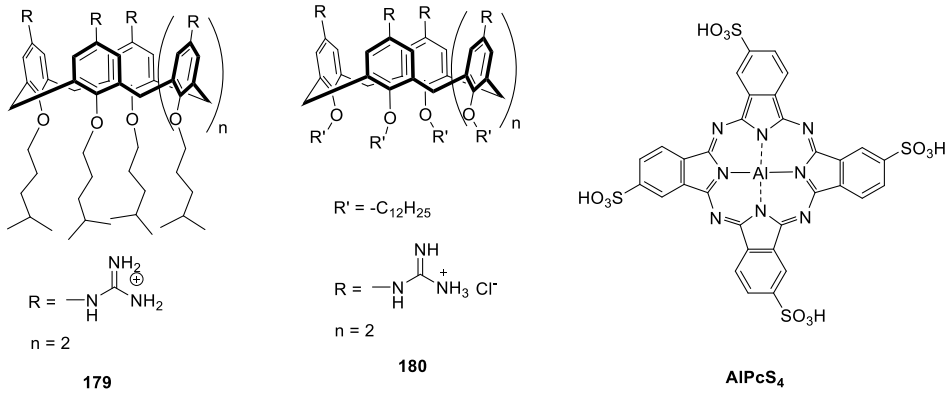

Figure 41. Molecular structures of calix[5]arene-based host **179**, **180** and sulfonated aluminum phthalocyanine ($AlPcS_4$).

Recently, Guo *et al.* demonstrated an IDA-based, cancer-specific photo-theranostics (imaging and therapy) protocol.[330] First, a 1:1 ratio of guanidinium-decorated *tetrakis*-dodecyl calix[5]arene **180** (Figure 41) and 4-(dodecyloxy)benzamido-terminated methoxy poly(ethylene glycol) (PEG-12C) were used to assemble a micelle. Subsequently, one of four photosensitizers (PS) were loaded into the micelle. The resulting NPs were fluorescence and photoactivity silent. However, incubation in the microenvironment of cancerous cells led to the displacement of the PS by the overexpressed ATP, resulting in a turn-on fluorescence and photoactivity response. Supported by *in vitro* results demonstrating the light-induced phototoxicity of the NPs in 4T1 breast cancer cells, the authors tested the potential of the NPs in 4T1 xenograft models. After intravenous injection, the NPs displayed preferential tumor accumulation and tumor-ATP driven activation, with a high tumor-to-normal organ ratio relative to controls. The NPs also

exhibited excellent therapeutic potential upon irradiation at 660nm, with significant tumor ablation and without any systemic toxicity observed.

Developing drug carriers that can selectively deliver the active drug to the tumor site, whilst avoiding undesired interactions with blood plasma proteins, could be a solution to resistance issues. Towards this the Barroso-Flores research group conducted MD analyses of possible binding interaction between imatinib and calixarenes of various core sizes (calix[5]arene, calix[6]arene and calix[8]arene) and different functional groups on the upper rims.[331] This revealed that calix[6]arene was the appropriate size to act as a carrier for the drug. The presence of acidic groups, *i.e.,* -SO_3H and -$(CH_2)_2OH$, offered additional stabilization to the complex *via* interactions with the nitrogens of the drug.

3.2 Applications of calix[6]arene derivatives

As a first step towards the fabrication of self-assembled nano-carriers for application in biology and medicine, Fontana *et al*.[332] reported amphiphilic calix[6]arene derivatives **181a** and **181b** (Figure 42). These derivatives self-assemble in aqueous media to form micelles or vesicles, with fluorescence, TEM, and DLS studies indicating sizes ranging from 20-200 nm depending on the length of alkyl chain appended to the lower rim. These derivatives form the "wheel" component of pseudo-rotaxanes when 1,1-dialkyl-4,4-bipyridinium (**DOV**) are threaded through.[333] The viologen was shown to increase the permeability of the vesicle and hence facilitate the fast release of encapsulated molecules. Thus, fluorescent dye 5(6)-carboxyfluorescein (CF) was loaded into the vesicle and its release monitored by fluorescence before and after the threading of the DOV axle. This showed that CF release from **181a**·**DOV** was twice than free **181a**.

Intracellular thiols, such as glutathione (GSH), cysteine (Cys) and homocysteine (Hcy) are key to maintaining cellular redox balance.[334] However, aberrant concentrations of these are implicated in many biological disorders.[335] Rao *et al*.[336] reported calix[6]arene derivative **182** (Figure 42) appended with three, 7-oxanorbornadiene (OND) units at the lower rim for the selective turn-on fluorescence detection of Cys over Hcy and GSH. The selectivity was attributed to the calix[6]arene platform and the sterically hindered electrophilic Diels–Alder center (OND). Calix **182** showed time-dependent fluorescence enhancement at 520 nm in the presence of three equivalents of Cys, reaching a 12-fold

enhancement after 22-24 minutes. However, no response was observed even with ten equivalents of Hcy or fifty equivalents of GSH. The morphology of **182** in the absence and presence of Cys was investigated by SEM analysis. This revealed that **182** formed spherical nanoparticles having sizes of 80 ± 20 nm, and that their morphology changed according to the ratio of **182** and Cys. For example, flower-like assemblies were seen at 1:1, fiber-like at 1:3, and cabbagelike at 1:5 ratios. Moreover, these morphological changes were time dependent. Finally, confocal imaging of HeLa cells and Jurkat cells demonstrated that **182** was cell permeable and could efficiently image intracellular Cys.

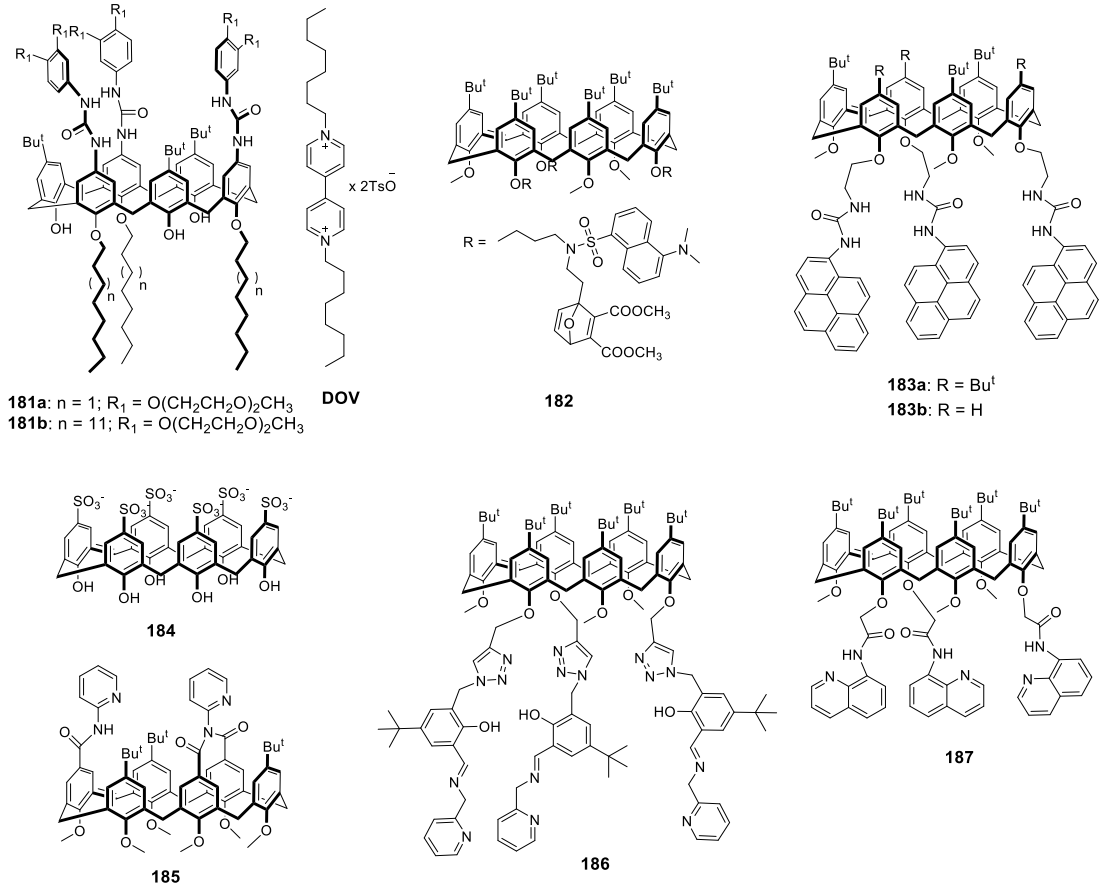

Figure 42. Molecular structures of calix[6]arene derivatives **181-187**.

Jabin *et al*.[337] have reported pyrene-substituted calix[6]arene-based fluorescent sensors **183a** and **183b** (Figure 42) and investigated their binding affinity for anions and ammonium salts as contact-pairs in different solvent systems. Addition of *tetra*-butylammonium sulfate ($(TBA)_2SO_4$), to a DMSO solution of **183a** revealed signal shifts

in the ^{1}H NMR signals suggesting strong hydrogen bonding between the urea groups and SO_4^{2-}. This selective binding was confirmed by fluorescence spectroscopy in which successive additions of salt led to fluorescence quenching of the monomer emission at 420 nm and slight increase in excimer emission at 506 nm. These spectral changes were attributed to the proximity of the pyrene moieties upon anion coordination. When the anion complexation was investigated in CH_2Cl_2, results were quite different. The shifts in the NMR signals were not only observed for the pyrene and urea NH, but also for the methylene units of TBA. Moreover, in contrast to DMSO, the fluorescence response in CH_2Cl_2 was also reversed, *i.e.,* binding led to an increase in monomer emission and a decrease in excimer emission. It was therefore suggested that in CH_2Cl_2, **183a** behaved as a heterotopic host for ammonium sulfate salts, whereby the sulfate anion interacts with the ureas, whilst the ammonium ions interact with the pyrene unit *via* cation-π interactions. The binding is cooperative since both ions can bind only as contact pairs. The log K_a values for the ammonium salt calculated using fluorescence titration curves was found to be 5.4 ± 0.1. Similar behavior was observed in **183b**.

Carnitine (β-hydroxy-γ-*N*-trimethylaminobutyric acid) is a biological nutrient that plays a critical role in molecular biology such as fatty acid metabolism and energy production,[338] deficiency of which is implicated in various disorders such as cardiomyopathy, diabetes, malnutrition, cirrhosis, obesity, and endocrine imbalances.[339] Li *et al*.[340] reported *p*-sulfonated calix[6]arene **184**, used for modifying a graphene oxide (GO) mono-layer that acted as a turn-on fluorescence probe for the *in vitro* detection of L-carnitine *via* an IDA mechanism (Figure 42). The increased thickness of the GO layer upon addition of **184**, as determined by AFM, was form 1.00 ± 0.2 nm (typical of single-layer GO) to 1.40 ± 0.2 nm. Further confirmation was provided by UV-vis spectroscopy, XPS and Fourier transform infrared (FT-IR). The complementary dye for the modified GO, was safranine T, which bound through electrostatic interactions with **184**. The bound dye was quenched *via* a FRET mechanism. When exposed to different analytes, only L-carnitine displaced safranin T from the surface. The limit of detection as low as 1.54 μM. Imaging was also successfully carried out in human liver cancer (HepG2) cells.

In separate investigation, Mohanty *et al.*[341] investigated the effect of pH on the binding behavior of **184** (Figure 42) with acridine. Fluorescence spectroscopic analysis

revealed that calix **184** bound acridine most strongly in acidic media, where the protonated N-atom (pK_a of acridinium ion = 5.58) forms attractive Coulombic interactions with the host. The fluorescence response of guest binding was significant. At pH 4.3 acridine showed significant fluorescence quenching at 477 nm upon the incremental addition of **184** (0.1 mM to 2 mM). In contrast, in basic solution only a slow decrease in fluorescence band at 430 nm was observed. The formation of the inclusion complex had a significant effect on the pK_a of acridinium, which was found to shift upward by ~2 units. This shift suggested that bound acridine **i**s approximately fifty times stronger a base than in the free form. Interestingly, the acridinium complex acted as a fluorescence turn-on chemosensor for Gd^{2+} *via* an IDA mechanism.

There are relatively few reports of higher calixarene as anion receptors, and towards addressing this Li *et al*.[342] reported 2-aminopyridyl-bridged calix[6]arene **185** (Figure 42) for F^- sensing. NMR studies suggested that probe **185** adopts a distorted cone conformation. The selective response of probe **185** towards F^- ions was demonstrated by ~92% quenching of fluorescence upon complexation. Probe **185** could detect F^- ions at concentrations as low as 0.02 μM.

Calix[6]arene chemosensor **186** (Figure 42) possessing three triazole-linked picolylimine moieties at the lower rim has been found to selectively coordinating La^{3+} ions.[343] Coordination of La^{3+} was accompanied by a sixteen-fold increase in the turn-on fluorescence response at 490 nm (λ_{ex} = 390 nm), with a 65 $\pm$ 5 ppb minimum detection limit determined. The La^{3+} complex was able to reversibly detect the F^- ion as observed by visual color change under UV light.

Rao *et al.* reported calix[6]arene probe **187** appended with three amide-linked 8-aminoquinoline functionalities on the lower rim (Figure 42)[344] for the selective recognition of Cu^{2+} and Zn^{2+} ions. With the addition of Cu^{2+}, a decrease in the fluorescence emission of 201 at 390 nm (λ_{ex} = 330 nm) was observed. In contrast, upon titration with Zn^{2+}, the emission at 390 nm decreased but there is simultaneous emergence of a new emission band at 490 nm. Cu^{2+} competed for **187 (**$K_a = 4.31 \times 10^4\ M^{-1}$) in the presence of Zn^{2+} ($K_a = 1.50 \times 10^4\ M^{-1}$). In both cases, mass analysis revealed a 1:1 stoichiometry.

3.3 Applications of calix[8]arene derivatives

Cunsolo *and* co-workers[345] reported polycationic calix[8]arene derivatives **188a-d** (Figure 43) with improved neutralization ability towards the important anticoagulant heparin.[346] Fluorescence and NMR spectroscopy demonstrated **188a-d** exhibited significant and specific binding to negatively charged heparin in aqueous solutions. This was further confirmed by an activated partial thromboplastin time assay measuring the rate of blood coagulation. The results showed that despite a higher charge density on **188c** relative to **188d**, the latter showed better neutralization of Hep. Evidently, other factors were involved in heparin inhibition than just charge density.

Ponterinin *et al*.[347] reported sulfonated calix[8]arene derivative **189** (Figure 43) and studied its solvent-dependent complexation behavior for merocyanine guests **Mc1** and **Mc2**. Probe **189** was shown to have similar affinity for both guests, irrespective of the nature of the organic solvent. Binging was attributed to van der Waals interactions between the alkyl chains of host and the guest. However, in water **189** showed selective binding of **Mc1** over **Mc2**, in which the alkyl chains self-assemble *via* the hydrophobic interaction to form a closed lid. As a result, the guest forms a complex only through the hydrophilic upper rim, and in this arrangement only smaller the **Mc1** can fit. This point also explained the higher water solubility of **Mc1** in the presence of **189**.

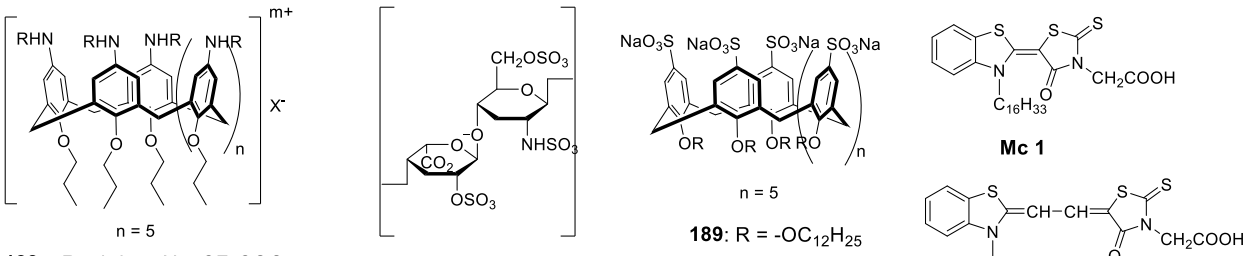

188a: R = L-Lys, X = CF_3COO^-
188b: R = $CO(CH_2)_6NH_2$, X = CF_3COO^-
188c: R = L-Lys, X = Cl^-
188d: R = $CO(CH_2)_6NH_2$, X = Cl^-

189: R = $-OC_{12}H_{25}$

Figure 43. Molecular structures of calix[8]arene derivatives **188a-d**, and **189**.

4. Conclusions and future perspectives

The structural features of calixarenes, their pre-organized non-polar cavity and ion-binding sites, variable but well-defined conformations, and tunable functionality, are key

to their general utility. As a result, fluorescent calixarenes and their complexes have proven to be exceedingly useful in a wide range of applications. Conjugating various fluorogenic groups to the calixarene scaffolds leads to the development of smart fluorescent probes that have been applied toward molecular sensors, bioimaging, drug- and gene-delivery systems, self-assembled aggregates, and smart materials. More specifically, as we have outlined, the combination of fluorogenic moieties and different anion and cation binding sites into calix[4]arene scaffolds, has led to sensors for a wide range of ions. The low detection limit and high selectivity for target ions, without any noticeable interference from multiple interfering analytes, have been well documented. On the other hand, controlling recognition in the non-polar pocket has engendered sensors for important classes of small organic targets such as nitro-aromatics. Utilizing both types of recognition, fluorescent calixarenes have also found utility in bioapplications. This review has also highlighted the fundamental fluorescence studies with calixarene derivatives, and how these are opening up the possibility of smart materials, both hard and soft. Additionally, the “imbalance” in the applications of calix[4]arenes and applications of higher calixarenes has also been outlined. A number of key developments with calix[5]/[6]/[8] have emerged, but new ways to synthesize and control the conformation of these derivatives would be immensely beneficial.

Despite many contributions and tremendous advances, there are still many challenges associated with the chemical detection area that need to be addressed. Importantly, this includes the detection of anions in aqueous media. With the exception of *p*-sulfonato-calix[4]arenes, the poor aqueous solubility of fluorescent calixarenes has hindered the potential of this class as effective hosts in aqueous media. Furthermore, the high hydration energies of anions has exacerbated the difficulties of anion detection in water and aqueous solutions by calixarenes. Poor water solubility has also negatively impacted the practical application of these systems in large-scale detection/screening/removal processes, for example, of the remediation of environmental pollutants. Other concerns relate to the bio-applicability of calixarenes derivatives. Although, *p*-sulfonato-calix[4]arene and its derivatives have been utilized for bio-assays and drug delivery formulations, the true potential of this class of host has not been realized thus far. Numerous efforts need to be focused in this area. This requires derivatizing

calix-scaffolds with water-soluble auxiliaries such as arginine, and pegylation suitable for biomedical and drugs delivery applications. Additionally, studying their interactions with biomolecules, cells, and tissues of interest, and investigating their cell permeability behavior, all need to be deeply studied. From clinical translation point of view, safety assurance is paramount, and various regulatory hurdles must also be addressed for successful applicatio. Perhaps more fundamentally, determining reliable and scalable approaches to the large-scale manufacture of water-soluble calixarenes is also important. All of these work will require sustained effort not just from individual research labs, but from major scientific and financial bodies. Much work is still to be done.

In sum, this manuscript has described the recent development and future potential of fluorescent calixarenes as third generation hosts for multiple applications ranging from molecular sensors to advance functional materials. With all these considerations, and possible wide range applications, the future of calixarene field is bright. Technologies are advancing, and scientists around the world are striving every day to solve the unmet need in this area: from fundamental studies to translational application. Although, the journey may be long, scientific partnerships between academic and industrial institutions will guarantee impactful progress in the coming decades. We hope this review will be beneficial to readers in on all the different levels/facets of calixarene research, and inspire them to realize and understand the true potential of calixarenes in modern technological and biomedicical applications.

Biographies

Rajesh Kumar was born in Pathankot, India in 1978. He received his Ph.D. degree in organic chemistry with Prof. Manoj Kumar from Department of Chemistry, Guru Nanak Dev University, Amritsar, India. Then he joined Prof. Jong Seung Kim's lab, Korea University, Seoul as research professor from Sept 2011 to June 2015. He moved to University of Calgary in June 2015 as postdoctoral fellow and then Canam Bioresearch as research scientist. His research interest concerns development of fluorescent biomarkers, drug delivery systems, and nanomedicines for cancer therapy.

Amit Sharma was born in Nagrota Bagwan, Kangra, H.P., India in 1983. He received his Ph.D. from Guru Nanak Dev University, Amritsar, India under the supervision of Prof. Kamaljit Singh. Thereafter, he joined Sphaera Pharma Pvt. Ltd, India as a research scientist (2011-2014). Later, he joined Prof. J. S. Kim's research group in 2014 as research professor. His research interest concerns the development of smart biomarkers, supramolecular scafolds, drug delivery systems and nano-formulations for chemotherapy.

Hardev Singh was born in Amritsar, India, in 1982. He received his Ph.D. degree in Organic Chemistry under the supervision of Prof. Vandana Bhalla, Department of Chemistry, Guru Nanak Dev University, Amritsar, India. After two years post-doctoral fellowship at Ajou University with Prof. Hwan Myung Kim, he joined Prof. Jong Seung Kim's lab as research professor in 2015. In February 2018, he moved to University of Manitoba, Canada where he is presently working as research associate. His research interest includes development of novel molecular imaging probes and targeted drug delivery systems (DDS's) for the cancer therapy, and fabrication of smart theranostic wound dressings.

Paolo Suating obtained his BSc in chemistry in 2016 from Northern Illinois University under the supervision of Dr. Marc Adler. His research focused on organosilicon chemistry, specifically in the stereoelectronics of organosilicon species, and the applications of silatranes. He is now in the Ph.D. program of Tulane University in New Orleans, under the supervision of Dr. Bruce Gibb. His current research is in the synthesis and properties of deep-cavity cavitands.

Hyeong Seok Kim received his bachelor's degree from the Department of Chemistry at the Catholic University of Korea in 2015. Curently, he is pursuing his Ph.D. degree under the guidance of Prof. Jong Seung Kim at Korea university. His current research interests are fluorescent probes for the detection of biomolecules as well as drug delivery systems for cancer therapy.

Inseob Shim was born in Daegu, Korea, in 1994. He received his bachelor's degree in 2016 and master's degree in 2018 from the department of chemistry at Korea University in Seoul, South Korea. He is pursuing his Ph.D. degree under guidance of prof.

Jong Seung Kim, department of chemistry at Korea University. He is mainly engaged in the design and synthesis of drug delivery systems.

Kyoung Sunwoo was born in Austin, Texas, USA, in 1990. She received her bachelor's degree in 2014 from the Department of Chemistry at Korea University in Seoul, South Korea and she is pursuing her PhD degree under guidance of Prof. Jong Seung Kim, Department of chemistry at Korea University. Her research interests include the design and synthesis of fluorescent reporters for drug delivery systems.

Bruce Gibb was born in Aberdeen, Scotland in 1965. He received his Ph.D. from Robert Gordons Institute of Technology in 1992. After postdoctoral fellowships at the University of British Columbia and New York University, he joined the faculty at the University of New Orleans in 1996. In 2012 he moved to Tulane University. His research interests center around the fundamental understanding of molecular recognition in aqueous solution, and how this can be applied to the development of water-based tools for novel chemical conversions and separations.

Jong Seung Kim was born in Daejon, Korea in 1963. He received Ph.D. from Department of Chemistry and Biochemistry at Texas Tech University. After one-year postdoctoral fellowship at University of Houston, he joined the faculty at Konyang University in 1994 and transferred to Dankook University in 2003. In 2007, he then moved to the Department of Chemistry at Korea University in Seoul as a professor.

Acknowledgment

This work was supported by the National Research Foundation of Korea (CRI 2018R1A3B1052702, J.S.K). BCG acknowledges the support of the National Science Foundation (CHE-1807101).

Abbrevations

PET	Photoinduced electron transfer
ICT	Intramolecular charge transfer
ESIPT	Excited state intramolecular proton transfer
MLCT	Metal-to-ligand charge transfer
BODIPY	Boron-dipyrromethene
DFT	Density functional theory
HOMO	Highest occupied molecular orbitals
TREN	Tris(2-aminoethyl)amine)

CHEF	Chelation-Enhanced Fluorescence
TEM	Transmission electron microscopy
AFM	Atomic force microscopy
ROS	Reactive oxygen species
EPR	Electron paramagnetic resonance
FRET	Förster resonance energy transfer
PDMS	Polydimethylsiloxane
HSA	Human serum albumin
BSA	Bovine serum albumin
LA	α-lactalbumin
PCT	Photo-induced charge transfer
IDA	Indicator displacement assay
PD	Parkinson's disease
CA	Contact angle
NTPs	Nucleoside triphosphates
ATP	Adenosine triphosphate
GTP	Guanosine triphosphate
CTP	Cytidine triphosphate
TTP	Thymidine triphosphate
UTP	Uridine triphosphate
AIE	Aggregation-induce emission
SEM	Scanning electron microscopy
BINOL	1,1’-bi(2-naphthol)
DLS	Dynamic light scattering
ESI MS	Electro spray ionization mass spectrometry
TNT	Trinitrotoluene
RDX	1,3,5-trinitro-1,3,5-triazinane
PETN	Pentaerythritol tetranitrate
MALDI-MS	matrix-assisted laser desorption/ionization mass spectrometry
SWCNT	Single-walled carbon nanotubes
SDS	Sodium dodecyl sulfate
CTAB	Cetyl trimethylammonium bromide
XPS	X-ray photoelectron spectroscopy
QDs	Quantum dots
PAHs	Polyaromatic hydrocarbons
MRI	Magnetic resonance imaging
DDS	drug delivery systems
NBD	7-nitrobenzofurazan
NPs	Polymer nanoparticles
DAPI	4′,6′-diamidino-2-phenylindole
DOPE	2,3-di(oleolyoxy)propyl phosphatidyl ethanolamine
GFP	Green fluorescent protein
CT-DNA	Calf thymus DNA
LPS	Lipopolysaccharide
DOX	Doxorubicin
TPE	Tetraphenylethene

CV	Cyclic voltammetry
ITC	Isothermal titration calorimetry
PBI	Perylene bis-imide
CMC	Critical micelle concentration
GPC	Gel Permeation Chromatography
OLED	Organic light-emitting diode
CD	Circular Dichroism
NOESY	Nuclear Overhauser effect spectroscopy
G'	Storage modulus
G"	Loss modulus
LMWG	Low molecular weight gel
FE-SEM	Field emission scanning electron microscope
LPA	Lysophosphatidic acid
PS	Photosensitizers
GSH	Glutathione
Cys	Cysteine
Hcy	Homocysteine

References

(1) Amabilino, D. B.; Gale, P. A. Supramolecular chemistry anniversary. *Chem. Soc. Rev*. **2017**, *46*, 2376–2377.

(2) Ma, X.; Zhao, Y. Biomedical applications of supramolecular systems based on host−guest interactions. *Chem. Rev*. **2015**, *115*, 7794−7839.

(3) Ariga, K.; Kunitake, T. *Supramolecular chemistry: fundamentals and applications*: Advanced Textbook; Springer: Heidelberg, **2006**.

(4) Schneider, H.-J. r. *Applications of supramolecular chemistry for 21st century technology*; Taylor & Francis: Boca Raton, FL, **2012**.

(5) Avestro, A.-J.; Belowich, M. E.; Stoddart, J. F. Cooperative self-assembly: producing synthetic polymers with precise and concise primary structures. *Chem. Soc. Rev*. **2012**, *41*, 5881–5895.

(6) Gutsche, C. D. *Calixarenes*; Royal Society of Chemistry: Cambridge, U.K., **1989**.

(7) Gokel, G. W.; Leevy, W. M.; Weber, M. E. Crown ethers: sensors for ions and molecular scaffolds for materials and biological models. *Chem. Rev.* **2004**, *104*, 2723–2750.

(8) Lai, W.-F.; Rogach, A. L.; Wong, W.-T. Chemistry and engineering of cyclodextrins for molecular imaging. *Chem. Soc. Rev.* **2017**, *46*, 6379–6419.

(9) Szejtli, J. Introduction and general overview of cyclodextrin chemistry. *Chem. Rev*. **1998**, *98*, 1743–1754.

(10) Gokel, G. W. Crown ethers and cryptands, The Royal Society of Chemistry, London, England, **1991**.

(11) Murray, J.; Kim, K.; Ogoshi, T.; Yao, W.; Gibb, B. C. The aqueous supramolecular chemistry of cucurbit[n]urils, pillar[n]arenes and deep-cavity cavitands. *Chem. Soc. Rev*. **2017**, *46*, 2479–2496.

(12) Lee, J. W.; Samal, S.; Selvapalam, N.; Kim, H.-J.; Kim, K. Cucurbituril homologues and derivatives: new opportunities in supramolecular chemistry. *Acc. Chem. Res*. **2003**, *36*, 621–630.

(13) Neri, P.; Sessler, J. L.; Wang, M.-X. (eds) *Calixarenes and beyond,* Springer, **2016**.

(14) Joseph, R.; Rao, C. P. Ion and molecular recognition by lower rim 1,3-di-conjugates of calix[4]arene as receptors. *Chem. Rev.* **2011**, *111*, 4658–4702.

(15) Baklouti, L.; Harrowfield, J.; Pulpoka, B.; Vicens, J. 1,3-Alternate, the smart conformation of calix[4]arenes. *Mini-Rev. Org. Chem*. **2006**, *3*, 355–384.

(16) Kim, J. S.; Yang, S. H.; Rim, J. A.; Kim, J. Y.; Vicens, J.; Shinkai, S. Silver ion oscillation through calix[4]azacrown tube. *Tetrahedron Lett*. **2001**, *42*, 8047–8050.

(17) Shinkai, S. *Calixarenes as third supramolecular host*, in Advances in Supramolecular Chemistry, JAI Press Inc., **1993**, vol. 3, p. 97.

(18) Kim, J. S.; Quang, D. T. *Calixarene-derived fluorescent probes*. *Chem. Rev*. **2007**, *107*, 3780–3799.

(19) Bakic, M. T.; Jadresko, D.; Hrenar, T.; Horvat, G.; Pozar, J.; Galic, N.; Sokol, V.; Tomas, R.; Alihodzic, S.; Zinic, M.; et al. Fluorescent phenanthridine-based calix[4]arene derivatives: synthesis and thermodynamic and computational studies of their complexation withalkali-metal cations. *RSC Adv*. **2015**, *5*, 23900–23914.

(20) Melnikov, P.; Zanoni, L. Z. Clinical effects of cesium intake. *Biol. Trace Elem. Res*. **2010**, *135*, 1−9.

(21) Depauw, A.; Kumar, N.; Ha-Thi, M. H.; Leray, I. Calixarene-based fluorescent sensors for cesium cations containing BODIPY fluorophore. *J. Phys. Chem.* A **2015**, *119*, 6065−6073.

(22) Galic, N.; Buric, N.; Tomas, R.; Frkanec, L.; Tomis, V. Synthesis and cation binding properties of fluorescent calix[4]arene derivatives bearing tryptophan units at the lower rim. *Supramolecular Chemistry* **2011**, *23*, 389−397.

(23) Mank, M.; Griesbeck, O. Genetically encoded calcium indicators. *Chem. Rev*. **2008**, *108*, 1550–1564.

(24) LeGeros, R. Z. Calcium phosphate-based osteoinductive materials. *Chem. Rev*. **2008**, *108*, 4742–4753.

(25) Harder, S. From limestone to catalysis: application of calcium compounds as homogeneous catalysts. *Chem. Rev*. **2010**, *110*, 3852–3876.

(26) Kim, H. J.; Kim, J. S. BODIPY appended cone-calix[4]arene: selective fluorescence changes upon Ca^{2+} binding. *Tetrahedron Lett.* **2006**, *47*, 7051–7055.

(27) Zhan, J.; Fang, F.; Tian, D.; Li, H. Anthraquinone-modified calix[4]arene: click synthesis, selective calcium ion fluorescent chemosensor and INHIBIT logic gate. *Supramol. Chem*, **2012**, *24*, 272–278.

(28) Yamanaka, M.; Hara, K.; Kudo, J. Bactericidal actions of a silver ion solution on Escherichia coli, studied by energy-filtering transmission electron microscopy and proteomic analysis. *Appl*. *Environ*. *Microb*. **2005**, *71*, 7589–7593.

(29) Litwin, C. M.; Boyko, S. A.; Calderwood, S. B. Cloning, sequencing, and transcriptional regulation of the Vibrio cholerae for gene. *J. Bacteriol*. **1992**, *174*, 1897–1903.

(30) Zhang, J. F.; Zhou, Y.; Yoon, J.; Kim, J. S. Recent progress in fluorescent and colorimetric chemosensors for detection of precious metal ions (silver, gold and platinum ions). *Chem. Soc. Rev.* **2011**, *40*, 3416–3429.

(31) Ho, I-.; Haung, K.-C.; Chung, W.-S. 1,3-Alternate calix[4]arene as a homobinuclear ditopic fluorescent chemosensor for Ag^+ ions. *Chem. Asian J*. **2011**, 6, 2738-2746.

(32) Wang, N.-J.; Sun, C.-M.; Chung, W.-S. A highly selective fluorescent chemosensor for Ag^+ based on calix[4]arene with lower-rim proximal triazolylpyrenes. *Sens. Actuators B Chem.* **2012**, *171– 172*, 984– 993.

(33) Good, P. F.; Olanow, C. W.; Perl, D. P. Neuromelanin-containing neurons of the substantia nigra accumulate iron and aluminum in Parkinson's disease: a LAMMA study. *Brain Res*. **1992**, *593*, 343–346.

(34) Kawahara, M.; Muramoto, K.; Kobayashi, K.; Mori, H.; Kuroda, Y. Aluminum promotes the aggregation of Alzheimer's amyloid beta-protein in vitro. *Biochem. Biophys. Res. Commun.* **1994**, *198*, 531–535.

(35) Ruan, Y.-B.; Depauw, A.; Leray, I. Aggregation-induced emission enhancement upon Al^{3+} complexation with a tetrasulfonated calix[4]bisazacrown fluorescent molecular sensor. *Org. Biomol. Chem.* **2014**, *12*, 4335–4341.

(36) Othman, A. B.; Lee, J. W.; Huh, Y.-D.; Abidi, R.; Kim, J. S.; Vicens, J. A novel pyrenyl-appended tricalix[4]arene forfluorescence-sensing of Al(III). *Tetrahedron* **2007**, *63*, 10793–10800.

(37) Valeur, B. *Molecular fluorescence. principles and applications*; Wiley-VCH: Weinheim, **2002**.

(38) Okamoto, S.; Eltis, L. D. The biological occurrence and trafficking of cobalt. *Metallomics* **2011**, *3*, 963–970.

(39) Mummidivarapu, V. V. S.; Hinge, V. K.; Tabbasum, K.; Gonnade, R. G.; Rao, C. P. Triazole-linked anthracenyl-appended calix[4]arene conjugate as receptor for co(ii): synthesis, spectroscopy, microscopy, and computational studies. *J. Org. Chem*. **2013**, *78*, 3570−3576.

(40) Malmstrom, B. G.; Leckner, J. The chemical biology of copper. *Curr. Opin. Chem. Biol*. **1998**, *2*, 286–292.

(41) Uauy, R.; Olivares, M.; Gonzalez, M. Essentiality of copper in humans. *Am. J. Clin. Nutr.* **1998**, *67*, 952S–959S.

(42) Peers, G.; Price, N. M. Copper-containing plastocyanin used for electron transport by an oceanic diatom. *Nature*, **2006**, *44*, 341-344.

(43) Uriu-Adams, J. Y.; Keen, C. L. Copper, oxidative stress, and human health. *Mol. Aspects Med*. **2005**, *26*, 268–298.

(44) Desai, V.; Kaler, S. G. Role of copper in human neurological disorders. *Am. J. Clin. Nutr*. **2008**, 88, 855S–858S.

(45) Halfdanarson, T. R.; Kumar, N.; Li, C.-Y.; Phyliky, R. L.; Hogan, W. J. Hematological manifestations of copper deficiency: a retrospective review. *Eur. J. Haematol*., **2008**, *80*, 523–531.

(46) Yang, Q.; Zhu, X.; Yan, C.; Sun, J. Determination of trace copper(II) by Triton X-100 sensitized fluorescence quenching of a novel calix[4]arene Schiff base derivative, *Anal. Methods* **2014**, *6*, 575–580.

(47) Li, G.-K.; Xu, Z.-X.; Chen, C.-F.; Huang, Z.-T. A highly efficient and selective turn-on fluorescent sensor for Cu^{2+} ion based on calix[4]arene bearing four iminoquinoline subunits on the upper rim, *Chem. Commun.* **2008**, 1774–1776.

(48) Pathak, R. K.; Hinge, V. K.; Mondala, P.; Rao, C. P. Ratiometric fluorescence off-on-off sensor for Cu^{2+} in aqueous buffer by a lower rim triazole linked benzimidazole conjugate of calix[4]arene. *Dalton Trans*. **2012**, *41*, 10652–10660.

(49) Kumar, M.; Babu, J. N.; Bhalla, V. Fluorescent chemosensor for Cu^{2+} ion based on iminoanthryl appended calix[4]arene. *J. Incl. Phenom. Macrocycl. Chem*. **2010**, *66*, 139–145.

(50) Fischer, C.; Stapf, M.; Seichter, W.; Weber, E. Fluorescent chemosensors based on a new type of lower rim-dansylated and bridge-substituted calix[4]arenes, *Supramol. Chem.* **2013**, *25*, 371–383.

(51) Ho, I-T.; Chu, J.-H.; Chung, W.-S. Calix[4]arene with lower-rim β-amino α,β-unsaturated ketones containing bis-chelating sites as a highly selective fluorescence turn-on chemosensor for two copper(ii) ions. *Eur. J. Org. Chem.* **2011**, 1472–1481.

(52) Halouani, H.; Dumazet-Bonnamour, I.; Perrin, M.; Lamartine, R. First synthesis and structure of β-ketoimine calix[4]arenes: complexation and extraction studies. *J. Org. Chem.* **2004**, *69*, 6521–6527.

(53) Chang, K.-C.; Luo, L.-Y.; Diau, E. W.-G.; Chung, W.-S.; Highly selective fluorescent sensing of Cu^{2+} ion by an arylisoxazole modified calix[4]arene, *Tetrahedron Lett*. **2008**, *49*, 5013–5016.

(54) de Silva, A. P.; Gunaratne, H. Q. N.; Lynch, P. L. M. Luminescence and charge transfer. Part 4. 'On–off' fluorescent PET (photoinduced electron transfer) sensors with pyridine receptors: 1,3-diaryl-5-pyridyl-4,5-dihydropyrazoles. *J. Chem. Soc. Perkin Trans*. 2, **1995**, 685–690.

(55) Chae, M.-Y.; Cherian, X. M.; Czarnik, A. W. New reagents for the syntheses of fluorescent chemosensors. Anthrylogous ethylene dibromides. *J. Org. Chem*. **1993**, *58*, 5797–5801.

(56) Chawla, H. M.; Shukla, R.; Pandey, S. Novel fluorescein appended calix[4]arenes for preferential recognition of Cu^{2+} ions. *Tetrahedron Lett*. **2013**, *54*, 2063–2066.

(57) Dunn, L. L.; Rahmanto, Y. S.; Richardson, D. R. Iron uptake and metabolism in the new millennium. *Trends Cell Biol*. **2007**, *17*, 93–100.

(58) Walter, P. B.; Knutson, M. D.; Paler-Martinez, A.; Lee, S.; Xu, Y.; Viteri, F. E.; Ames, B. N. Iron deficiency and iron excess damage mitochondria and mitochondrial DNA in rats. *Proc. Natl. Acad. Sci*. USA **2002**, *99*, 2264–2269.

(59) Pathak, R. K.; Dessingou, J.; Hinge, V. K.; Thawari, A. G.; Basu, S. K.; Rao, C. P. Quinoline driven fluorescence turn on 1,3-bis-calix[4]arene conjugate-based receptor to discriminate Fe^{3+} from Fe^{2+}. *Anal. Chem*. **2013**, *85*, 3707−3714.

(60) Chawla, H. M.; Gupta, T. Novel bis-calix[4]arene based molecular probe for ferric iron through colorimetric, ratiometric, and fluorescence enhancement response. *Tetrahedron Lett.* **2015**, *56*, 793–796.

(61) Chen, Y.-J.; Yang, S.-C.; Tsai, C.-C.; Chang, K.-C.; Chuang, W.-H.; Chu, W.-L.; Kovalev, V.; Chung, W.-S. Anthryl-1,2,4-oxadiazole-substituted calix[4]arenes as highly selective fluorescent chemodosimeters for Fe^{3+}. *Chem. Asian J*. **2015**, *10*, 1025–1034.

(62) *Mercury Update: Impact on Fish Advisories*. EPA Fact Sheet EPA-823-F-01-011; EPA, Office of Water: Washington, DC, 2001.

(63) Renzoni, A.; Zino, F.; Franchi, E. Mercury levels along the food chain and risk for exposed populations. *Environ. Res.* **1998**, *77*, 68–72.

(64) Benoit, J. M.; Fitzgerald, W. F.; Damman, A. W. The biogeochemistry of an ombrotrophic bog: evaluation of use as an archive of atmosphere mercury deposition. *Environ. Res.* **1998**, *78*, 118–133.

(65) Malm, O. Gold mining as a source of mercury exposure in the Brazilian Amazon. *Environ. Res.* **1998**, *77*, 73–78.

(66) Boening, D. W. Ecological effects, transport, and fate of mercury: a general review. *Chemosphere* **2000**, *40*, 1335–1351.

(67) Othman, A. B.; Lee, J. W.; Wu, J. S.; Kim, J. S.; Abidi, R.; Thuéry. P.; Strub, J. M.; Dorsselaer, A. V.; Vicens, J. Calix[4]arene-based, Hg^{2+}-induced intramolecular fluorescence resonance energy transfer chemosensor. *J. Org. Chem.* **2007**, *72*, 7634–7640.

(68) Lee, Y. H.; Lee, M. H.; Zhang, J. F.; Kim, J. S. Pyrene excimer-based calix[4]arene fret chemosensor for mercury(II). *J. Org. Chem*. **2010**, *75*, 7159–7165.

(69) Dhir, A.; Bhalla, V.; Kumar, M. Ratiometric sensing of Hg^{2+} based on the calix[4]arene of *partial cone* conformation possessing a dansyl moiety. *Org. Lett.,* **2008**, 10, 4891–4894.

(70) Kim, K. S.; Kim, S. H.; Kim, H. J.; Lee, S. H.; Lee, S. W.; Ko, J.; Bartsch, R. A.; Kim, J. S. Indium(III)-induced fluorescent excimer formation and extinction in calix[4]arene-fluoroionophores. *Inorg. Chem.* **2005**, *44*, 7866–7875.

(71) Dinake, P.; Prokhorova, P. E.; Talanov, V. S.; Butcher, R. J.; Talanova, G. G. A new fluorogenic calix[4]arene N-dansylcarboxamide in the cone conformation for selective optical recognition of mercury(II). *Tetrahedron Lett*. **2010**, *51*, 5016–5019.

(72) Li, G.-K.; Liu, M.; Yang, G.-Q.; Chen, C.-F.; Huang, Z.-T. An effective Hg^{2+}-selective fluorescent chemosensor based on a calix[4]arene bearing four dansyl amides. *Chinese J. Chem.* **2008**, *26*, 1440–1446.

(73) Metivier, R.; Leray, I.; Valeur, B. A highly sensitive and selective fluorescent molecular sensor for Pb(II) based on a calix[4]arene bearing four dansyl groups. *Chem. Commun*. **2003**, 996–997.

(74) Arena, G.; Attanasio, F.; Zhang, D.; Yang, Y.; Bartsch, R. A.; Sgarlata, C. Selective sensing of Hg^{2+} by a proton-ionizable calix[4]arene fluoroionophore. *Anal. Bioanal. Chem*. **2013**, *405*,1133–1137.

(75) Kumar, M.; Kumar, N.; Bhalla, V.; Kaur, A. Calix[4]arene-based fluorescent receptor for selective turn-on detection of Hg^{2+} ions. *Supramol. Chem.* **2013**, *25*, 28–33.

(76) Bandela, A. K.; Chinta, J. P.; Rao, C. P. Role of the conformational changes brought in the arms of the 1,3-di-capped conjugate of calix[4]arene (L) in turning on the fluorescence of L by Hg^{2+}. *Dalton Trans.*, **2011**, *40*, 11367–11370.

(77) Joseph, R.; Ramanujam, B.; Acharya, A.; Khutia, A.; Rao, C. P. Experimental and computational studies of selective recognition of Hg^{2+} by amide linked lower rim 1,3-dibenzimidazole derivative of calix[4]arene: species characterization in solution and that in the isolated complex, including the delineation of the nanostructures. *J. Org. Chem.* **2008**, *73*, 5745–5758.

(78) Tian, D.; Yan, H.; Li, H. A selective fluorescent probe of Hg^{2+} based on triazole-linked 8-oxyquinoline calix[4]arene by click chemistry. *Supramol. Chem*. **2010**, *22*, 249–255.

(79) Papanikolaou, N. C.; Hatzidaki, E. G.; Belivanis, S.; Tzanakakis, G. N.; Tsatsakis, A.M. Lead toxicity update. A brief review. *Med. Sci. Monitor* **2005**, *11*, RA329–336.

(80) Toscano, C. D.; Guilarte, T. R. Lead neurotoxicity: from exposure to molecular effects. *Brain Res. Rev.* **2005**, *49*, 529–554.

(81) Hutchinson, T. C.; Meema, K. M. in Lead, mecury, cadmium and arsenic in the environment, Wiley, New York, **1987**.

(82) Guidelines for drinking-water quality, 3rd ed., Vol. 1, World Health Organization, Geneva, **2004**, 188–189.

(83) Jeon, N. J.; Ryu, B. J.; Nam, K. C. Pb^{2+} On-off switchable 1,3-alternate calix[4]arene chemosensor containing urea and pyrene moieties, *Bull. Korean Chem. Soc*. **2012**, *33*, 3129–3132.

(84) Buie, N. M.; Talanov, V. S.; Butcher, R. J.; Talanova, G. G. New fluorogenic dansyl-containing calix[4]arene in the *partial cone* conformation for highly sensitive and selective recognition of lead(II). *Inorg. Chem*. **2008**, *47*, 3549–3558.

(85) Sahin, O.; Yilmaz, M. Synthesis and fluorescence sensing properties of novel pyrene-armed calix[4] arene derivatives. *Tetrahedron* **2011**, *67*, 3501–3508.

(86) Faye, D.; Lefevre, J.-P.; Delaire, J. A.; Leray, I. A selective lead sensor based on a fluorescent molecular probe grafted on a PDMS microfluidic chip. *J. Photoch. Photobio*. *A: Chemistry* **2012**, *234*, 115–122.

(87) Prasad, A. S. Zinc in human health: effect of zinc on immune cells. *Mol. Med*. **2008**, *14*, 353–357.

(88) Stewart, A. J.; Blindauer, C. A.; Berezenko, S.; Sleep, D.; Sadler, P. J. Interdomain zinc site on human albumin. *Proc. Natl. Acad. Sci.* U. S. A., **2003**, *100*, 3701–3706.

(89) Pathak, R. k.; Dikundwar, A. G.; Row, T. N. G.; Rao, C. P. A lower rim triazole linked calix[4]arene conjugate as a fluorescence switch on sensor for Zn^{2+} in blood serum milieu. *Chem. Commun*. **2010**, *46*, 4345–4347.

(90) Zhu, L.-N.; Gong, S.-L.; Gong, S.-L.; Yang, C.-L.; Qin, J.-G. Novel pyrene-armed calix[4]arenes through triazole connection: ratiometric fluorescent chemosensor for Zn^{2+} and promising structure for integrated logic gates. *Chinese J. Chem.* **2008**, *26*, 1424—1430.

(91) Park, S. Y.; Yoon, J. H.; Hong, C. S.; Souane, R.; Kim, J. S.; Matthews, S. E.; Vicens, J. A pyrenyl-appended triazole-based calix[4]arene as a fluorescent sensor for Cd^{2+} and Zn^{2+}. *J. Org. Chem.* **2008**, *73*, 8212–8218.

(92) Mummidivarapu, V. V. S.; Tabbasum, K.; Chinta, J. P.; Rao, C. P. 1,3-Di-amidoquinoline conjugate of calix[4]arene (L) as a ratiometric and colorimetric sensor for Zn^{2+}: Spectroscopy, microscopy and computational studies, *Dalton Trans.* **2012**, *41*, 1671–1674.

(93) Zhang, J. F.; Bhuniya, S.; Lee, Y. H.; Bae, C.; Lee, J. H.; Kim, J. S. Novel 2,2'-bipyridine-modified calix[4]arenes: ratiometric fluorescent chemosensors for Zn^{2+} ion. *Tetrahedron Lett.* **2010**, *51*, 3719–3723.

(94) Chawla, H. M.; Shukla, R.; Pandey, S. Preferential recognition of zinc ions through a new anthraquinonoidal calix[4]arene. *Tetrahedron Lett*. **2012**, *53*, 2996–2999.

(95) Steed, J. W.; Atwood, J. L. *Supramolecular Chemistry*, John Wiley & Sons Ltd, **2009**.

(96) Alvarez-Leefmans, F. J.; Delpire. E. *Physiology and pathology of chloride transporters and channels in the nervous system* Eds., Academic Press, **2009**.

(97) Quinton, P. M. Cystic fibrosis: a disease in electrolyte transport. *FASEB J*. **1990**, 10, 2709–2717.

(98) Ruzafa, D.; Conejero-Lara, F.; Morel, B. Modulation of the stability of amyloidogenic precursors by anion binding strongly influences the rate of amyloid nucleation. *Phys. Chem. Chem. Phys*, **2013**, *15*, 15508.

(99) Ratnaike, R. N. Acute and chronic arsenic toxicity. *Postgrad Med J*. 2003, *79*, 391–396.

(100) Tantry, B. A.; Shrivastava, D.; Taher, I.; Tantry, M. N. Arsenic exposure: mechanisms of action and related health effects. *J. Environ Anal Toxicol.* **2015**, *5*, 327.

(101) Srinivasan, A.; Viraraghavan, T. Perchlorate: Health effects and technologies for its removal from water resources. *Int. J. Environ. Res. Public Health* **2009**, *6*, 1418–1442.

(102) Leung, A. M.; Pearce, E. N.; Braverman, L. E.; Environmental perchlorate exposure: potential adverse thyroid effects. *Curr Opin Endocrinol Diabetes Obes.* **2014**, *21*, 372–376.

(103) Gale, P.; Busschaert, N.; Haynes, C.; Karagiannidis, L.; Kirby, I. Anion receptor chemistry: highlights from 2011 and 2012. *Chem. Soc. Rev.* **2014**, *43*, 205–241.

(104) Kirk, L. K. *Biochemistry of the Halogens and Inorganic Halides*; Plenum Press: New York, **1991**.

(105) Kleerekoper, M. The role of fluoride in the prevention of osteoporosis. *Endocrinol. Metab. Clin. North Am*. **1998**, *27*, 441–452.

(106) Aaseth, J.; Shimshi, M.; Gabrilove, J. L.; Birketvedt, G. S. Fluoride: A toxic or therapeutic agent in the treatment of osteoporosis? *J. Trace Elem. Exp. Med*. **2004**, *17*, 83–92.

(107) Carton, R. J. Review of the 2006 united states national research council report: fluoride in drinking water. *Fluoride* **2006**, *39*, 163–172.

(108) Environmental Health Criteria 227, IPCS International Programme on Chemical Safety; World Health Organization: Geneva, Switzerland, **2002**.

(109) Michigami, Y.; Kuroda, Y.; Ueda, K.; Yamamoto, Y. Determination of urinary fluoride by ion chromatography. *Anal. Chim. Acta* **1993**, *274*, 299–302.

(110) Kim, S. K.; Bok, J. H.; Bartsch, R. A.; Lee, J. Y.; Kim, J. S. Fluoride-selective PCT chemosensor based on formation of a static pyrene excimer. *Org. Lett*., **2005**, *7*, 4839–4842.

(111) Dusemund, C.; Sandanayake, K. R. A. S.; Shinkai, S. J. Selective fluoride recognition with ferroceneboronic acid. *Chem. Soc., Chem. Commun*. **1995**, 333–334.

(112) Anzenbacher, P., Jr.; Jursı´kova´, K.; Lynch, V. M.; Gale, P. A.; Sessler, J. L. Calix[4]pyrroles containing deep cavities and fixed walls. synthesis, structural studies, and anion binding properties of the isomeric products derived from the condensation of p-hydroxyacetophenone and pyrrole. *J. Am. Chem. Soc*. **1999**, *121*, 11020–11021.

(113) Miao, R.; Zheng, Q.-Y.; Chen, C.-F.; Huang, Z.-T. A C-linked peptidocalix[4]arene bearing four dansyl groups: a highly selective fluorescence chemosensor for fluoride ions. *Tetrahedron Lett*. **2004**, *45*, 4959–4962.

(114) Frisch, M. J.; Trucks, G. W.; Schlegel, H. B.; Scuseria, G. E.; Robb, M. A.; Cheeseman, J. R.; Zakrzewski, V. G.; Montgomery, J. A., Jr.; Stratmann, R. E.; Burant, J. C. et al. Gaussian 98, revision A6; Gaussian Inc.: Pittsburgh, PA, **1999**.

(115) Lee, S. H.; Kim, H. J.; Lee, Y. O.; Vicensb, J.; Kim, J. S. Fluoride sensing with a PCT-based calix[4]arene. *Tetrahedron Lett.* **2006**, *47*, 4373–4376.

(116) Yun, S.; Ihm, H.; Kim, H. G.; Lee, C. W.; Indrajit, B.; Oh, K. S.; Gong, Y. J.; Lee, J. W.; Yoon, J.; Lee, H. C. et al. Molecular recognition of fluoride anion: benzene-based tripodal imidazolium receptor. *J. Org. Chem*. **2003**, *68*, 2467–2470.

(117) Kim, S. K.; Yoon, J. A new fluorescent PET chemosensor for fluoride ions. *Chem. Commun*. **2002**, 770-771.

(118) Vance, D. H.; Czarnik, A. W. Real-time assay of inorganic pyrophosphatase using a high-affinity chelation-enhanced fluorescence chemosensor. *J. Am. Chem. Soc*. **1994**, *116*, 9397–9398.

(119) Jung. H. S.; Kim, H. J.; Vicens, J.; Kim, J. S. A new fluorescent chemosensor for F^- based on inhibition of excited-state intramolecular proton transfer. *Tetrahedron Lett*. **2009**, *50*, 983–987.

(120) Cho, E. J.; Moon, J. W.; Ko, S. W.; Lee, J. Y.; Kim, S. K.; Yoon, J.; Nam, K. C. A new fluoride selective fluorescent as well as chromogenic chemosensor containing a naphthalene urea derivative. *J. Am. Chem. Soc*. **2003**, *125*, 12376–12377.

(121) Kim, H. J.; Kim, S. K.; Lee, J. Y.; Kim, J. S. Fluoride-sensing calix-luminophores based on regioselective binding. *J. Org. Chem*. **2006**, *71*, 6611–6614.

(122) Kim, J. Y.; Kim, G.; Kim, C. R.; Lee, S. H.; Lee, J. H.; Kim, J. S. UV band splitting of chromogenic azo-coupled calix[4]crown upon cation complexation. *J. Org. Chem*. **2003**, *68*, 1933–1937.

(123) Quinlan, E.; Matthews, S. E.; Gunnlaugsson, T. Colorimetric recognition of anions using preorganized tetra-amidourea derived calix[4]arene sensors. *J. Org. Chem*. **2007**, *72*, 7497–7503.

(124) Camiolo, S.; Gale, P.; Hursthouse, M. B.; Light, M. E. Nitrophenyl derivatives of pyrrole 2,5-diamides: structural behaviour, anion binding and colour change signalled deprotonation. *Org. Biomol. Chem*. **2003**, *1*, 741–744.

(125) Gunnlaugsson, T.; Kruger, P. E.; Jensen, P.; Pfeffer, F. M.; Hussey, G. M. Simple naphthalimide based anion sensors: deprotonation induced colour changes and CO_2 fixation. *Tetrahedron Lett*. **2003**, *44*, 8909-8913.

(126) Chawla, H. M.; Shrivastava, R.; Sahu, S. N. A new class of functionalized calix[4]arenes as neutral receptors for colorimetric detection of fluoride ions. *New J. Chem*., **2008**, *32*, 1999–2005.

(127) Schazmann, B.; Alhashimy, N.; Diamond, D. Chloride selective calix[4]arene optical sensor combining urea functionality with pyrene excimer transduction. *J. Am. Chem. Soc*. **2006**, *128*, 8607–8614.

(128) Machuca, H. G.; Campano, C. Q.; Jullian, C.; De la Fuente, J.; Mahana, H. P.; Escobar, C. A.; Dobado, J. A.; Saitz, C. Study by fluorescence of calix[4]arenes bearing heterocycles with anions: highly selective detection of iodide. *J. Incl. Phenom. Macrocycl. Chem*. **2014**, *80*, 369–375.

(129) Amendola, V.; Boiooccchi, M.; Fabbrizzi, L.; Fusco, N. Putting the anion into the cage-fluoride. Inclusion in the smallest trisimidazolium macrotricycle. *Eur. J. Org. Chem.* **2011**, *32*, 6434–6444.

(130) Vasquez, M.; Fabrizzi, L; Taglietti, A.; Pedrido, R. M.; Gonza´lez Noya, A.M.; Bermejo, M. R. A colorimetric approach to anion sensing: a selective chemosensor of fluoride Ions, in which color is generated by anion-enhanced p delocalization. *Angew. Chem. Int. Ed.* **2004**, *43*, 1962–1965.

(131) Jeon, N. J.; Ryu, B. J.; Lee, B. H.; Nam, K. C. Fluorescent sensing of tetrahedral anions with a pyrene urea derivative of calix[4]arene chemosensor. *Bull. Korean Chem. Soc.* **2009**, *30*, 1675–1677.

(132) Sun, X. H.; Li, W.; Xia, P. F.; Luo, H. B.; Wei, Y.; Wong, M. S. Cheng, Y. T.; Shuang, S. phenyl-calix[4]arene-based fluorescent sensors: cooperative binding for carboxylates, *J. Org. Chem.* **2007**, *72*, 2419–2426.

(133) Qing, G. Y; He, Y.; Wang, F.; Qin, H.; Hu, C.; Yang, X. Enantioselective fluorescent sensors for chiral carboxylates based on calix[4]arenes bearing an L-tryptophan unit. *Eur. J. Org. Chem.* **2007**, 1768–1778.

(134) Qing, G. Y.; Wang, F.; He, Y. B.; Hu, C. G.; Yang, X. Highly selective fluorescent recognition of amino alcohol based on chiral calix[4]arenes bearing L-tryptophan unit. *Supramol. Chem.* **2008**, *20*, 635–641.

(135) Nguyenc, B. T.; Anslyn, E. V. Indicator–displacement assays. *Coordin. Chem. Rev*. **2006**, *250*, 3118–3127.

(136) Norouzy, A.; Azizi, Z.; Nau, W. M. Indicator displacement assays inside live cells. *Angew. Chem. Int. Ed*. **2015**, *54*, 792–795.

(137) Koner, A. L.; Schatz, J.; Nau, W. M.; Pischel, U. Selective sensing of citrate by a supramolecular 1,8-naphthalimide/calix[4]arene assembly *via* complexation-modulated pKa shifts in a ternary complex. *J. Org. Chem*. **2007**, *72*, 3889–3895.

(138) Blachier, F.; Wu, G.; Yin, Y. (eds), *Nutritional and physiological functions of amino acids in pigs*, Springer, **2013**.

(139) Siegel, G. J.; Agranoff, B. W.; Albers, R. W.; et al., editors. Basic neurochemistry: molecular, cellular and medical aspects. 6th edition. Philadelphia: Lippincott-Raven; **1999**. Chapter 15.

(140) Baughman, R. W.; Gilbert, C. D. Aspartate and glutamate as possible neurotransmitters in the visual cortex. *J. Neurosci.* **1981**, *1*, 427–439.

(141) Fonnum, F. Glutamate: a neurotransmitter in mammalian brain. *J. Neurochem.* **1984**, *42*, 1–11.

(142) Li, S. Y.; Xu, Y. W.; Zeng, S. Q.; Xiao, L. M.; Duan, H. Q.; Lin, X. L.; Liu, J. M.; Su, C. Y. Highly selective fluorescent calix[4]arene chemosensor for acidic amino acids in pure aqueous media. *Tetrahedron Lett.* **2012**, *53*, 2918–2921.

(143) Zhang, X.; Li, J.; Feng, N.; Luo, L.; Dai, Z.; Yang, L.; Tian, D.; Li, H.; A tryptophan responsive fluorescent and wettable dual-signal switch. *Org. Biomol. Chem.* **2014**, *12*, 6824–6830.

(144) Xu, L.; Chen, W.; Mulchandani, A.; Yan, Y. Reversible conversion of conducting polymer films from superhydrophobic to superhydrophilic. *Angew. Chem., Int. Ed.* **2005**, 44, 6009–6012.

(145) Mendes, P. Stimuli-responsive surfaces for bio-applications. *Chem. Soc. Rev.* **2008**, *37*, 2512–2529.

(146) Stuart, M.; Huck, W.; Genzer, J.; Müller, M.; Ober, C.; Stamm, M.; Sukhorukov, G.; Szleifer, I.; Tsukruk, V.; Urban, M. et al. Emerging applications of stimuli-responsive polymer materials. *Nat. Mater.* **2010**, *9*, 101–113.

(147) Mummidivarapu, V. V. S.; Hinge, V. K.; Samanta, K.; Yarramala, D. S.; Rao, C. P. Supramolecular complexation of biological phosphates with an acyclic triazolium-linked anthracenyl-1,3-diconjugate of calix[4]arene: synthesis, characterization, spectroscopy, microscopy, and computational studies. *Chem. Eur. J.* **2014**, *20*, 14378–14386.

(148) Xu, Z.; Singh, N. J.; Lim, J.; Pan, J.; Kim, H. N.; Park, S.; Kim, K. S.; Yoon, J. Unique sandwich stacking of pyrene-adenine-pyrene for selective and ratiometric fluorescent sensing of ATP at physiological pH. *J. Am. Chem. Soc.* **2009**, *131*, 15528–15533.

(149) Li, C.; Numata, M.; Takeuchi, M.; Shinkai, S. A sensitive colorimetric and fluorescent probe based on a polythiophene derivative for the detection of ATP. *Angew. Chem. Int. Ed.* **2005**, *44*, 6371–6374.

(150) Chang, K.-C.; Su, I.-H.; Senthilvelan, A.; Chung, W.-S. Triazole-modified calix[4]crown as a novel fluorescent on-off switchable chemosensor. *Org. Lett.* **2007**, *9*, 3363–3366.

(151) Kim, S. H.; Choi, J. K.; Kim, S. K.; Sim, W.; Kim, J. S. On/off fluorescence switch of a calix[4]arene by metal ion exchange. *Tetrahedron Lett.* **2006**, *47*, 3737–3741.

(152) Kim, S. K.; Lee, S. H.; Lee, J. Y.; Lee, J. Y.; Bartsch, R. A.; Kim, J. S. An excimer-based, binuclear, on-off switchable calix[4]crown chemosensor. *J. Am. Chem. Soc.* **2004**, *126*, 16499–164506.

(153) Lee, J. Y.; Kim, S. K.; Jung, J. H.; Kim, J. S. Bifunctional fluorescent calix[4]arene chemosensor for both a cation and an anion. *J. Org. Chem.* **2005**, *70*, 1463–1466.

(154) Wang, H. W.; Feng, Y. Q.; Chen, C.; Xue, J. Q. Two novel fluorescent calix[4]arene derivatives with benzoazole units in 1,3-alternate conformation for selective recognition to Fe^{3+} and Cr^{3+}. *Chinese Chem. Lett.* **2009**, *20*, 1271–1274.

(155) Patra, S.; Lo, R.; Chakraborty, A.; Gunupuru, R.; Maity, D.; Ganguly, B.; Paul, P. Calix[4]arene based fluorescent chemosensor bearing coumarin as fluorogenic unit: Synthesis, characterization, ion-binding property and molecular modeling. *Polyhedron* **2013**, *50*, 592–601.

(156) Yao, J. N.; Dou, W.; Qin, W. W.; Liu, W. S. A new coumarin-based chemosensor for Fe^{3+} in water. *Inorg. Chem. Commun.* **2009**, *12*, 116–118.

(157) de Silva, A. P.; Gunaratne, H. Q. N.; Gunnlaugsson, T.; Huxley, A. J. M.; McCoy, C. P.; Rademacher, J. T.; Rice, T. E. Signaling recognition events with fluorescent sensors and switches. *Chem. Rev.* **1997**, *97*, 1515–1566.

(158) Oliveira, E.; Baptista, R. M. F.; Costa, S. P. G.; Raposo, M. M. M.; Lodeiro, C. Exploring the emissive properties of new azacrown compounds bearing aryl, furyl, or thienyl moieties: a special case of chelation enhancement of fluorescence upon interaction with Ca^{2+}, Cu^{2+}, or Ni^{2+}. *Inorg. Chem.* **2010**, *49*, 10847–10857.

(159) Lee, M. H.; Quang, D. T.; Jung, H. S.; Yoon, J.; Lee, C. H.; Kim, J. S. Ion-induced FRET on-off in fluorescent calix[4]arene. *J. Org. Chem.* **2007,** *72*, 4242–4245.

(160) Casnati, A.; Ungaro, R.; Asfari, Z.; Vicens, J. *In calixarenes* 2001; Asfari, Z., Bo¨hmer, V., Harrowfield, J., Eds.; Kluwer Academic Publishers: Dordrecht, The Netherlands, **2001**; p 365.

(161) Senthilvelan, A.; Ho, I. T.; Chang, K. C.; Lee, G. H.; Liu, Y. H.; Chung, W. S. Cooperative recognition of a copper cation and anion by a calix[4]arene substituted at the lower rim by a beta-amino-alpha,beta-unsaturated ketone. *Chem-Eur. J.* **2009**, *15*, 6152–6160.

(162) Tas, E.; Kilic, A.; Konak, N.; Yilmaz, I., The sterically hindered salicylaldimine ligands with their copper(II) metal complexes: Synthesis, spectroscopy, electrochemical and thin-layer spectroelectrochemical features. *Polyhedron* **2008**, *27*, 1024–1032.

(163) Sahin, O.; Yilmaz, M. Synthesis and fluorescence sensing properties of a new naphthalimide derivative of calix[4]arene. *Tetrahedron Lett*. **2012**, *53*, 2319–2324.

(164) Xu, Z.; Kim, S.; Kim, H. N.; Han, S. J.; Lee, C.; Kim, J. S.; Qian, X. H.; Yoon, J. A naphthalimide-calixarene as a two-faced and highly selective fluorescent chemosensor for Cu^{2+} or F^{-}. *Tetrahedron Lett.* **2007,** *48*, 9151–9154.

(165) Xu, Z. C.; Qian, X. H.; Cui, J. N. Colorimetric and ratiometric fluorescent chemosensor with a large red-shift in emission: Cu(II)-only sensing by deprotonation of secondary amines as receptor conjugated to naphthalimide fluorophore. *Org. Lett.* **2005**, *7*, 3029–3032.

(166) Joseph, R.; Chinta, J. P.; Rao, C. P. Calix[4]arene-based 1,3-diconjugate of salicylyl imine having dibenzyl amine moiety (I): synthesis, characterization, receptor properties toward Fe^{2+}, Cu^{2+}, and Zn^{2+}, crystal structures of its Zn^{2+} and Cu^{2+} complexes, and selective phosphate sensing by the [ZnL]. *Inorg. Chem.* **2011**, *50*, 7050–7058.

(167) Sahin, O., Synthesis and spectral properties of pyrene based calix[4]arene. *J. Mol. Struct.* **2013**, *1041*, 175–182.

(168) Hu, X. Y.; Zhang, X. L.; Song, H. L.; He, C.; Bao, Y. M.; Tang, Q.; Duan, C. Y. A novel copper(II) complex-based fluorescence probe for nitric oxide detecting and imaging. *Tetrahedron* **2012**, *68*, 8371–8375.

(169) Gao, C. J.; Jin, X. J.; Yan, X. H.; An, P.; Zhang, Y.; Liu, L. L.; Tian, H.; Liu, W. S.; Yao, X. J.; Tang, Y. A small molecular fluorescent sensor for highly selectivity of zinc ion. *Sen Actuators. B. Chem.* **2013**, *176*, 775–781.

(170) Song, F. Y.; Ma, X.; Hou, J. L.; Huang, X. B.; Cheng, Y. X.; Zhu, C. J. (R,R)-salen/salan-based polymer fluorescence sensors for Zn^{2+} detection. *Polymer* **2011**, *52*, 6029–6036.

(171) Yuan, M. J.; Li, Y. L.; Li, J. B.; Li, C. H.; Liu, X. F.; Lv, J.; Xu, J. L.; Liu, H. B.; Wang, S.; Zhu, D. A colorimetric and fluorometric dual-modal assay for mercury ion by a molecule. *Org. Lett.* **2007**, *9*, 2313–2316.

(172) Hsieh, W. H.; Wan, C. F.; Liao, D. J.; Wu, A. T. A turn-on Schiff base fluorescence sensor for zinc ion. *Tetrahedron Lett.* **2012**, *53*, 5848–5851.

(173) Sahin, O.; Akceylan, E. A phenanthrene-based calix[4]arene as a fluorescent sensor for Cu^{2+} and F^-. *Tetrahedron* **2014**, *70*, 6944–6950.

(174) Sutariya, P. G.; Pandya, A.; Lodha, A.; Menon, S. K. Fluorescence switch on-off-on receptor constructed of quinoline allied calix[4]arene for selective recognition of Cu^{2+} from blood serum and F^- from industrial waste water. *Analyst* **2013**, *138*, 2531–2535.

(175) Sutariya, P. G.; Pandya, A.; Lodha, A.; Menon, S. K. A pyrenyl linked calix[4]arene fluorescence probe for recognition of ferric and phosphate ions. *RSC Adv.* **2014**, *4*, 34922–34926.

(176) Sutariya, P. G.; Pandya, A.; Modi, N. R.; Menon, S. K. A highly efficient PET switch on-off-on fluorescence receptor based on calix[4]arene for the selective recognition of Cd^{2+} and Sr^{2+}. *Analyst* **2013**, *138*, 2244–2248.

(177) Erdemir, S.; Malkondu, S.; Kocyigit, O.; Alici, O. A novel colorimetric and fluorescent sensor based on calix[4]arene possessing triphenylamine units. *Spectrochim. Acta A.* **2013**, *114*, 190–196.

(178) Liu, Y.; Li, Z.; Zhang, H. Y.; Wang, H.; Li, C. J. Colorimetric sensor and inverse fluorescent behavior of anions by calix[4]arene possessing imidazo[4,5-f]-1,10-phenanthroline groups and its Ru(II) Complex. *Supramol. Chem.* **2008**, *20*, 419–426.

(179) Miao, F.; Zhou, J.; Tian, D.; Li, H. Enantioselective recognition of mandelic acid with (R)-1,1-bi-2-naphthol-linked calix[4]arene *via* fluorescence and dynamic light scattering. *Org. Lett.* **2012**, *14*, 3572–3575.

(180) Mummidsivarapu, V. V. S.; Hinge, V. K.; Rao, C. P. Interaction of a dinuclear fluorescent Cd(II) complex of calix[4]arene conjugate with phosphates and its applicability in cell imaging, *Dalton Trans.*, **2015**, *44*, 1130–1141.

(181) Dessingou, J.; Tabbasum, K.; Mitra, A.; Hinge, V. K.; Rao, C. P. lower rim 1,3-di{4-antipyrine}amide conjugate of calix[4]arene: synthesis, characterization, and selective recognition of Hg^{2+} and its sensitivity toward pyrimidine bases. *J. Org. Chem.* **2012**, *77*, 1406–1413.

(182) Joseph, R.; Ramanujam, B.; Acharya, A.; Rao, C. P. Lower rim 1,3-di{bis(2-picolyl)}amide derivative of calix[4]arene (L) as ratiometric primary sensor toward Ag^{+} and the complex of Ag^{+} as secondary sensor toward cys: experimental, computational, and microscopy studies and INHIBIT logic gate properties of L. *J. Org. Chem.* **2009**, *74*, 8181–8190.

(183) Souchon, V.; Maisonneuve, S.; David, O.; Leray, I.; Xie, J.; Valeur, B. Photophysics of cyclic multichromophoric systems based on beta-cyclodextrin and calix[4]arene with appended pyridin-2 '-yl-1,2,3-triazole groups. *Photoch. Photobio. Sci.* **2008**, *7*, 1323–1331.

(184) Joseph, R.; Ramanujam, B.; Acharya, A.; Rao, C. P. Fluorescence switch-on sensor for Cu^{2+} by an amide linked lower rim 1,3-bis(2-picolyl)amine derivative of calix[4]arene in aqueous methanol. *Tetrahedron Lett.* **2009**, *50*, 2735–2739.

(185) Pathak, R. K.; Hinge, V. K.; Mondal, M.; Rao, C. P. Triazole-linked-thiophene conjugate of calix[4]arene: its selective recognition of Zn^{2+} and as biomimetic model in supporting the events of the metal detoxification and oxidative stress involving metallothionein. *J. Org. Chem.* **2011**, *76*, 10039–10049.

(186) Chang, C. J.; Jaworski, J.; Nolan, E. M.; Sheng, M.; Lippard, S. J. A tautomeric zinc sensor for ratiometric fluorescence imaging: Application to nitric oxide-induced release of intracellular zinc. *P. Natl. Acad. Sci. USA* **2004**, *101*, 1129–1134.

(187) Pathak, R. K.; Tabbasum, K.; Rai, A.; Panda, D.; Rao, C. P. Pyrophosphate sensing by a fluorescent Zn^{2+} bound triazole linked imino-thiophenyl conjugate of calix[4]arene in HEPES buffer medium: spectroscopy. microscopy, and cellular studies. *Anal. Chem.* **2012**, *84*, 5117–5123.

(188) Pathak, R. K.; Tabbasum, K.; Rai, A.; Panda, D.; Rao, C. P. A Zn^{2+} specific triazole based calix[4]arene conjugate (L) as a fluorescence sensor for histidine and cysteine in HEPES buffer milieu. *Analyst* **2012**, *137*, 4069–4075.

(189) Pathak, R. K.; Hinge, V. K.; Mahesh, K.; Rai, A.; Panda, D.; Rao, C. P. Cd^{2+} complex of a triazole-based calix[4]arene conjugate as a selective fluorescent chemosensor for Cys. *Anal. Chem.* **2012**, *84*, 6907–6913.

(190) Pathak, R. K.; Dessingou, J.; Rao, C. P. Multiple sensor array of Mn^{2+}, Fe^{2+}, Co^{2+}, Ni^{2+}, Cu^{2+}, and Zn^{2+} complexes of a triazole linked imino-phenol based calix[4]arene conjugate for the selective recognition of Asp, Glu, Cys, and His. *Anal. Chem.* **2012**, *84*, 8294–8300.

(191) Pathak, R. K.; Hinge, V. K.; Rai, A.; Panda, D.; Rao, C. P. Imino-phenolic-pyridyl conjugates of calix[4]arene (L1 and L2) as primary fluorescence switch-on sensors for Zn^{2+} in solution and in HeLa cells and the recognition of pyrophosphate and ATP by [ZnL2]. *Inorg. Chem.* **2012**, *51*, 4994–5005.

(192) Nehra, A.; Yarramala, D. S.; Hinge, V. K.; Samanta, K.; Rao, C. P. Differentiating phosphates by an Mg^{2+} complex of the conjugate of calix[4]arene *via* the formation of ternary species and causing

changes in the aggregation: spectroscopy, microscopy, and computational modeling. *Anal. Chem.* **2015**, *87*, 9344–9351.

(193) Nehra, A.; Hinge, V. K.; Rao, C. P. Phenylene-diimine-capped conjugate of lower rim 1,3-calix[4]arene as molecular receptor for Mg^{2+} *via* arm conformational changes followed by aggregation and mimicking the species by molecular mechanics. *J. Org. Chem.* **2014**, *79*, 5763–5770.

(194) Lee, Y. H.; Liu, H.; Lee, J. Y.; Kim, S. K. S. H.; Kim, S. K. S. H.; Sessler, J. L.; Kim, Y.; Kim, J. S. Dipyrenylcalix[4]arene-A fluorescence-based chemosensor for trinitroaromatic explosives. *Chem-Eur. J.* **2010**, *16*, 5895–5901.

(195) Kandpal, M.; Bandela, A. K.; Hinge, V. K.; Rao, V. R.; Rao, C. P. Fluorescence and piezoresistive cantilever sensing of trinitrotoluene by an upper-rim tetrabenzimidazole conjugate of calix[4]arene and delineation of the features of the complex by molecular dynamics. *ACS Appl. Mater. Interfaces* **2013**, *5*, 13448–13456.

(196) Cao, X.; Luo, L.; Zhang, F.; Miao, F.; Tian, D.; Li, H. Synthesis of a deep cavity calix[4]arene by fourfold Sonogashira cross-coupling reaction and selective fluorescent recognition toward p-nitrophenol. *Tetrahedron Lett.* **2014**, *55*, 2029–2032.

(197) Zhan, J.; Zhu, X.; Fang, F.; Miao, F.; Tian, D.; Li, H. Sensitive fluorescence sensor for nitroaniline isomers based on calix[4]arene bearing naphthyl groups. *Tetrahedron* **2012**, *68*, 5579–5582.

(198) Boonkitpatarakul, K.; Yodta, Y.; Niamnont, N.; Sukwattanasinitt, M. Fluorescent phenylethynylene calix[4]arenes for sensing TNT in aqueous media and vapor phase. *RSC Adv.* **2015**, *5*, 33306–33311.

(199) Wang, F.; Yang, Y.; Swager, T. M. Molecular recognition for high selectivity in carbon nanotube/polythiophene chemiresistors. *Angew. Chem. Int. Ed.* **2008**, *47*, 8394–8396.

(200) Molad, A.; Goldberg, I.; Vigalok, A. Tubular conjugated polymer for chemosensory applications. *J. Am. Chem. Soc.* **2012**, *134*, 7290–7292.

(201) Chinta, J. P.; Rao, C. P. Triazole linked lower rim glycosyl appended 1,3-calix[4]arene conjugates: Synthesis, characterization, and their interaction with jacalin. *Carbohydr. Res.* **2013**, *369*, 58–62.

(202) Yang, Q.; Qin, X.; Yan, C.; Zhu, X. A novel fluorescent chemosensor for safranine T based on calixarene-1,3-diacyl hydrazone. *Sens. Actuators B Chem.* **2015**, *212*, 183–189.

(203) Ma, L.; Zhu, X. Determination of emodin by hexadecyl trimethyl ammonium bromide sensitized fluorescence quenching method of the derivatives of calix[4]arene. *Spectrochim. Acta A* **2012**, *95*, 246–251.

(204) Sun, Y.; Mao, X.; Luo, L.; Tian, D.; Li, H. Calix[4]arene triazole-linked pyrene: click synthesis, assembly on graphene oxide, and highly sensitive carbaryl sensing in serum. *Org. Biomol. Chem.* **2015**, *13*, 9294–9299.

(205) Li, H.; Qu, F. Selective inclusion of polycyclic aromatic hydrocarbons (PAHs) on calixarene coated silica nanospheres englobed with CdTe nanocrystals. *J. Mater. Chem.* **2007**, *17*, 3536–3544.

(206) Sidorov, V.; Kotch, F. W.; Abdrakhmanova, G.; Mizani, R.; Fettinger, J. C.; Davis, J. T. Ion channel formation from a calix[4]arene amide that binds HCl. *J. Am. Chem. Soc.* **2002**, *124*, 2267–2278.

(207) Iqbal, K. S.; Allen, M. C.; Fucassi, F.; Cragg, P. J., Artificial transmembrane ion channels from commercial surfactants. *Chem. Commun.* **2007**, 3951–3953.

(208) Aime, S.; Barge, A.; Botta, M.; Casnati, A.; Fragai, M.; Luchinat, C.; Ungaro, R. A calix[4]arene Gd-III complex endowed with high stability, relaxivity, and binding affinity to serum albumin. *Angew. Chem. Int. Ed.* **2001**, *40*, 4737–4739.

(209) Schuhle, D. T.; Schatz, J.; Laurent, S.; Elst, L. V.; Muller, R. N.; Stuart, M. C. A.; Peters, J. A. Calix[4]arenes as molecular platforms for magnetic resonance imaging (MRI) contrast agents. *Chem-Eur. J.* **2009,** *15*, 3290–3296.

(210) Dings, R. P. M.; Chen, X. M.; Hellebrekers, D. M. E. I.; van Eijk, L. I.; Zhang, Y.; Hoye, T. R.; Griffioen, A. W.; Mayo, K. H. Design of nonpeptidic topomimetics of antiangiogenic proteins with antitumor activities. *J. Natl. Cancer I* **2006**, *98*, 932–936.

(211) Loiseau, F. A.; Hill, A. M.; Hii, K. K. M. Preparation of macrocyclon analogues: calix[8]arenes with extended polyethylene glycol chains. *Tetrahedron* **2007**, *63*, 9947–9959.

(212) Da Silva, E.; Lazar, A. N.; Coleman, A. W., Bioharmaceutical applications of calixarenes. *J. Drug Deliv. Sci. Tec.* **2004**, *14*, 3–20.

(213) Lalor, R.; Baillie-Johnson, H.; Redshaw, C.; Matthews, S. E.; Mueller, A., Cellular uptake of a fluorescent calix[4]arene derivative. *J. Am. Chem. Soc.* **2008**, *130*, 2892–2893.

(214) Consoli, G. M.; Granata, G.; Fragassi, G.; Grossi, M.; Sallese, M.; Geraci, C., Design and synthesis of a multivalent fluorescent folate-calix[4]arene conjugate: cancer cell penetration and intracellular localization. *Org. Biomol. Chem.* **2015**, *13*, 3298–3307.

(215) Shulov, I.; Rodik, R. V.; Arntz, Y.; Reisch, A.; Kalchenko, V. I.; Klymchenko, A. S. Protein-sized bright fluorogenic nanoparticles based on cross-linked calixarene micelles with cyanine corona. *Angew. Chem. Int. Ed.* **2016**, *55*, 15884–15888.

(216) Hong, Y. N.; Lam, J. W. Y.; Tang, B. Z. Aggregation-induced emission. *Chem. Soc. Rev.* **2011,** *40*, 5361–5388.

(217) Wu, C.; Chiu, D. T. Highly fluorescent semiconducting polymer dots for biology and medicine. *Angew. Chem. Int. Ed*. **2013**, *52*, 3086 – 3109.

(218) Boukerb, A. M.; Rousset, A.; Galanos, N.; Mear, J. B.; Thepaut, M.; Grandjean, T.; Gillon, E.; Cecioni, S.; Abderrahmen, C.; Faure, K. et al. Antiadhesive properties of glycoclusters against pseudomonas aeruginosa lung infection. *J. Med. Chem.* **2014**, *57*, 10275–10289.

(219) Sansone, F.; Dudic, M.; Donofrio, G.; Rivetti, C.; Baldini, L.; Casnati, A.; Cellai, S.; Ungaro, R. DNA condensation and cell transfection properties of guanidinium calixarenes: dependence on macrocycle lipophilicity, size, and conformation. *J. Am. Chem. Soc.* **2006**, *128*, 14528–14536.

(220) Bagnacani, V.; Sansone, F.; Donofrio, G.; Baldini, L.; Casnati, A.; Ungaro, R. Macrocyclic nonviral vectors: high cell transfection efficiency and low toxicity in a lower rim guanidinium calix[4]arene. *Org. Lett.* **2008**, *10*, 3953–3956.

(221) Bagnacani, V.; Franceschi, V.; Fantuzzi, L.; Casnati, A.; Donofrio, G.; Sansone, F.; Ungaro, R. Lower rim guanidinocalix[4]arenes: macrocyclic nonviral vectors for cell transfection. *Bioconjug. Chem.* **2012**, *23*, 993–1002.

(222) Bagnacani, V.; Franceschi, V.; Bassi, M.; Lomazzi, M.; Donofrio, G.; Sansone, F.; Casnati, A.; Ungaro, R., Arginine clustering on calix[4]arene macrocycles for improved cell penetration and DNA delivery. *Nat. Commun.* **2013**, *4*, 1721.

(223) Gallego-Yerga, L.; Lomazzi, M.; Franceschi, V.; Sansone, F.; Mellet, C. O.; Donofrio, G.; Casnati, A.; Fernandez, J. M. G. Cyclodextrin- and calixarene-based polycationic amphiphiles as gene delivery systems: a structure-activity relationship study. *Org. Biomol. Chem.* **2015**, *13*, 1708–1723.

(224) Nault, L.; Cumbo, A.; Pretot, R. F.; Sciotti, M. A.; Shahgaldian, P. Cell transfection using layer-by-layer (LbL) coated calixarene-based solid lipid nanoparticles (SLNs). *Chem. Comm.* **2010**, *46*, 5581–5583.

(225) Rodik, R. V.; Klymchenko, A. S.; Jain, N.; Miroshnichenko, S. I.; Richert, L.; Kalchenko, V. I.; Mely, Y. Virus-sized DNA nanoparticles for gene delivery based on micelles of cationic calixarenes. *Chem-Eur. J.* **2011**, *17*, 5526–5538.

(226) Rodik, R. V.; Anthony, A. S.; Kalchenko, V. I.; Mely, Y.; Klymchenko, A. S. Cationic amphiphilic calixarenes to compact DNA into small nanoparticles for gene delivery. *New J. Chem.* **2015**, *39*, 1654–1664.

(227) Mochizuki, S.; Nishina, K.; Fujii, S.; Sakurai, K. The transfection efficiency of calix[4]arene-based lipids: the role of the alkyl chain length. *Biomater Sci-Uk* **2015**, *3*, 317–322.

(228) Barran-Berdon, A. L.; Yelamos, B.; Garcia-Rio, L.; Domenech, O.; Aicart, E.; Junquera, E. Polycationic macrocyclic scaffolds as potential non-viral vectors of dna: A multidisciplinary study. *ACS Appl. Mater. Inter.* **2015**, *7*, 14404–14414.

(229) Rullaud, V.; Moridi, N.; Shahgaldian, P. Sequence-specific DNA interactions with calixarene-based langmuir monolayers. *Langmuir* **2014**, *30*, 8675–8679.

(230) Alavijeh, N. S.; Zadmard, R.; Balalaie, S.; Alavijeh, M. S.; Soltani, N. DNA binding and recognition of a cc mismatch in a DNA duplex by water-soluble peptidocalix[4]arenes: synthesis and applications. *Org. Lett.* **2016**, *18*, 4766–4769.

(231) Lalor, R.; DiGesso, J. L.; Mueller, A.; Matthews, S. E. Efficient gene transfection with functionalised multicalixarenes. *Chem. Comm.* **2007**, 4907–4909.

(232) Gschwind, H. P.; Pfaar, U.; Waldmeier, F.; Zollinger, M.; Sayer, C.; Zbinden, P.; Hayes, M.; Pokorny, R.; Seiberling, M.; Ben-Am, M. et al. Metabolism and disposition of imatinib mesylate in healthy volunteers. *Drug Metab. Dispos.* **2005**, *33*, 1503–1512.

(233) O'Brien, S. G.; Guilhot, F.; Larson, R. A.; Gathmann, I.; Baccarani, M.; Cervantes, F.; Cornelissen, J. J.; Fischer, T.; Hochhaus, A.; Hughes, T. et al. Imatinib compared with interferon and low-dose cytarabine for newly diagnosed chronic-phase chronic myeloid leukemia. *New Engl. J. Med.* **2003**, *348*, 994–1004.

(234) Linch, M.; Claus, J.; Benson, C., Update on imatinib for gastrointestinal stromal tumors: duration of treatment. *Oncotargets Ther.* **2013**, *6*, 1011–1023.

(235) Peng, B.; Hayes, M.; Resta, D.; Racine-Poon, A.; Druker, B. J.; Talpaz, M.; Sawyers, C. L.; Rosamilia, M.; Ford, J.; Lloyd, P.; Capdeville, R. Pharmacokinetics and pharmacodynamics of imatinib in a phase I trial with chronic myeloid leukemia patients. *J. Clin. Oncol.* **2004**, *22*, 935–942.

(236) Peng, B.; Lloyd, P.; Schran, H., Clinical pharmacokinetics of imatinib. *Clin. Pharmacokinet.* **2005,** *44*, 879–894.

(237) Peng, B.; Dutreix, C.; Mehring, G.; Hayes, M. J.; Ben-Am, M.; Seiberling, M.; Pokorny, R.; Capdeville, R.; Lloyd, P. Absolute bioavailability of imatinib (Glivec (R)) orally versus intravenous infusion. *J. Clin. Pharmacol.* **2004**, *44*, 158–162.

(238) Takahashi, N.; Miura, M.; Scott, S. A.; Kagaya, H.; Kameoka, Y.; Tagawa, H.; Saitoh, H.; Fujishima, N.; Yoshioka, T.; Hirokawa, M.; Sawada, K. Influence of CYP3A5 and drug transporter polymorphisms on imatinib trough concentration and clinical response among patients with chronic phase chronic myeloid leukemia. *J. Hum. Genet.* **2010**, *55*, 731–737.

(239) Eechoute, K.; Sparreboom, A.; Burger, H.; Franke, R. M.; Schiavon, G.; Verweij, J.; Loos, W. J.; Wiemer, E. A. C.; Mathijssen, R. H. J. Drug transporters and imatinib treatment: implications for clinical practice. *Clin. Cancer Res.* **2011**, *17*, 406–415.

(240) Adhikari, B. B.; Roshandel, S.; Fujii, A.; Schramm, M. P. Calixarene-mediated liquid membrane transport of choline conjugates 2: transport of drug-choline conjugates and neurotransmitters. *Eur. J. Org. Chem.* **2015**, 2683–2690.

(241) Granata, G.; Paterniti, I.; Geraci, C.; Cunsolo, F.; Esposito, E.; Cordaro, M.; Blanco, A. R.; Cuzzocrea, S.; Consoli, G. M. L. Potential eye drop based on a calix[4]arene nanoassembly for curcumin delivery: enhanced drug solubility, stability, and anti-inflammatory effect. *Mol. Pharm.* **2017**, *14*, 1610–1622.

(242) Alrawaiq, N. S.; Abdullah, A. A review of antioxidant polyphenol curcumin and its role in detoxification. *Int. J. Pharm. Technol. Res.* **2014**, *6*, 280−289.

(243) Moghadamtousi, S. Z.; Kadir, H. A.; Hassandarvish, P.; Tajik, H.; Abubakar, S.; Zandi, K. A review on antibacterial, antiviral, and antifungal activity of curcumin. *BioMed. Res. Int.* **2014,** *2014*, 12.

(244) Gupta, S. C.; Patchva, S.; Aggarwal, B. B. Therapeutic roles of curcumin: lessons learned from clinical trials. *AAPS J.* **2013**, *15*, 195-218.

(245) Anand, P.; Kunnumakkara, A. B.; Newman, R. A.; Aggarwal, B. B. Bioavailability of curcumin: problems and promises. *Mol. Pharmaceutics* **2007**, *4*, 807−818.

(246) Consoli, G. M. L.; Di Bari, I.; Blanco, A. R.; Nostro, A.; D'Arrigo, M.; Pistara, V.; Sortino, S. Design, synthesis, and antibacterial activity of a multivalent polycationic calix[4]arene-no photodonor conjugate. *ACS Med. Chem. Lett.* **2017**, *8*, 881–885.

(247) Narkhede, N.; Uttam, B.; Kandi, R.; Rao, C. P. Silica-calix hybrid composite of allyl calix[4]arene covalently linked to MCM-41 nanoparticles for sustained release of doxorubicin into cancer cells. *ACS Omega* **2018**, *3*, 229–239.

(248) Guo, D.-S.; Liu, Y. Supramolecular chemistry of p-sulfonatocalix[n]arenes and its biological applications. *Acc. Chem. Res*. **2014**, *47*, 1925−1934.

(249) Zhu, L.; Wu, W.; Zhu, M.-Q.; Han, J. J.; Hurst, J. K.; Li, A. D. Q. Reversibly photoswitchable dual-color fluorescent nanoparticles as new tools for live-cell imaging. *J. Am. Chem. Soc.* **2007**, *129*, 3524–3526.

(250) Wu, C.; Bull, B.; Szymanski, C.; Christensen, K.; McNeill, J. Multicolor conjugated polymer dots for biological fluorescence imaging. *ACS Nano* **2008**, *2*, 2415–2423.

(251) Yang, Y.; Wang, X.; Cui, Q.; Cao, Q.; Li, L. Self-assembly of fluorescent organic nanoparticles for iron(iii) sensing and cellular imaging. *ACS Appl. Mater. Interfaces*, **2016**, *8*, 7440–7448.

(252) Feng, X.; Liu, L.; Wang, S.; Zhu, D. Water-soluble fluorescent conjugated polymers and their interactions with biomacromolecules for sensitive biosensors. *Chem. Soc. Rev.* **2010**, *39*, 2411–2419.

(253) Pu, F.; Ju, E.; Ren, J.; Qu, X. Multiconfigurable logic gates based on fluorescence switching in adaptive coordination polymer nanoparticles. *Adv. Mater.* **2014**, 26, 1111–1117.

(254) Jiang, B. P.; Guo, D. S.; Liu, Y. C.; Wang, K. P.; Liu, Yu. Photomodulated fluorescence of supramolecular assemblies of sulfonatocalixarenes and tetraphenylethene. *ACS Nano* **2014**, *8*, 1609–1618.

(255) Guo, D.-S.; Liu, Y. Calixarene-based supramolecular polymerization in solution. *Chem. Soc. Rev*. **2012**, *41*, 5907–5921.

(256) Wang, K.; Guo, D.-S.; Wang, X.; Liu, Y. Multistimuli responsive supramolecular vesicles based on the recognition of p-sulfonatocalixarene and its controllable release of doxorubicin. *ACS Nano* **2011**, *5*, 2880–2994.

(257) Guo, D.-S.; Wang, K.; Wang, Y.-X.; Liu, Y. Cholinesterase-responsive supramolecular vesicle. *J. Am. Chem. Soc*. **2012**, *134*, 10244–10250.

(258) Basilio, N.; Gomez, B.; García-Río, L.; Francisco, V. Using calixarenes to model polyelectrolyte surfactant nucleation sites. *Chem-Eur. J.* **2013**, *19*, 4570–4576.

(259) Basilio, N.; Martín-Pastor, M.; García-Río, L. Insights into the structure of the supramolecular amphiphile formed by a sulfonated calix[6]arene and alkyltrimethylammonium surfactants. *Langmuir* **2012**, *28*, 6561–6568.

(260) Lau, V.; Heyne, B. Calix[4]arene sulfonate as a template for forming fluorescent thiazole orange H-aggregates, *Chem. Commun.* **2010**, *46*, 3595–3597.

(261) Bivier, T.; Boggioni, A.; Secco, F.; Turriani, X.; Venturini, M.; Yarmoluk, S. Influence of cyanine dye structure on self-aggregation and interaction with nucleic acids: a kinetic approach to TO and BO binding. *Arch. Biochem. Biophys.*, **2007**, 465, 90–100.

(262) Fei, X. Gu, Y. Ban, Y. Liu Z. and Zhang, B. Thiazole orange derivatives: synthesis, fluorescence properties, and labeling cancer cells. *Bioorg. Med. Chem.* **2009**, 17, 585–591.

(263) Gadde, S.; Batchelor, E. K.; Kaifer, A. E. Controlling the formation of cyanine dye H- and J-aggregates with cucurbituril hosts in the presence of anionic polyelectrolytes. *Chem.–Eur. J.***2009**, *15*, 6025–6031.

(264) Wang, Y. X.; Zhang, Y. M.; Liu, Y. Photolysis of an amphiphilic assembly by calixarene-induced aggregation. *J. Am. Chem. Soc.* **2015**, *137*, 4543–4549.

(265) Kubát, P.; Šebera, J.; Záliš, S.; Langmaier, J.; Fuciman, M.; Polívka, T.; Lang, K. Charge transfer in porphyrin–calixarene complexes: ultrafast kinetics, cyclic voltammetry, and DFT calculations. *Phys. Chem. Chem. Phys.* **2011**, *13*, 6947–6954.

(266) Hennig, A.; Bakirci, H.; Nau, W. M., Label-free continuous enzyme assays with macrocycle-fluorescent dye complexes. *Nat. Methods* **2007**, *4*, 629–632.

(267) Nau, W. M.; Ghale, G.; Hennig, A.; Bakirci, H.; Bailey, D. M. Substrate-selective supramolecular tandem assays: monitoring enzyme inhibition of arginase and diamine oxidase by fluorescent dye displacement from calixarene and cucurbituril macrocycles. *J. Am. Chem. Soc.* **2009**, *131*, 11558–11570.

(268) Christianson, D. W. Arginase: Structure, mechanism, and physiological role in male and female sexual arousal. *Acc. Chem. Res.*. **2005**, *38*, 191–201.

(269) Guo, D. S.; Uzunova, V. D.; Su, X.; Liu, Y.; Nau, W. M. Operational calixarene-based fluorescent sensing systems for choline and acetylcholine and their application to enzymatic reactions. *Chem. Sci*. **2011**, *2*, 1722–1734.

(270) Ikeda, A.; Shinkai, S. Unusually high ionophoricity of 1,3-alternate-calix[4]arenes: π-donor participation in the complexation of cations? *Tetrahedron Lett.* **1992**, *33*, 7385–7388.

(271) Maskiewicz, R.; Sogah, D.; Bruice, T. C. Chemiluminescent reactions of lucigenin. 1. reactions of lucigenin with hydrogen peroxide, *J. Am. Chem. Soc.* **1979**, *101*, 5347–5354.

(272) Massouli, J.; Sussman, J.; Bon, S.; Silman, I. Structure and functions of acetylcholinesterase and butyrylcholinesterase. *Brain Res.* **1993**, *98*, 139–146.

(273) Cokugras, A. N. Butyrylcholinesterase: structure and physiological importance. *Turk. J. Biochem.* **2003**, *28*, 54–61.

(274) Lane, R. M.; Potkin, S. G.; Enz, A. Targeting acetylcholinesterase and butyrylcholinesterase in dementia. *Int. J. Neuropsychopharmacol*. **2006**, *9*, 101–124.

(275) Guo, D. S.; Yang, J.; Liu, Y. Specifically monitoring butyrylcholinesterase by supramolecular tandem assay, *Chem-Eur. J.* **2013**, *19*, 8755–8759.

(276) Guo, D.-S.; Wang, K.; Liu, Y. Selective binding behaviors of p-sulfonatocalixarenes in aqueous solution. *J. Incl. Phenom. Macrocycl. Chem.* **2008**, *62*, 1– 21.

(277) Benson, G. J.; Thurmon, J. C. Clinical pharmacology of succinylcholine. *J. Am. Vet. Med. Assoc.* **1980**, *176*, 646–647.

(278) Wang, Y. X.; Guo, D. S.; Duan, Y. C.; Wang, Y. J.; Liu, Y. Amphiphilic p-sulfonatocalix[4]arene as ‘‘drug chaperone’’ for escorting anticancer drugs, *Sci. Rep.* **2015**, 5, 9019.

(279) Droumaguet, B. L.; Nicolas, J.; Brambilla, D.; Mura, M.; Maksimenko, A.; Kimpe, L. D.; Salvati, E.; Zona, E.; Airoldi, C.; Canovi, M. et al. Versatile and efficient targeting using a single nanoparticulate platform: application to cancer and alzheimer's disease. *ACS Nano*. **2012**, 6, 5866–5879.

(280) Yang, Y.; Zhang, Y. M.; Chen, Y.; Chen, J. T.; Liu, Y. Targeted polysaccharide nanoparticle for adamplatin prodrug delivery. *J. Med. Chem.* **2013**, *56*, 9725–9736.

(281) Wang, Y. X.; Zhang, Y. M.; Wang, Y. L.; Liu, Y. Multifunctional vehicle of amphiphilic calix[4]arene mediated by liposome. *Chem. Mater.* **2015**, 27, 2848−2854.

(282) Hippius, C.; van Stokkum, I. H. M.; Zangrando, E.; Williams, R. M.; Würthner, F. Excited state interactions in calix[4]arene−perylene bisimide dye conjugates: global and target analysis of supramolecular building blocks. *J. Phys. Chem. C* **2007,** *111*, 13988–13996.

(283) Hippius, C.; van Stokkum, I. H. M.; Gsänger, M.; Groeneveld, M. M.; Williams, R. M.; Würthner, F. Sequential FRET processes in calix[4]arene-linked orange-red-green perylene bisimide dye zigzag arrays. *J. Phys. Chem. C* **2008**, *112*, 2476–2486.

(284) Hippius, C.; van Stokkum, I. H. M.; Zangrando, E.; Williams, R. M.; Wykes, M.; Beljonne, D.; Würthner, F. Ground- and excited-state pinched cone equilibria in calix[4]arenes bearing two perylene bisimide dyes. *J. Phys. Chem. C* **2008**, *112*, 14626–14638.

(285) Vân Anh, N.; Schlosser, F.; Groeneveld, M. M.; van Stokkum, I. H. M.; Würthner, F.; Williams, R. M. Photoinduced interactions in a pyrene-calix[4]arene-perylene bisimide dye system: probing ground-state conformations with excited-state dynamics of charge separation and recombination. *J. Phys. Chem. C* **2009**, *113*, 18358–18368.

(286) Siekierzycka, J. R.; Hippius, C.; Würthner, F.; Williams, R. M.; Brouwer, A. M. Polymer glass transitions switch electron transfer in individual molecules. *J. Am. Chem. Soc.* **2010**, *132*, 1240–1242.

(287) Issac, A.; Hildner, R.; Ernst, D.; Hippius, C.; Würthner, F.; Köhler, J. Single molecule studies of calix[4]arene-linked perylene bisimide dimers: relationship between blinking, lifetime and/or spectral fluctuations. *Phys. Chem. Chem. Phys.* **2012**, *14*, 10789–10798.

(288) Issac, A.; Hildner, R.; Hippius, C.; Würthner, F.; Köhler, J. Stepwise decrease of fluorescence versus sequential photobleaching in a single multichromophoric system. *ACS Nano* **2014**, *8*, 1708-1717.

(289) Hennrich, G.; Murillo, M. T.; Prados, P.; Al-Saraierh, H.; El-Dali, A.; Thompson, D. W.; Collins, J.; Georghiou, P. E.; Teshome, A.; Asselberghs, I. et al. Alkynyl expanded donor–acceptor calixarenes: geometry and second-order nonlinear optical properties. *Chem-Eur. J.* **2007**, *13*, 7753–7761.

(290) Chan, K. L.; Lim, J. P. F.; Yang, X.; Dodabalapur, A.; Jabbour, G. E.; Sellinger, A. High-efficiency pyrene-based blue light emitting diodes: aggregation suppression using a calixarene 3D-scaffold. *Chem. Commun.* **2012**, *48*, 5106–5108.

(291) Fan, H. H.; Li, K. F.; Zhang, X. L.; Yang, W.; Wong, M. S.; Cheah, K. W. Efficient two- to five-photon excited violet emission of calix[4]arene-based multiple donor–accepter assembly. *Chem. Commun.* **2011**, *47*, 3879–3881.

(292) Rodler, F.; Schade, B.; Jäger, C. M.; Backes, S.; Hampel, F.; Böttcher, C.; Clark, T.; Hirsch, A. Amphiphilic perylene–calix[4]arene hybrids: synthesis and tunable self-assembly. *J. Am. Chem. Soc.* **2015**, *137*, 3308–3317.

(293) Becherer, M. S.; Schade, B.; Böttcher, C.; Hirsch, A. Supramolecular assembly of self-labeled amphicalixarenes. *Chem-Eur. J.* **2009**, *15*, 1637–1648.

(294) Yihwa, C.; Kellermann, M.; Becherer, M.; Hirsch, A.; Bohne, C. Pyrene binding to persistent micelles formed from a dendro-calixarene. *Photochem. Photobiol. Sci.* **2007**, *6*, 525–531.

(295) Martin, A. D.; Boulos, R. A.; Stubbs, K. A.; Raston, C. L. Phosphonated calix[4]arene-based amphiphiles as scaffolds for fluorescent nano-fibres. *Chem. Commun.* **2011**, *47*, 7329–7331.

(296) Tulli, L. G.; Wang, W.; Lindemann, W. R.; Kuzmenko, I.; Meier, W.; Vaknin, D.; Shahgaldian, P. Interfacial binding of divalent cations to calixarene-based Langmuir monolayers. *Langmuir* **2015**, *31*, 2351–2359.

(297) Cheipesh, T. A.; Zagorulko, E. S.; McHedlov-Petrossyan, N. O.; Rodik, R. V.; Kalchenko, V. I. The difference between the aggregates of short-tailed and long-tailed cationic calix[4]arene in water as detected using fluorescein dyes. *J. Mol. Liq.* **2014**, *193*, 232–238.

(298) Bisht, T.; Garg, B.; Chauhan, S. M. S. Hydrogen bonded non-covalent synthesis by reaction of porphyrin appended calix[4]arene with 5,5-diethylbarbituric acid in solution. *J. Incl. Phenom. Macrocycl. Chem.* **2014**, *78*, 103–111.

(299) Costa, A. I.; Ferreira, L. F. V.; Prata, J. V. Novel fluorescent (p-phenylene ethynylene)-calix[4]arene-based polymer: design, synthesis, and properties. *J. Polym. Sci. A* **2008**, *49*, 6477–6488.

(300) Barata, P. D.; Costa, A. I.; Prata, J. V. Calix[4]arene–carbazole-containing polymers: Synthesis and properties. *React. Funct. Polym.* **2012**, *72*, 627–634.

(301) Ogoshi, T.; Nishida, Y.; Yamagishi, T.-a.; Nakamoto, Y. Synthesis and host–guest properties of an alternating copolymer containing calix[4]arene and calix[6]arene in its main chain. *Polym. Chem.* **2010**, *1*, 203–206.

(302) Willner, I. Stimuli-controlled hydrogels and their applications. *Acc. Chem. Res*. **2017**, *50*, 657–658.

(303) Culver, H. R.; Clegg, J. R.; Peppas, N. A. Analyte-responsive hydrogels: intelligent materials for biosensing and drug delivery. *Acc. Chem. Res.* **2017**, *50*, 170–178.

(304) Moore, A. N.; Hartgerink J. D. Self-assembling multidomain peptide nanofibers for delivery of bioactive molecules and tissue regeneration. *Acc. Chem. Res.* **2017**, *50*, 714–722.

(305) Kim, Y.; Kathaperumal, M.; Chen, V. W.; Park, Y.; Fuentes-Hernandez, C.; Pan, M.-J.; Kippelen, B.; Perry, J. W. Bilayer structure with ultrahigh energy/power density using hybrid sol–gel dielectric and charge-blocking monolayer. *Adv. Energy Mater*. **2015**, *5*, 1500767.

(306) Chen, Q.; Feng, Y.; Zhang, D.; Zhang, G.; Fan, Q.; Sun, S.; Zhu, D. Light-triggered self-assembly of a spiropyran-functionalized dendron into nano-/micrometer-sized particles and photoresponsive organogel with switchable fluorescence. *Adv. Funct. Mater*. **2010**, *20*, 36−42.

(307) Hoeben, F. J. M.; Jonkheijm, P.; Meijer, E. W.; Schenning, A. P. H. J. About supramolecular assemblies of π-conjugated systems. *Chem. Rev*. **2005**, *105*, 1491−1546.

(308) Babu, S. S.; Praveen, V. K.; Ajayaghosh, A. Functional π-gelators and their applications. *Chem. Rev*. **2014**, *114*, 1973−2129.

(309) Aoki, M.; Nakashima, K.; Kawabata, H.; Tsutsui, S.; Shinkai, S. Molecular design and characterizations of new calixarene-based gelators of organic fluids. *J. Chem. Soc., Perkin Trans.* 2, **1993**, 347–354.

(310) Bandela, A. K.; Hinge, V. K.; Yarramala, D. S.; Rao, C. P. Versatile, reversible, and reusable gel of a monocholesteryl conjugated calix[4]arene as functional material to store and release dyes and drugs including doxorubicin, curcumin, and tocopherol. *ACS Appl. Mater. Interfaces* **2015**, *7*, 11555−11566.

(311) Kaiser, T. E.; Wang, H.; Stepanenko, V.; Wurthner, F. supramolecular construction of fluorescent j-aggregates based on hydrogen-bonded perylene dyes. *Angew. Chem., Int. Ed*. **2007**, *46*, 5541−5544.

(312) Park, J.; Lee, J. H.; Jaworski, J.; Shinkai, S.; Jung, J. H. Luminescent calix[4]arene-based metallogel formed at different solvent composition. *Inorg. Chem.* **2014**, *53*, 7181–7187.

(313) Zheng, Y-S.; Ran, S-Y.; Hua, Y,-J.; Liu, X,-X. Enantioselective self-assembly of chiral calix[4]arene acid with amines. *Chem. Commun.* **2009**, 1121–1123.

(314) Tsai, C.-C.; Cheng, Y.-T.; Shen, L.-C.; Chang, K.-C.; Ho, I-T.; Chu, J.-H.; Chung, W.-S. Biscalix[4]arene derivative as a very efficient phase selective gelator for oil spill recovery. *Org. Lett.* **2013**, *15*, 5830–5833.

(315) Lee, J. H.; Jung, S. H.; Lee, S. S.; Kwon, K.-Y.; Sakurai, K.; Jaworski, J.; Jung, J. H. Ultraviolet patterned calixarene-derived supramolecular gels and films with spatially resolved mechanical and fluorescent properties. *ACS Nano* **2017**, *11*, 4155−4164.

(316) Sun, X. H.; Chan, C. S.; Wong, M. S.; Wong, W. Y. Synthesis of tetra-oligothiophene-substituted calix[4]arenes and their optical and electrochemical properties. *Tetrahedron* **2006**, *62*, 7846–7853.

(317) O'Malley, S.; Alhashimy, N.; O'Mahony, J.; Kieran, A.; Pryce, M.; Nolan, K. The selective preparation of partial cone O-aryl calix[4]arene ethers from 1,3-dimethoxycalix[4]arene: a new platform for the preparation of non-aggregated dyes. *Tetrahedron Lett.* **2007**, *48*, 681-684.

(318) Prata, J. V.; Costa, A. I.; Pescitelli, G.; Teixeira, C. M. A fluorescent bicyclic calix[4]arene-oxacyclophane with planar chirality: Resolution, chiroptical properties, and absolute configuration. *Tetrahedron Asymmetry* **2014**, *25*, 547–553.

(319) Joshi, K. V.; Joshi, B. K.; Pandya, A.; Sutariya, P. G.; Menon, S. K. Calixarene capped ZnS quantum dots as an optical nanoprobe for detection and determination of menadione. *Analyst*, **2012**, *137*, 4647–4650.

(320) Mamor, A. F. D.; Cleverley, R. M.; Zapata-Ormachea, M. L. Thermodynamics of calixarene chemistry. *Chem. Rev.* **1998**, *98*, 2495–2526.

(321) Poul, N. L.; Mest, Y. L.; Jabin, I.; Reinaud, O. Supramolecular modeling of mono-copper enzyme active sites with calix[6]arene-based funnel complexes. *Acc. Chem. Res.* **2015**, 48, 2097−2106.

(322) Specht, A.; Bernard, P.; Goeldner, M.; Peng, L. Mutually induced formation of host–guest complexes between p-sulfonated calix[8]arene and photolabile cholinergic ligands. *Angew. Chem., Int. Ed*. **2002**, *41*, 4706–4708.

(323) Rieth, L. R.; Eaton, R. F.; Coates, G. W. Polymerization of ureidopyrimidinone-functionalized olefins by using late-transition metal ziegler–natta catalysts: synthesis of thermoplastic elastomeric polyolefins. *Angew. Chem. Int. Ed.* **2001**, *40*, 2153–2156.

(324) Kubo, Y.; Kitada, Y.; Wakabayashi, R.; Kishida, T.; Ayabe, M.; Kaneko, K.; Takeuchi, M.; Shinkai, S. A Supramolecular bundling approach toward the alignment of conjugated polymers. *Angew. Chem.* **2006**, *118*, 1578–1583.

(325) Xu, H.; Rudkevich, D. M. Reversible chemistry of CO_2 in the preparation of fluorescent supramolecular polymers. *J. Org. Chem.* **2004**, *69*, 8609–8617.

(326) Haino, H.; Hirai, E.; Fujiwara, Y.; Kashihara, K. Supramolecular cross-linking of [60]fullerene-tagged polyphenylacetylene by the host–guest interaction of calix[5]arene and [60]fullerene. *Angew. Chem. Int. Ed.* **2010**, *49*, 7899–7903.

(327) Haino, T.; Araki, H.; Fujiwara, Y.; Tanimoto, Y.; Fukazawa, Y. Fullerene sensors based on calix[5]arene. *Chem. Commun.* **2002**, 2148–2149.

(328) Hirao, T.; Tosaka, M.; Yamago, S.; Haino, T. Supramolecular fullerene polymers and networks directed by molecular recognition between calix[5]arene and C60. *Chem-Eur. J.* **2014**, *20*, 16138–16146.

(329) Zheng, Z.; Geng, W. C.; Gao, J.; Wang, Y. Y.; Sun, H. W.; Guo, D. S. Ultrasensitive and specific fluorescence detection of a cancer biomarker *via* nanomolar binding to a guanidinium-modified calixarene. *Chem. Sci.* **2018**, *9*, 2087–2091.

(330) Gao, J.; Li, J.; Geng, W. C.; Chen, F. Y.; Duan, X.; Zheng, Z.; Ding, D.; Guo, D. S. Biomarker displacement activation: a general host-guest strategy for targeted phototheranostics in vivo. *J. Am. Chem. Soc.* **2018**, *140*, 4945–4953.

(331) Galindo-Murillo, R.; Sandoval-Salinas, M. E.; Barroso-Flores, J. In silico design of monomolecular drug carriers for the tyrosine kinase inhibitor drug imatinib based on calix- and thiacalix[n]arene host molecules: A DFT and molecular dynamics study. *J. Chem. Theory Comput.* **2014**, *10*, 825–834.

(332) Bussolati, R.; Carrieri, P.; Secchi, A.; Arduini, A.; Credi, A.; Semeraro, M.; Venturi, M.; Silvi, S.; Velluto, D.; Zappacostad, R. et al. Hierarchical self-assembly of amphiphilic calix[6]arene wheels and viologen axles in water. *Org. Biomol. Chem.* **2013**, *11*, 5944–5953.

(333) Arduini, A.; Bussolati, R.; Credi, A.; Faimani, G.; Garaudee, S.; Pochini, A.; Secchi, A.; Semeraro, M.; Silvi, S.; Venturi, M. Towards controlling the threading direction of a calix[6]arene wheel by using nonsymmetric axles. *Chem.–Eur. J.* **2009**, *15*, 3230–3242.

(334) Wood, Z. A.; Schroder, E.; Harris, R.; Poole, L. B. Trends, Structure, mechanism and regulation of peroxiredoxins. *Biochem. Sci.* **2003**, *28*, 32–40.

(335) Townsend, T.; Solo-Gabriele, H.; Tolaymat, T.; Stook, K.; Hosein, N. Chromium, copper, and arsenic concentrations in soil underneath cca-treated wood structures. *Soil Sediment Contam.* **2003**, *12*, 779–798.

(336) Mummidivarapu, V. V. S.; Yarramala, D. S.; Kondaveeti, K. K.; Rao, C. P. Time- and concentration-dependent reactivity of cys, hcy, and gsh on the diels−alder-grafted 1,3,5-tris conjugate of calix[6]arene to bring selectivity for cys: spectroscopy, microscopy, and its reactivity in cells. *J. Org. Chem.* **2014**, *79*, 10477−10486.

(337) Brunetti, E.; Picron, J. F.; Flidrova, K.; Bruylants, G.; Bartik, K.; Jabin, I. Fluorescent chemosensors for anions and contact ion pairs with a cavity-based selectivity. *J. Org. Chem.* **2014**, *79*, 6179−6188.

(338) Puyana, M. C.; Ruiz, C. G.; Crego, A. L.; Marina, M. L. Development of a CE-MS2 method for the enantiomeric separation of L/D-carnitine: Application to the analysis of infant formulas, *Electrophoresis* **2009**, *30*, 337–348.

(339) Flanagan, J. L.; Simmons, P. A.; Vehige, J.; Willcox, M. D. P.; Garrett, Q. Role of carnitine in disease, *Nutrition & Metabolism* **2010**, *7*, 30.

(340) Mao, X.; Tian, D.; Li, H. p-Sulfonated calix[6]arene modified graphene as a 'turn on' fluorescent probe for L-carnitine in living cells, *Chem. Commun.*, **2012**, *48*, 4851–4853.

(341) Jadhav, A.; Kalyani, V. S.; Barooah, N.; Malkhede, D. D.; Mohanty, J. Molecular-recognition-assisted pKa shifts and metal-ion-induced fluorescence regeneration in p-sulfonatocalix[6]arene-encapsulated acridine, *ChemPhysChem.* **2015**, *16*, 420–427.

(342) Mai, J. H.; Liu, J. M.; Li, S. Y.; Jiang, H. F. A fluorescent probe for fluoride ion based on 2-aminopyridyl-bridged calix[6]arene, *Chin. Chem. Lett.*, **2009**, *20*, 1191–1194.

(343) Mummidivarapu, V. V. S.; Nehra, A.; Hinge, V. K.; Rao, C. P. Triazole linked picolylimine conjugate of calix[6]arene as a sequential sensor for La^{3+} followed by F^{-}. *Org. Lett.* **2012,** *14*, 2968–2971.

(344) Mummidivarapu, V. V. S.; Bandaru, S.; Yarramala, D. S.; Samanta, K.; Mhatre, D. S.; Rao, C. P. Binding and ratiometric dual ion recognition of Zn^{2+} and Cu^{2+} by 1,3,5-tris-amidoquinoline conjugate of calix[6]arene by spectroscopy and its supramolecular features by microscopy. *Anal. Chem.* **2015**, *87*, 4988–4995.

(345) Mecca, T.; Consoli, G. M. L.; Geraci, C.; Spina, R. L.; Cunsolo, F. Polycationic calix[8]arenes able to recognize and neutralize heparin. *Org. Biomol. Chem.* **2006**, *4*, 3763–3768.

(346) Rabenstein, D. L. Heparin and heparan sulfate: structure and function. *Nat. Prod. Rep.* **2002**, *19*, 312–331.

(347) Lodi, A.; Caselli, M.; Casnati, A.; Momicchioli, F.; Sansone, F.; Vanossi, D.; Ponterini, G. Solvent-dependent host–guest complexation of two homologous merocyanines by a water-soluble calix[8]arene: spectroscopic analysis and structural calculations. *J. Mol. Struct.* **2007**, *846*, 49–54.